Functional studies on a novel cytochrome *c* from *Rhodobacter sphaeroides*

Bor-Ran Li

Doctor of Philosophy
University of Edinburgh
2009

謹獻給　　佳憓與琴淑

DECLARATION

I declare that this thesis was composed by my self and that I carried out the work presented here, except where indicated in the text. It has not been submitted in part, or in whole, for any other degree. Some of the results have already been pubished.

Bor-Ran Li
7th July 1009

ACKNOWLEDGEMENTS

First of all, I would like to thanks, in particular, my supervisor Professor Steve Chapman for the opportunity to conduct my research within his laboratory and for his input and support. Thanks also to my examiners, Professor Yellowlees and Dr. Watmough, for their advices to this thesis and made it better. I also have to thank Professor Graeme Reid and Dr. Simon Daff for their conduct on my research. Special thanks go to Dr. Chris Mowat and Dr. Ross Anderson for their invaluable assistant and patience for my study and English. I am also grateful to Dr. Caroline Miles and Dr. Laurie Cooper for their help with molecular cloning and constructing the knockouts. Thanks also to Dr. John Ingledew for his help with EPR spectroscopy. I would like to thank all past and present members of the Chapman/Reid group, Caroline II, Andy, Sally, Loura, Davide, Chiara, Sarah, Sidong, Fei, Ben, Laura and Georage, for their various help and making my life in lab an enjoyable one. Genuine thanks give to my family and all closest Taiwanese friends in Edinburgh for their encouragement in the passed three years. Last I have to give my final thanks to EaStCHEM for three years finance support.

ABSTRACT

SHP (*Sphaeroides* Heme Protein) is a monoheme cytochrome *c* of unknown function. In general, ligands cannot bind to ferric SHP, but some diatomic molecules, such as O_2 or NO, can bind to ferrous SHP. The gene encoding SHP and genes encoding a diheme cytochrome *c* (DHC) and a *b*-type cytochrome (Cyt-*b*) are found in the same chromosome region in different species [1-3]. In the case of *Shewanella oneidensis* MR-1, mRNA levels for SHP, DHC, and Cyt-*b* are up-regulated by nearly 10-fold when grown under anaerobic conditions using nitrate as the electron acceptor [4]. Thus it is possible that the physiological role of SHP may be in nitrate metabolism. However, nitrate is too big to be a candidate substrate for SHP, and some nitrification steps need more than one electron transfer (SHP is a monoheme cytochrome). Therefore, we will focus on the nitrite reductase, nitric oxide reductase and nitric oxide dioxygenase activities of SHP.

In this thesis it is shown that SHP can catalyse the reaction between oxygen and nitric oxide to give a nitrate ion as the final product. Thus a possible aerobic function for SHP as a nitric oxide dioxygenase is proposed. Aerobically, SHP is proposed to be a nitric oxide dioxygenase [5] which utilizes the same mechanism as other NO dioxygenases, flavohemoglobin (HMP) and neuroglobin (Ngb) [6-8]. This mechanism is proposed to proceed via an oxy-ferrous complex (SHP^{2+}-O_2) which reacts with nitric oxide. A mechanism for the catalytic reaction with ferrous-NO complex is described. SHP^{2+}-NO can be quickly converted back to ferrous SHP by reacting with superoxide liberated by SHP^{2+}-O_2 or from another source. In addition it is also found that *Shewanella* MR-1 wild type reveals a higher NO tolerance than the SHP knockout strain in aerobic conditions.

The catalytic mechanism of NO dioxygenase is oxygen-dependent, but the SHP mRNA up-regulation in *Shewanella oneidensis* MR-1 grown with nitrate under anaerobic conditions indicates that SHP may also perform some anaerobic function

and may possibly be involved in nitrate metabolism. This work found that SHP reveals anaerobic nitrite reductase activity. However, the catalytic efficiency of SHP is considerably lower than other nitrite reductases. This infers that although SHP can reduce nitrite *in vitro*, it is unlikely to function as a nitrite reductase *in vivo*. Ferrous SHP binds NO with a K_d of less than 1 μM, and does not auto-oxidise. Therefore, under anaerobic conditions SHP^{2+}-NO must be processed by some other mechanism. In addition, biochemical results reveal that the SHP/DHC complex has NO reductase activity under anaerobic conditions. Unfortunately, this function was not proved *in vivo*.

SHP was initially isolated from *Rhodobacter sphaeroides* and its structure was reported in 2000 [3]. Based upon this structure, SHP is clearly a class I cytochrome *c* with one axial histidine ligand to the heme iron. Unusually, however, it has an asparagine residue as the other axial heme ligand, and as such is unique among cytochromes *c*. For this reason it may be assumed that the asparagine plays a special role. This study reveals several potential reasons why SHP utilises asparagine as a heme ligand. Firstly, in the ferric form, asparagine 88 binds to the heme iron to prevent small molecules binding. Secondly, in the ferrous form it moves to allow oxygen to bind and form the oxy-ferrous complex, using hydrogen bonding for stability. Thirdly, using asparagine as a heme ligand creates a suitable redox potential for reduction by DHC, thus allowing NO dioxygenation.

ABBREVIATIONS

Amino Acids

A	Ala	Alanine	**M**	Met	Methionine
C	Cys	Cysteine	**N**	Asn	Asparagine
D	Asp	Aspartate	**P**	Pro	Proline
E	Glu	Glutamic acid	**Q**	Gln	Glutamine
F	Phe	Phenylalanine	**R**	Arg	Arginine
G	Gly	Glycine	**S**	Ser	Serine
H	His	Histidine	**T**	Thr	Threonine
I	Ile	Isoleucine	**V**	Val	Valine
K	Lys	Lysine	**W**	Trp	Tryptophan
L	Leu	Leucine	**Y**	Tyr	Tyrosine

Protein Abbreviations

SHP	*Sphaeroides* Heme Protein
DHC	diheme cytochrome *c*
Cyt *b*	cytochrome *b*
HMP	flavohemoglobin
Ngb	Neuroglobin
Fcc$_3$	Flavocytochrome c_3

Kinetic and Electrochemical Parameters

k_{cat}	Rate constant at substrate saturation
k_{et}	Kinetic rate constants of electron transfer

k_{obs}	Rate constant for observed association (s^{-1})
k_1	Rate constant for the fast phase of a biphasic reaction (s^{-1})
k_2	Rate constant for the slow phase of a biphasic reaction (s^{-1})
K_m	Michaelis constant
K_d	Dissociation constant
k_{on}	The on rate constant ($M^{-1}s^{-1}$)
k_{off}	The off rate constant (s^{-1})

Buffers

TRIS	Tris[hydroxymethyl]aminoethane
HEPES	N-[2-Hydroxyethyl]piperazine-N'-[2-ethane-sulfonic acid]
KP_i	Potassium Phosphate: K_2HPO_4/KH_2PO_4
MES	2-[N-Morpholino]ethanesulfonic acid
MOPS	3-[N-Morpholino]propanesulfonic acid
PIPES	Piperazine-N,N'bis(2-ethanesulfonic acid)

Chemical Abbreviations

ADP	Adenosine Diphosphate
ATP	Adenosine Triphosphate
dH_2O	Distilled Water
DTT	Dithiothreitol
DMSO	Dimethyl Sulphoxide
EDTA	Ethylene diamine tetra-acetic acid
EtOH	Ethanol
FAD	Flavin Adenine Dinucleotide
FMN	Flavin Mononucleotide

IPTG	Isopropyl-β-D-thiogalactopyranoside
MGD	*bis*(Molybdopterin guanine Dinucleotide) molybdenum
MK	Menaquinone
MMK	Methylmenaquinone
NADH	β-Nicotinamide adenine dinucleotide
NADPH	β-Nicotinamide adenine dinucleotide phosphate
SDS	Sodium dodecylsulfate
TMBZ	3,3',5,5'-Tetramethylbenzidine
UQ	Ubiquinone

Standard Units

m	metre	M	molar
g	gram	^{o}C	degree Celcius
l	litre	V	volt
s	second	Å	Angstrom

Textual Abbreviations

Abs	Absorbance
Da	Daltons
ε_x	Extinction coefficient at wavelength *x*
E_o	Standard Reduction Potential
FPLC	Fast Protein Liquid Chromotography
I	Ionic Strength
LB	Luria Bertani
OTTLE	Optically Transparent Thin Layer Electrode
ox	oxidised

PAGE	Polyacrylamide Gel Electrophoresis
PDB	Protein Data Bank (http://www.rcsb.org/pdb)
red	reduced
SHE	Standard Hydrogen Electrode
TIGR	The Institute for Genomic Research (http://www.tigr.org)
UV	Ultraviolet
Vis	Visible
ΔG^o	Standard Free Energy Change

CONTENTS

LIST OF FIGURES

LIST OF TABLES

Chapter I

INTRODUCITON

1 INTRODUCTION

1.1 Respiration

Cellular respiration is a metabolic process that converts biochemical energy from nutrients into adenosine triphosphate (ATP). Many of the catabolic reactions involved in respiration are redox reactions that involve the oxidation of one molecule and the reduction of another [9, 10].

The common nutrients used by animal and plant cells in respiration include glucose, amino acids and lipids, and the common electron acceptor used is molecular oxygen (O_2). Using oxygen as a final electron acceptor in respiration is described as aerobic respiration. Some bacteria and archaea can use not only oxygen as an electron acceptor, but also a broad range of inorganic molecules, such as sulfur or various metal ions. Such respiratory processes are referred to as anaerobic respiration [9-12].

1.1.1 Aerobic respiration

As a source of energy and electrons glucose is the most efficient, becoming oxidized as shown in the equation below.

$$C_6H_{12}O_{6\,(aq)} + 6O_{2\,(g)} \rightarrow 6CO_{2\,(g)} + 6H_2O_{\,(l)} \qquad \Delta G = -2880 \text{ kJ per mole of } C_6H_{12}O_6$$

In vivo, the energy released from glucose oxidation is stored as ATP, which is the main unit of energy currency in living organisms. This simple equation masks the complexity of the process of glucose metabolism. Using mitochondria as an example, the whole process can be separated into 4 parts. These include glycolysis, Acetyl-CoA formation, the citric acid cycle (Krebs cycle) and the electron-transport chain [10, 11, 13, 14].

How is energy transformed from glucose to ATP?

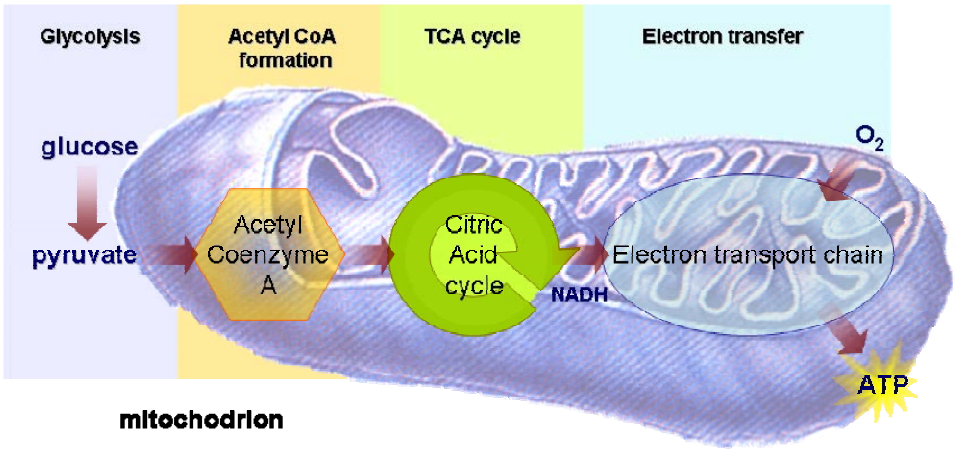

Figure 1.1: The process of energy transformation from glucose to ATP.

As Figure 1.1 shows, in glycolysis, the first step of aerobic respiration glucose is converted to pyruvate (pyruvic acid). This is the most common pathway for the oxidation of glucose and results in the formation of two ATP and two NADH (Nicotinamide Adenine Dinucleotide) molecules from one glucose molecule [10, 13, 15]. In the second step pyruvate is oxidized by pyruvate dehydrogenase to produce one CO_2 molecule and one acetyl-CoA (acetyl-coenzyme A), which is a central compound in metabolism. In this step, one NAD^+ is reduced to NADH [10, 13, 16]. Acetyl-CoA then enters the third step, the citric acid cycle. Each glucose molecule can generate two acetyl-CoA groups for this cycle (one 6-carbon glucose is oxidized to two 3-carbon pyruvate molecules, each of which is decarboxylated to produce an acetyl-CoA molecule). Electrons are liberated in the citric acid cycle and are transferred to NAD^+ and FAD to form the reduced electron carriers NADH and $FADH_2$. The net result is that oxidation of one molecule of glucose in the citric acid cycle produces six molecules of NADH, two molecules of $FADH_2$, and two molecules of ATP [10, 13]. It also produces six molecules of CO_2 in the decarboxylation steps of the citric acid cycle. The final step is electron transport. Electrons are brought to the electron-transport chain by NADH generated during the previous steps. NADH transfers electrons to complex I (NADH-quinone oxidoreductase) as the first step, and

then through subsequent steps electrons are finally transferred to the terminal electron acceptor, O_2 [13]. In the final electron transfer step, O_2 is reduced to H_2O molecule. Ultimately, metabolism of one glucose molecule in aerobic conditions leads to the production of 6 CO_2, 6 H_2O and 36 ATP molecules [10, 13].

The mitochondrial electron-transport chain

The mitochondrial electron-transport chain couples oxidation of an electron donor (NADH) to reduction of an electron acceptor (O_2) to transfer protons across a inner-membrane *via* a set of mediating biochemical reactions. These H^+ ions are used to drive ATP synthesis as they move back across the inner-membrane [17-20]. The whole electron transport process involves more than twenty discrete electron carriers, and most of these are membrane proteins. These membrane protein complexes are known as complex I, II, III, IV and V (Figure 1.2).

Complex I (NADH quinone oxidoreductase)

Complex I is a large complex whose detailed structure is still unclear. As Figure 1.2 shows, complex I contains FMN (flavin mononucleotide) and several Fe-S clusters [21-27]. In the mitochondria, complex I functions as an NADH dehydrogenase (also called NADH quinone oxidoreductase) [28-32]. The reactions occur as follows; firstly, NADH is oxidized to NAD^+, reducing FMN to $FMNH_2$ in one two-electron step. The next electron carrier is a Fe-S cluster, which can only accept one electron at a time. $FMNH_2$ is oxidized in two one-electron steps [33, 34]. The first electron generated from $FMNH_2$ is transferred through an Fe-S cluster to an oxidized quinone to form a semiquinone intermediate. Then, this semiquinone receives the other electron to form the quinol form (QH_2) [33-35]. During this process, four protons (H^+) are translocated across the inner mitochondrial membrane, from the matrix to the intermembrane space. This creates a proton gradient that will be later used to generate ATP [36-40].

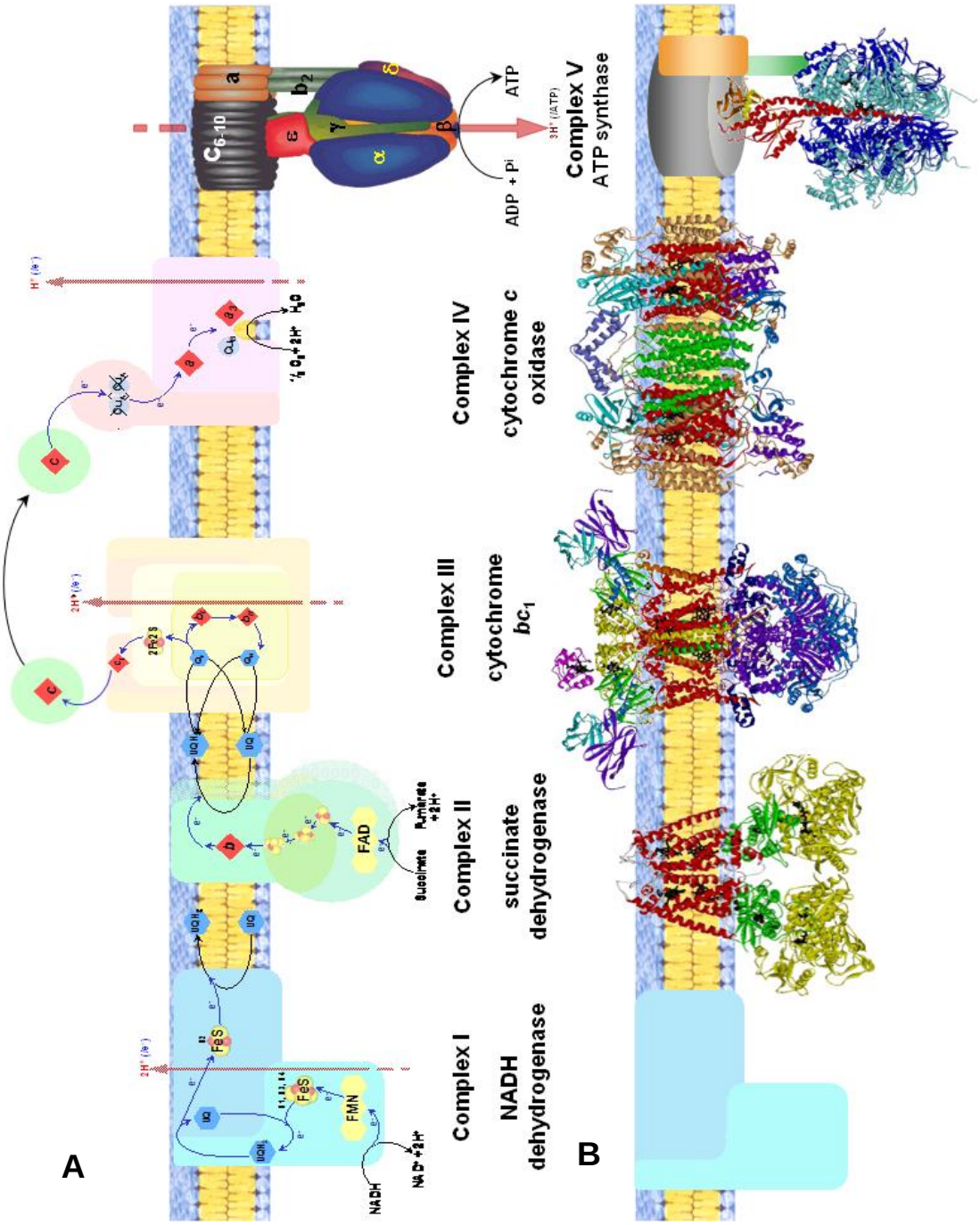

Figure 1.2: The arrangement of the aerobic respiratory pathway. *The schematic in Panel A shows the electron transport complexes I-IV with their cofactors and the flow of electrons. Complexes I, III and IV pump protons across the membrane, producing an electrochemical gradient that is used by Complex V to drive ATP synthesis. Panel B shows the crystal structures (where available) of the respiratory complexes. The structure shown for succinate dehydrogenase is that of the closely related fumarate reductase from Wolinella succinogenes. Figure modified from Ph.D thesis of Emma L. Rothery, 2004.*

Complex II (succinate dehydrogenase)

Complex II catalyses the two-electron oxidation of succinate to form fumarate and couples this to the reduction of quinone (Q) to quinol (QH_2) [41-43]. The quinol produced here and by complex I transfers electrons to complex III [44-48] (Figure 1.2). Succinate and fumarate are indispensable compounds in the citric acid cycle. Compared to the role played in the electron-transport chain, complex II plays a more important role in the citric acid cycle.

Complex III (cytochrome *bc*$_1$ complex)

Complex III contains cytochrome *b* and cytochrome c_1 units, and is therefore also called the cytochrome bc_1 complex. As Figure 1.2 shows, its function is to remove 4 electrons from two QH_2 and sequentially transfer two of them to two cytochrome *c* molecules *via* an Fe-S cluster. The other two electrons are sequentially passed across the protein to the quinone. The quinone is then reduced to quinol by combining with two protons from the matrix. The bc_1 complex does not pump protons; it helps build the proton gradient by the uptake and release of protons by quinone on opposite sides of the membrane [44-48].

Complex IV (cytochrome *c* oxidase): As Figure 1.2 shows, the function of complex IV is to transfer electrons to the terminal electron accepter, molecular oxygen (O_2). Electrons are removed from four molecules of reduced cytochrome *c*, which are generated by complex III. After receiving 4 electrons, molecular oxygen (O_2) can combine with 4 H^+ (from matrix) to produce two molecules of water (H_2O). At the same time, it moves protons across the membrane, producing a proton gradient [49-52].

Complex V (ATP synthesis): Complex V is composed of an F_1 and an F_0 particle. The F1 particle consists of a knob-like structure which is attached to stalk proteins linked to the F_0 base (Figure. 1.2) [53]. As described above, complexes I, II, and IV all pump protons into the space between the inner and outer mitochondrial membrane.

In this way, a proton gradient across the inner mitochondrial membrane is established. As the protons pass through complex V, the osmotic energy of the proton gradient is converted into chemical energy, in the form of ATP [36, 37, 53].

1.1.2 Anaerobic respiration

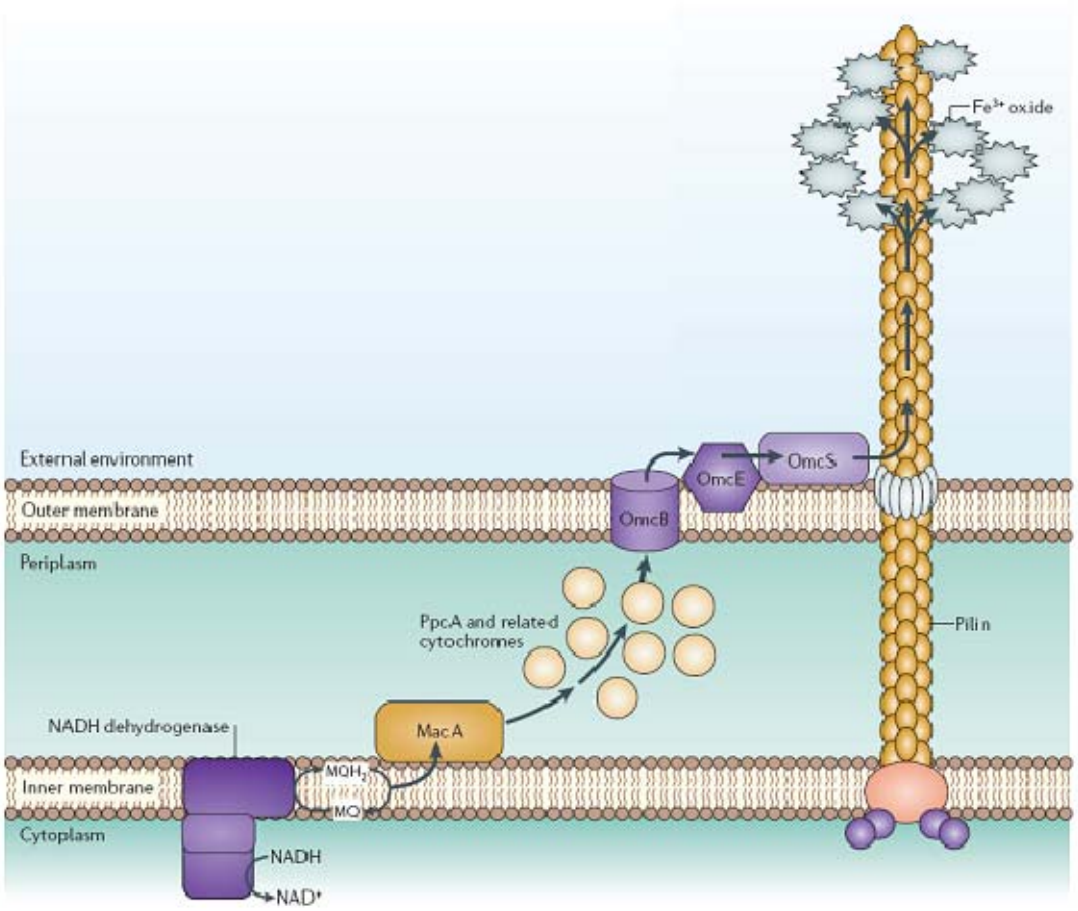

Figure 1.3: A mechanism for extracellular electron transfer by Geobacter sulfurreducens [54]. *Potential route for electron transfer to Fe^{3+} oxides in Geobacter sulfurreducens. This model is based on a previous model and subsequent findings. MacA, PpcA, OmcB, OmcE and OmcS are c-type cytochromes which genetic studies have indicated are required for optimal Fe^{3+} reduction. The proposed electron flow between the cytochromes is based on their reported location within the bacterial cell. MQH2, menaquinol; MQ, menaquinone. Figure modified from Lovely, Nature Reviews (2006).*

In anaerobic conditions, microbes can generate energy by two different processes. One of these is fermentation, and the other one is anaerobic respiration. Using glucose as the nutrient (as an example) in the fermentation processes it is converted to pyruvate and then fermented to form end products. The end product depends on the organism, but could be lactic acid, ethanol or other organic compounds [10, 55]. However, compared with respiration, only a little energy (in the form of ATP) can be generated by fermentation. The process of anaerobic respiration is very similar to aerobic respiration. It also generates pyruvate in the first step, and then produces acetyl-CoA to enter the citric acid cycle. ATP is generated through the transfer of electrons from NADH to an external electron acceptor other than O_2 [10, 55]. The final electron acceptor could be nitrate (NO_3^-), nitrite (NO_2^-), sulfate (SO_4^{2-}), carbon dioxide (CO_2), iron (Fe^{3+}) or other organic and inorganic molecules, and the choice of final electron acceptor is species dependent [54, 56]. Even when the same electron acceptor is used the anaerobic electron-transport chains are distinct in different organisms. Using *Shewanella* and *Geobacter* as example, both of them can use iron as the terminal electron acceptor, but their anaerobic electron-transport chains are slightly different (Figure 1.3) [54, 56].

1.1.3 Potential applications of microbial anaerobic respiration

Bioremediation: As described above, microbes can use a broad range of inorganic molecules as electron acceptors during anaerobic respiration. *Geobacter* species are naturally present in subsurface environments and these bacteria have been demonstrated to utilise the soluble contaminant species U^{6+} as a terminal electron acceptor. When *Geobacter* species and an acetate solution (as electron donor) are present in a U^{6+} contaminated zone, soluble uranium (U^{6+}) will be reduced to a highly insoluble form (U^{4+}). In this way further migration of the uranium is effectively prevented [57-59].

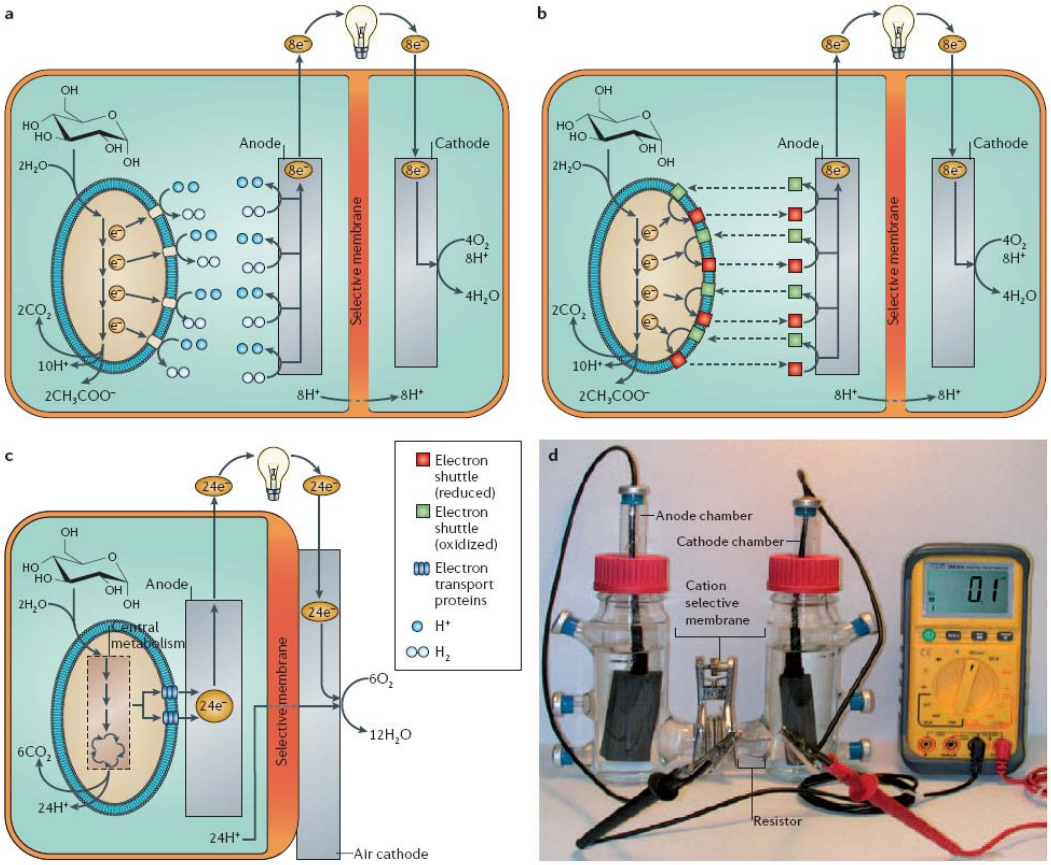

Figure 1.4: Examples of microbial fuel cells producing electricity through different mechanisms of electron transfer to the anode [54]. *(a) A fermentative microorganism converts glucose to an end product, hydrogen, which reacts with the anode to produce electrons and protons. This process only partially recovers the electrons available in the organic fuel as electricity, and results in the accumulation of organic products in the anode chamber. (b) An electron-shuttling mediator accepts electrons from reduced cell constituents and transfers the electrons to the anode. In most instances, the cells that have been used in such fuel cells only incompletely oxidize their organic fuels as shown. (c) The oxidation of glucose to carbon dioxide with direct electron transfer to the electrode surface. In this example, the system is illustrated with an air cathode rather than a cathode submerged in water. (d) A two-chambered microbial fuel cell. This system is not optimized for maximum power production but is convenient for microbiological studies. Figure modified from Lovely, Nature Reviews (2006).*

Microbial fuel cells: The definition of a fuel cell is a device unit which can convert chemical energy into electrical energy. In microbial fuel cells, the energy is generated from the microbial degradation of the organic content [54, 60, 61]. These organic compounds (fuel sources) cannot be directly used in current inorganic fuel cells, because, unlike hydrogen, they are not electrochemically active. Glucose is an obvious example of this. However, through the anaerobic respiration process in microorganisms (as described in the section 1.1.2), glucose will be taken into the cell and oxidized to CO_2 by the citric acid cycle with concomitant generation of NADH [9, 10, 55]. The electrons released from NADH in the electron-transport chain are transferred across the inner membrane, periplasm, and outer membrane through various electron carriers, such as *c*-type cytochromes [54, 56, 61]. Finally these electrons are transferred to extracellular electron acceptors that include iron (Fe^{3+}) or other oxidized metals. Therefore, when these microbes grow on an iron anode, electrons are transferred from the cell to the iron anode [60, 61]. This same process will occur as a result of anaerobic fermentation. As Figure 1.4 shows, one glucose molecule can generate 24 electrons from anaerobic respiration and less electrons from fermentation in theory [54, 56, 61]. Therefore, anaerobic respiration is the most efficient way to convert chemical energy stored in glucose into electrical energy.

1.2 Biological electron transfer and Marcus theory

Electron transfer reactions do not usually involve the making and breaking of bonds and are referred to as redox reactions. The most fundamental of chemical processes is the simple, one-electron transfer. It is important in biology, for example being utilized extensively in photosynthesis and respiration *via* electron-transport chains. The Marcus Theory for electron transfer originated in 1956 and is still used to explain the rates of electron transfer reactions in chemistry and biochemistry.

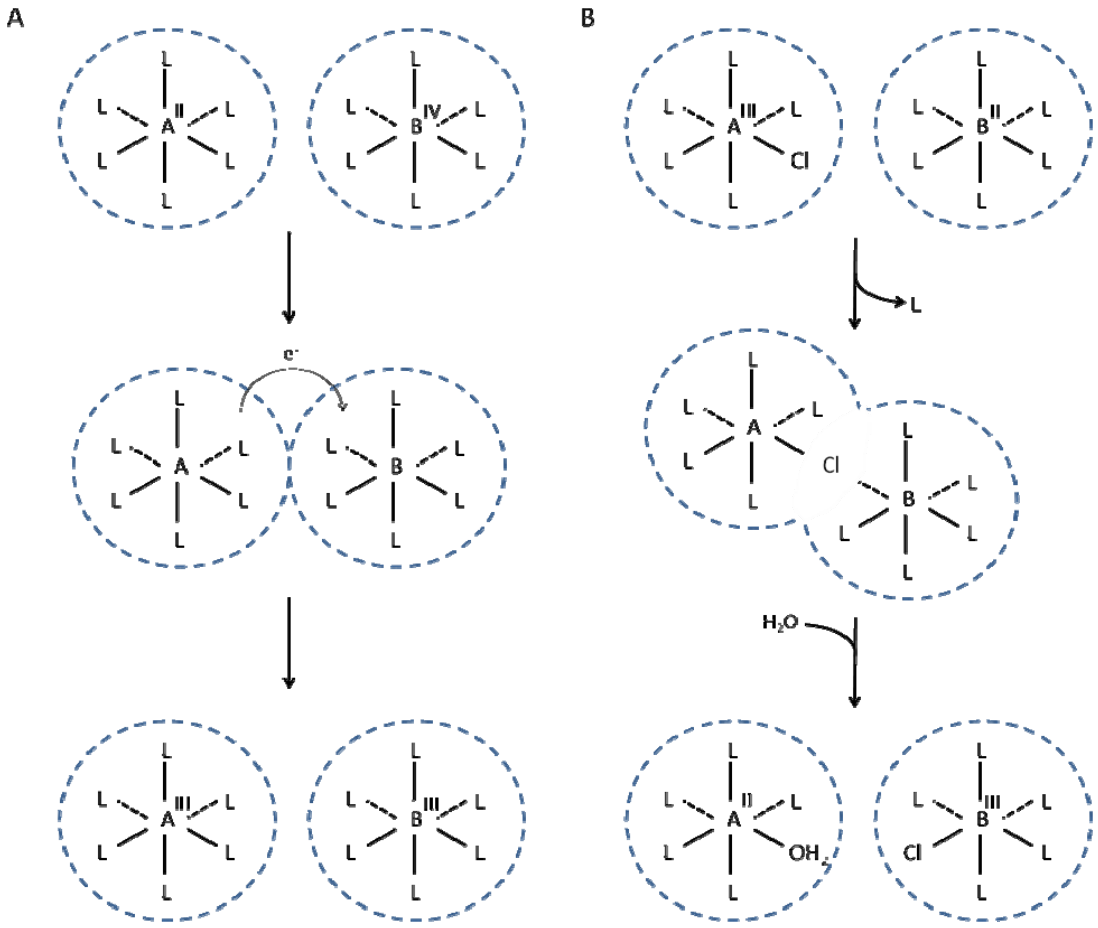

Figure 1.5: Outer- and inner-sphere electron transfer. *Panel A shows a schematic of outer-sphere electron transfer: the reacting ions diffuse together until their coordination spheres come into contact. An electron migrates from one ion to the other and the ions diffuse apart. Panel B shows a schematic of inner-sphere electron transfer: the reacting ions diffuse together until their coordination spheres come into contact at which point a ligand substitution reaction occurs, forming a transitory ligand-bridged species. The bridging ligand transfers from one ion to the other, leading to changes in both the oxidation states of the redox centres and the composition of the coordination spheres. Figure modified from Shriver and Atkins (1990)*[62].

1.2.1 Electron Transfer in Biological Systems

Inner- and outer-sphere electron transfer reactions (Figure1.5) occur in biological processes. The respiratory electron-transport chain is an example of a system in which both types of reaction are observed. It is of further use to examine adiabatic

and non-adiabatic electron transfer in biological systems:

Adiabatic Electron Transfer: As defined in Figure 1.5, inner-sphere redox reactions involve the formation of ligand-bridged intermediates before electron transfer can occur. Therefore, in comparison to the outer-sphere reaction, the energetic barrier to the formation of the transition state is large. This is in accordance with the Franck-Condon principle, which states that as nuclei are significantly more massive than electrons, an electronic transition (or electron rearrangement) occurs so fast that the relative positions of the nuclei remain unchanged. In contrast to this, outer-sphere electron transfer reactions are mechanistically facile and follow transition state theory.

Non-Adiabatic Electron Transfer: Electron transfer reactions between metal centres in proteins are considered to be non-adiabatic in nature. This is a consequence of the large inter-metal centre distances and the insulating character of their protein surroundings. These factors combine to result in very weak coupling between the donor and acceptor potential energy surfaces, leading to a low probability of a successful reaction. An elementary description of non-adiabatic electron transfer is given by Marcus Theory [63].

1.2.2 Marcus Theory

Marcus Theory, developed by Rudolph A. Marcus in 1956 was originally used to address outer sphere electron transfer reactions, in which the two chemical species aren't directly bonded to each other (Figure 1.5). It was extended to explain inner sphere electron transfer reactions by Noel S. Hush (Hush's formulation is known as Marcus-Hush theory), in which the bridging ligand transfers from one ion to the other, leading to a change in the oxidation state of the redox centres and a change in the composition of the coordination spheres (Figure 1.5) [64, 65].

The restrictions of Marcus Theory

Marcus Theory provides a convenient model to describe non-adiabatic electron

transfer processes. There are several other restrictions which are placed on his model. Firstly, both reactants and products, undergoing simple harmonic oscillations, are represented as single separate parabolic energy wells. Secondly, energy is neither lost nor gained during the transfer process. The total energy of the system must remain constant until the electron transfer process is complete, and the reaction can essentially be considered as a redistribution of electrons. Thirdly, according to the Frank-Condon principle, electron transitions occur so rapidly that there is no change in the nuclear configuration of either species.

The Marcus Theory equation for the rate of electron transfer

The reorganisation energy (λ) of the system is the energy required to rearrange the atomic nuclei of the reactants into those of the products and is comprised of two separate components; the inner-sphere rearrangement energy, ΔG^*_{IS}, arising from changes within the inner spheres of the reacting centres (such as adjustments in bond lengths), and the outer-sphere rearrangement energy, ΔG^*_{OS}, which is due to changes in the surrounding medium (such as solvent reorientation or movements within the protein matrix). Determining the value of λ for reactions in proteins is consequently a complicated process, although methods have been developed to assist in its calculation [64]. The electron transfer rate (k_{ET}) is dependant on the activation barrier according to the Gaussian function:

$$k_{ET} = k_{max}\, e^{(-\Delta G^*/RT)}$$

The driving force, activation energy and reorganisation energy are related according to the following equation:

$$\Delta G^* = (\Delta G^o + \lambda)^2 / 4\lambda$$

According to it, the rate of electron transfer is given by:

$$k_{ET} = k_{max} \exp -(\Delta G^o + \lambda)^2 / 4\lambda RT$$

The position corresponds to the point at which the product and reactant potential energy parabolas intersect (Figure 1.6). Here, k_{ET} is the rate of electron transfer. k_{max} is the maximal rate of electron transfer (when ΔG* = 0). ΔG^o is the free energy change of the reaction, and λ is the reorganisation energy, the energy associated with relaxing the geometry of the system after electron transfer. R is the Boltzmann constant. T is the temperature in Kelvin.

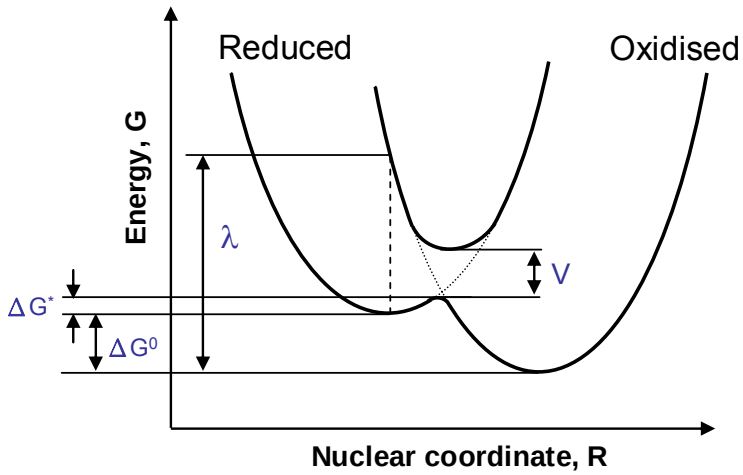

Figure 1.6: The reaction profile of an electron transfer reaction. *The diagram shows the two potential energy parabolas of the reactants (or reduced species, left) and the products (or oxidised species, right.) The activation energy of the reaction is shown by ΔG*, while the thermodynamic driving force is given by ΔG°, the standard free energy change of the reaction. The electronic interaction (or matrix coupling element) is defined by V and the reorganisation energy (the energy required to displace the configuration of the reactant nuclei to that of the products) is shown as λ.*

Three regions of electron transfer: normal, activationless and Marcus inverted

According to the Marcus electron transfer equation shown above, the thermodynamic driving force for a reaction is limited in three ways relating to the rate of electron transfer. Marcus Theory predicts an approximately parabolic dependence of the logarithm of the electron transfer rate upon – ΔG°, varying such that the rate increases with the driving force of the reaction to the maximum point of the parabola, when ΔG° = -λ. Once the driving force of the reaction exceeds this point, the rate of electron transfer decreases.

Marcus Theory predicts three regions for electron transfer, each requiring different conditions, as described in Figure 1.7. Figure 1.8 shows the potential energy diagrams relating to each case.

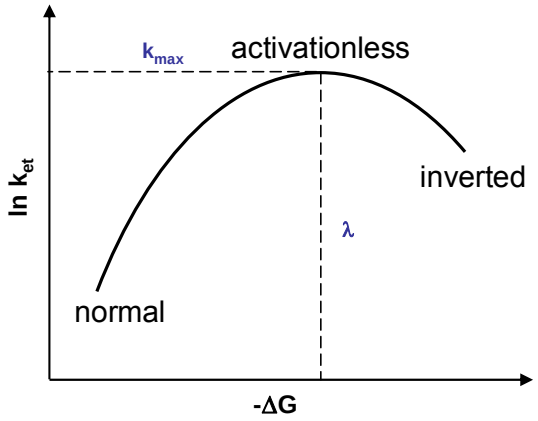

Figure 1.7: The relationship between the log of the electron transfer rate constant (k_{ET}) and the driving force (ΔG) according to Marcus Theory. *Three regions of electron transfer, normal, activationless and Marcus inverted are shown in the figure. The log of the electron transfer rate constant (k_{ET}) plotted as a function of the free energy of the reaction (ΔG°). The reorganisation energy of the reaction, λ, occurs at the apex of the curve.*

The normal region: when $\lambda > -\Delta G°$, the rate increases as the driving force increases.

The activationless region: when $\lambda = -\Delta G°$, there is no activation barrier to the reaction, therefore $k_{ET} = k_{max}$.

The Marcus inverted region: when $\lambda < -\Delta G°$, the rate of electron transfer decreases as the driving force increases.

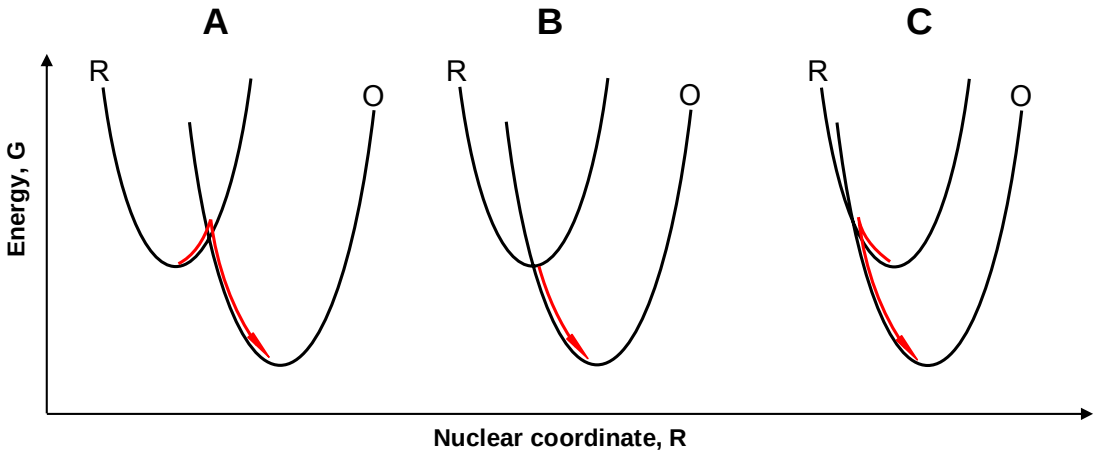

Figure 1.8: Three regions for electron transfer in Marcus Theory. *Relative positions of the potential energy wells for A: normal electron transfer, B: activationless electron transfer and C: electron transfer in the Marcus inverted region. Each of the three regions of electron transfer is shown in terms of the nuclear coordinates of their reactants and products. The activated complex is located at the intersection of the two potential energy curves.*

The maximum effective distance of electron transfer

The magnitude of the matrix coupling element is dependent on the distance between the two redox centres, R, and the nature of the intervening medium, β. These two factors are significant to the rate of the electron transfer reaction in the following way: the rate is proportional to the overlap between the donor and acceptor wavefunctions, and this overlap is dependent on both the distance between the two centres and the composition of the medium between them.

The extent of overlap between the orbitals decreases exponentially with distance, so that the rate of electron transfer increases as overlap increases. The rate of electron transfer can thus be expressed as a function of orbital overlap and the nature of the intervening medium:

$$k_{max} = 10^{13} \exp (-\beta (R - R_0))$$

It can therefore be determined that the maximum rate of electron transfer for a given reaction occurs at the maximum orbital overlap (the Van der Waals contact of the two centres) at 10^{13} s^{-1}. The rate decreases as the distance between the centres increases. Dutton has shown that at distances greater than 14 Å electron transfer is slowed to such an extent that it is unlikely to result in a productive reaction [63-67].

1.3 Redox cofactors in the cell

As mentioned in section 1.1, various electron carriers are involved in the electron-transport chain in both aerobic and anaerobic respiration. These electron carriers include some metal-containing molecules such as heme and iron-sulfur clusters, and some organic species such as FMN, NADH and quinones.

Heme is a prosthetic group that consists of an iron atom contained in the centre of a large heterocyclic organic ring called a porphyrin [68]. Proteins containing heme as their prosthetic subunit are called hemoproteins or cytochromes. There are more than 10 derivatives of heme. The most common type is heme *b*; other important types include heme *a* and heme *c*. The structures of major hemes are showed in Figure 1.9. There are many different hemes involved in the electron-transport chain. These include heme *a* in complex IV, heme *b* in complex II and III, and heme *c* in the water soluble cytochrome which transports electron from complex III to complex IV.

Not only functioning as an electron transporter (section 1.1), the biological functions of hemoproteins also include the storage and transport of diatomic gases, chemical catalysis or diatomic gas sensing [69-71]. The heme iron always serves as active centre during electron transfer or redox chemistry, and is also the site of binding of diatomics gases [72](e.g. globins).

Heme

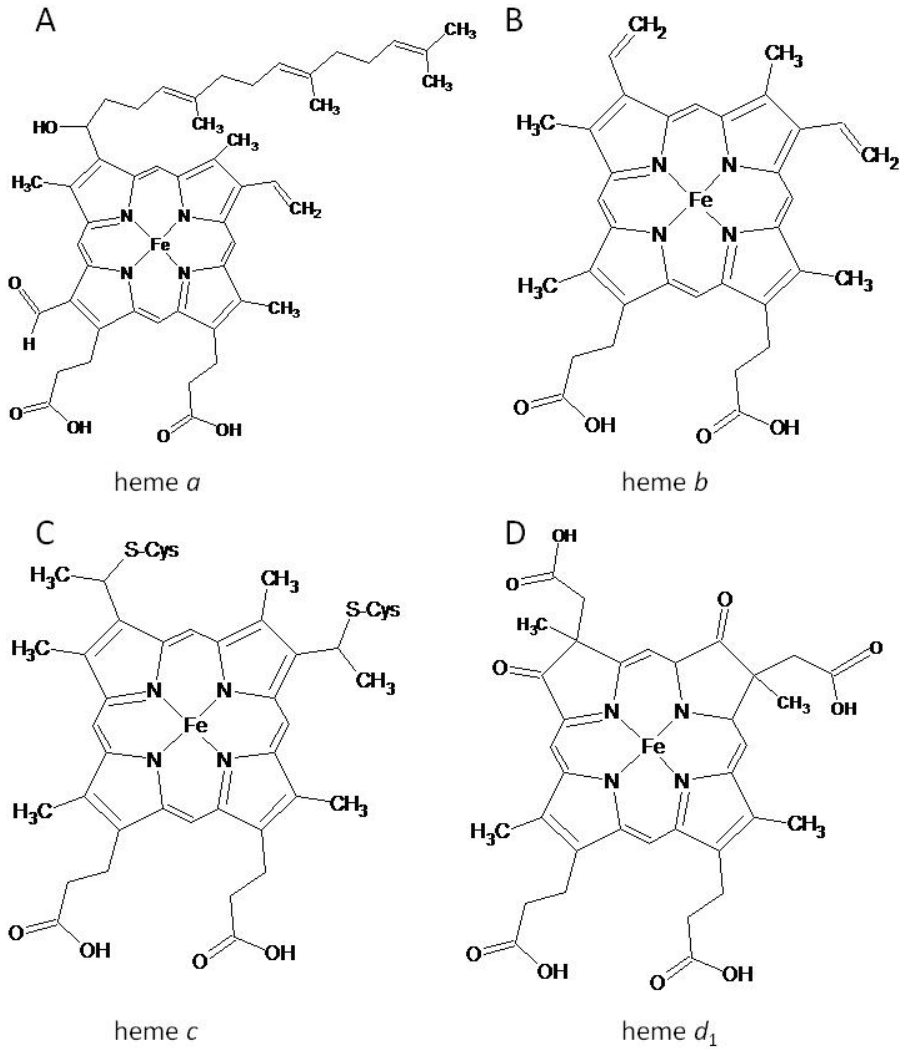

Figure 1.9: The structures of four different types of heme; a, b, c and d_1. *Structures A-D show the arrangements of the four different types of heme group, a,b,c and d_1 respectively. Structure B shows the configuration of the protoporphyrin IX system, heme b, and the remaining structures are modifications of this system. Heme a has an additional hydroxyethylfarnesyl side chain and formyl group. Heme c has two thioether linkages to cysteine residues, through which the heme is covalently attached to the protein backbone. Heme d contains two additional carboxylic acid groups and the porphyrin ring has fewer double bonds.*

Iron-sulfur clusters

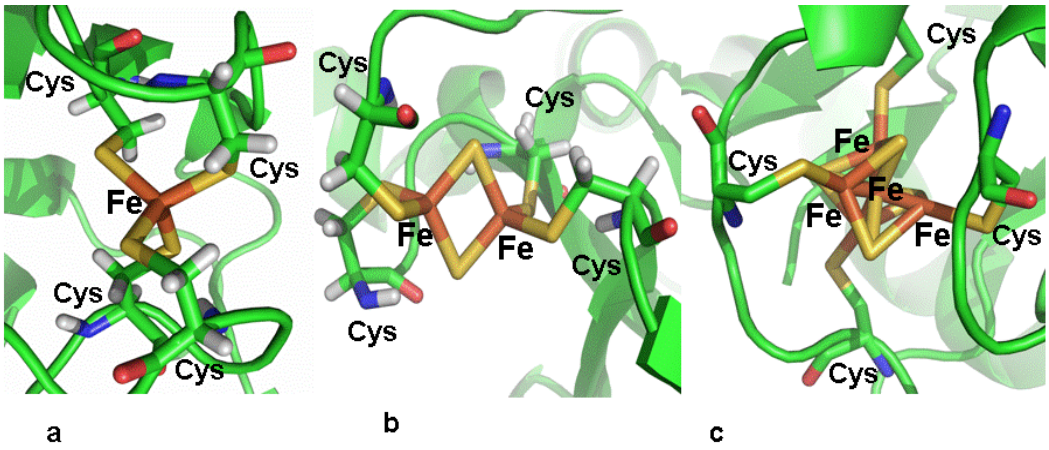

Figure 1.10: Iron-sulfur cluster centres. Iron is bound to the protein by the sulfur atoms of cysteine residues. *a) Crystal structure of rubredoxin from Clostridium pasteurianum showing a [1Fe-1S] cluster (PDB entry 4RXN) b)[2Fe-2S] ferredoxin-like cluster from Halobacterium salinarium (PDB entry 1E0Z) c) [3Fe-4S] cluster ferredoxin from Azotobacter vinelandii (PDB entry 1FDD). Figure adapted from Ph.D thesis of Chiara Bruckmanny, 2008.*

Iron-sulfur (Fe-S) clusters are ensembles of several iron and sulfur atoms. Iron atoms are covalently bound to the protein *via* cysteine residues and bound to other iron atoms via inorganic acid-labile sulfur bridges. Like hemes, Fe-S clusters also contain several derivatives, such as $[2Fe\text{-}2S]^{2+}$, $[4Fe\text{-}4S]^{n+}$ and $[3Fe\text{-}4S]^{n+}$ clusters. The structures are shown in Figure 1.10. In the electron-transport chain, these play electron transfer roles in complex I and complex III [44-48] (Figure 1.2).

Flavin

Flavins all contain a tricyclic heteronuclear isoalloxazine ring system. The source of flavin is the vitamin riboflavin which is generally modified to flavin adenine dinucleotide (FAD) or flavin mononucleotide (FMN) (Figure 1.11). The flavin group is capable of undergoing redox reactions, and can accept either one electron at a time or two electrons at once. FMN and FAD are important coenzymes that carry electrons from one reaction to another. For example, in complex I FMN is the active centre of the NADH dehydrogenase [21-27]. In the complex II, FAD is the cofactor of

the succinate dehydrogenase, an enzyme involved in the citric acid cycle [41-43].

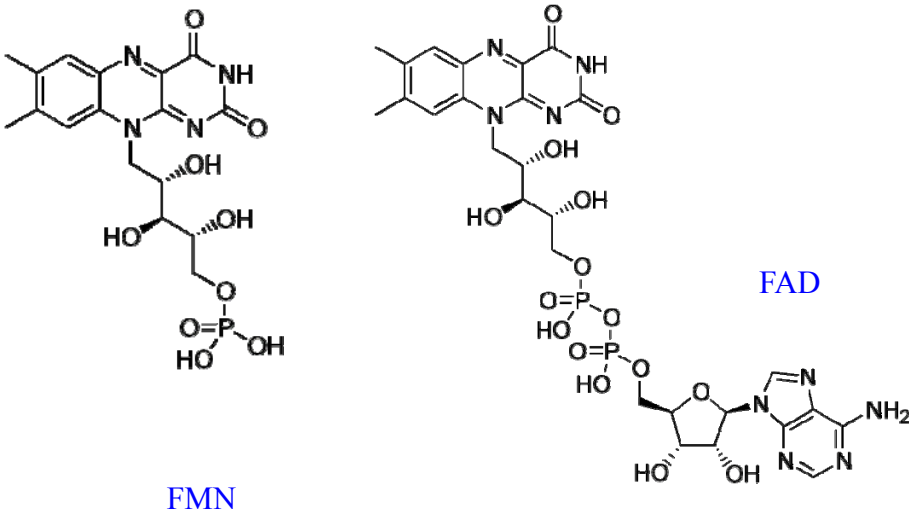

Figure 1.11: The structures of FMN and FAD.

NADH and NADPH

NAD^+ (Nicotinamide adenine dinucleotide) is a biological compound consisting of two nucleotides joined through their phosphate groups. One of these nucleotides contains an adenine base, and the other contains a nicotinamide base. Its structure is shown in Figure 1.12. In metabolism, NADH functions as an electron carrier and reducing agent. NAD^+ is the oxidized form, accepting electrons in the citric acid cycle and becoming the reduced form, NADH, which can then be used to donate electrons to complex I. NADH controls the activity of several key enzymes, including histone deacetylase [73], glyceraldehyde-3-phosphate dehydrogenase [74] and pyruvate dehydrogenase [75]. In organisms, NADH is synthesized from the amino acids tryptophan and aspartic acid, or alternatively taken up from nutrients as vitamin B_3.

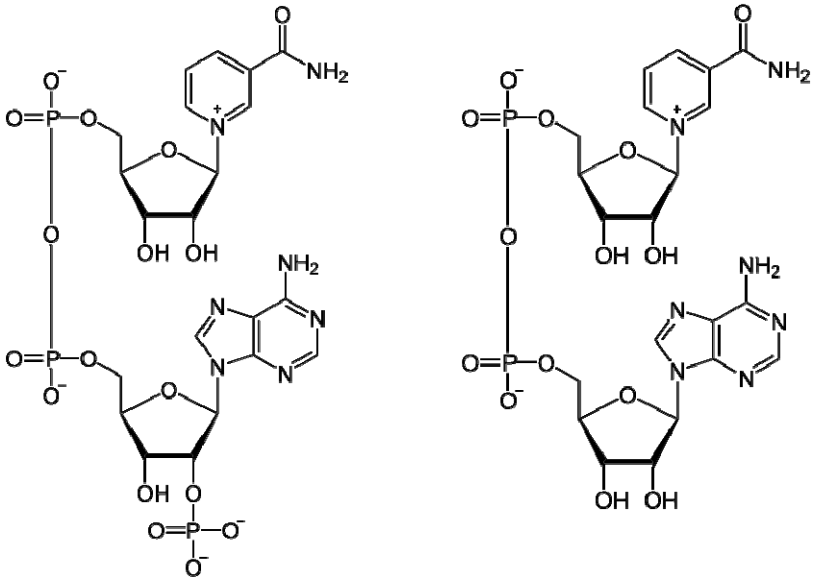

NADPH NADH

Figure 1.12: The structures of NADPH and NADH.

Nicotinamide adenine dinucleotide phosphate ($NADP^+$) is a derivative of NAD^+. In $NADP^+$, an additional phosphate group is on the 2' position of the adenine-carried ribose ring in the NAD^+ (structure is showed in Figure 1.12.). $NADP^+$ is the oxidized form and NADPH is the reduced form. Like the NAD^+/NADH system, the redox process in the $NADP^+$/NADPH system consists of the concomitant transfer of 2 electrons and a proton. Although the structures of $NADP^+$ and NAD^+ are almost the same, $NADP^+$ plays some different roles in metabolism, such as lipid and nicotinic acid synthesis.

Quinones

Quinones are highly hydrophobic molecules, due to their long isoprenoid tail groups. The length of the tail groups varies depending on the organism, but is usually 10 isoprene units in mammalian and 6 in bacterial cells. Quinones have the ability to exist in oxidized, semiquinone, and reduced forms and they act as electron carriers in membrane and lipid systems. Mammalian mitochondria use ubiquinone (UQ) in the

electron-transport chain, whereas bacteria utilize menaquinone (also known as vitamin K). Both can undergo $2e^- + 2H^+$ reduction to form quinol or partial reduction to a semiquinone (Figure 1.13) [10].

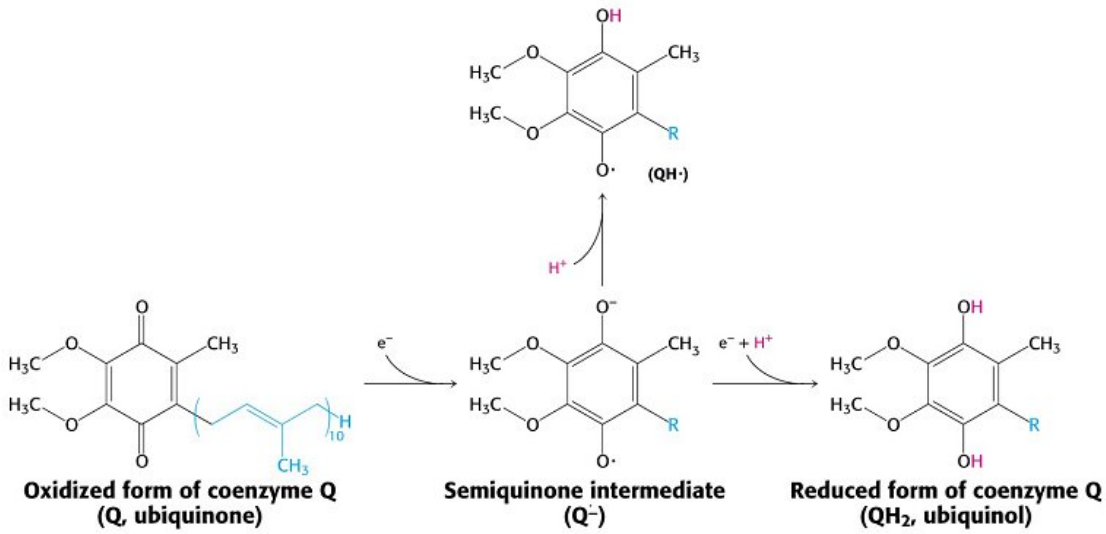

Figure 1.13: The structures of ubiquinone, semiquinone and ubiquinol

1.3 Two novel cytochromes *c*: SHP and DHC

Cytochromes are, in general, membrane-bound hemoproteins that contain one or several heme groups and carry out electron transport. They can be further classified according to the type of heme contained. For example, protein conjugates with *c*-type heme are called cytochrome *c* (cyt *c*). In this section, we will introduce the classes of cytochrome *c* and two cytochromes *c* of unknown function, SHP and DHC. These two proteins will be the subject of this thesis.

1.3.1 Cytochromes *c*

Cytochromes *c* generally function by a reversible change in the redox state of the central iron. The reduced, ferrous (Fe^{II}) form of cytochrome *c* is pink in solution,

with absorption bands at 551, 522 and 415 nm (Figure1.14). These bands are known as the α, β and γ (or Soret) band respectively. In the oxidized state it gives an orange solution with absorption bands at 530 and 400 nm .

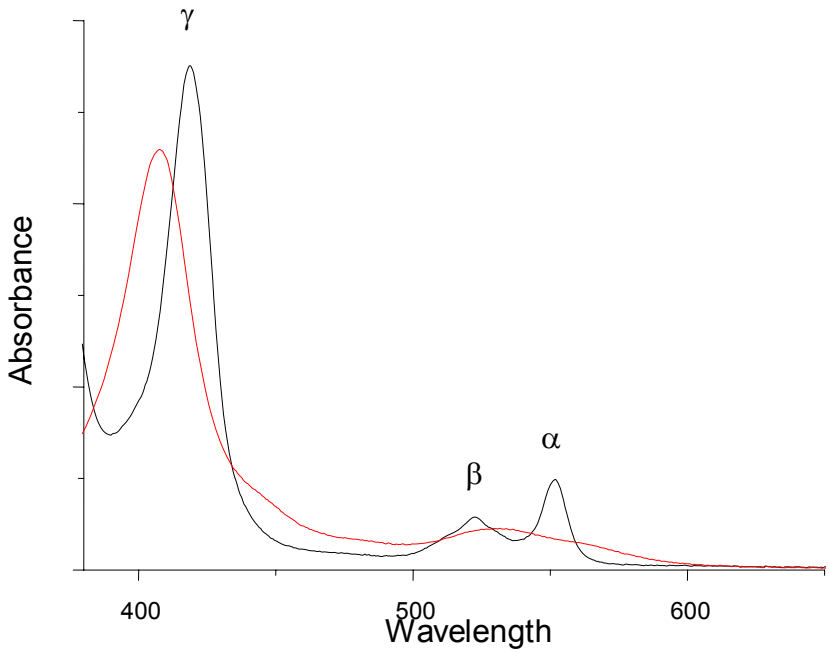

Figure 1.14: The Typical UV/visible absorption spectrum of a c-type cytochrome. *The reduced, ferrous (Fe^{II}), spectrum is shown in black, while the oxidised, ferric (Fe^{III}), spectrum is given in red. The α, β and γ bands are indicated on the reduced spectrum.*

Cytochromes *c* contain covalently bound heme. This is achieved by the use of a CXXCH amino acid motif which results in heme being bound *via* two thioether bonds involving vinyl groups on the porphyrin ring and sulfhydryl groups of cysteine residues. Generally speaking, the role cytochromes *c* play *in vivo* is one of electron transport. However, some of them also reveal enzymatic activity. Based on the number of hemes, properties of the axial iron ligands, 3-dimensional structures and redox potential, cytochromes *c* can be divided into four classes [76-78].

Class I includes cytochrome *c* itself, the low-spin soluble *c*-type heme protein

extensively found in the mitochondria and bacteria. The heme attachment site in this class is close to the N-terminus, and the proteins consist of approximately 80-120 amino acids. The structures of these proteins comprise three conserved helices forming a 'basket' around the heme group, which is solvent exposed on one side [78].

Class II includes both high-spin (His only heme coordination) and low-spin (His/Met heme coordination) cytochromes. Unlike class I, the heme-attachment site of the class II cytochromes *c* is close to the C-terminus, and the protein fold is composed of a four helix bundle [79].

Class III includes the low redox potential multiple-heme cytochromes, cyt c_7 and cyt c_3, and the high-molecular-weight cytochrome *c*, HMC. In this class, the proteins include multiple-hemes, and only 30-40 amino-acids per heme group. All of the hemes are bis-His coordination. In addition, the proteins in this class vary in structure and function, and the redox potentials range from 0 to -400 mV [80].

Class IV has two different definitions. One defines class IV as the cytochrome *c* holding other prosthetic groups as well as heme *c*, e.g. flavocytochrome *c* and cytochromes cd_1 [81, 82]. The other definition is that Class IV cytochromes *c* are tetraheme proteins containing both His/His and His/Met coordinated hemes, and form a structurally homogeneous family [83].

1.3.2 *Sphaeroides* heme protein (SHP)

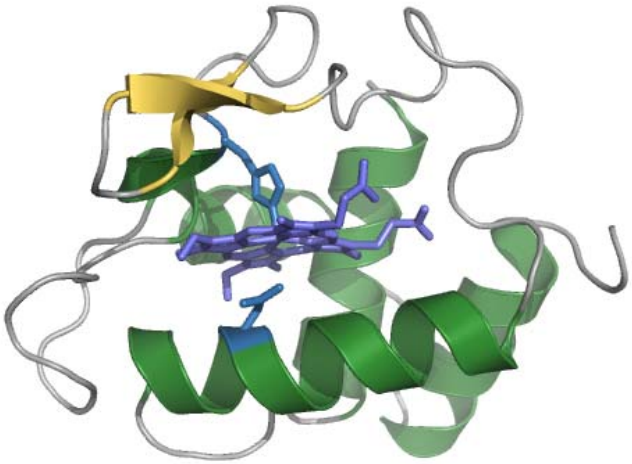

Figure 1.15: The structure of Rhodobacter sphaeroides SHP (1DW3). *The α-helices are shown in green, loops in gray, β-sheet in yellow, two heme ligands in blue, and heme in purple. This Figure was generated using PyMOL (DeLano Scientific; http://pymol. sourceforge.net/).*

Sphaeroides heme protein (SHP) is a monoheme c-type cytochrome (Figure 1.15) with a molecular weight of around 12.5 kDa. It is found in a number of diverse bacteria, which include *Rhodobacter sphaeroides* and *Shewanella oneidensis*. Ferrous SHP reveals the ability to bind dioxygen [1, 2, 84, 85]; like other oxygen binding proteins, reduced SHP also binds carbon monoxide, azide, cyanide and nitric oxide.

The crystal structures of the ferric, ferrous and ferrous-NO forms of *Rhodobacter sphaeroides* SHP were published in 2000 [1, 3], revealing it to be a class I cytochrome *c*. The cysteines which bind the heme group in the 112-residue protein are located at positions 43 and 46. Two extra cysteines in SHP (residues 89 and 97) form a disulfide bridge. According to these crystal structures, SHP reveals a novel sixth heme-ligating residue, asparagine. In the ferric form, this residue binds to the heme iron, but is labile upon reduction of the iron. Currently SHP is the only known cytochrome *c* that utilizes asparagine as sixth heme ligand. Therefore it is interesting to know what the function of this special protein is and why asparagine performs

such an unusual role.

From previous studies [85] it is known that *S. oneidensis*, *R. sphaeroides* and *M. methylotrophus* contain SHP homologues. In the *Shewanella* and *Rhodobacter* proteins, the sixth ligand are the conserved asparagines, but in the *Methylophilus* cytochrome c″ the sixth heme residue is a histidine. Therefore, although the amino sequences of these three proteins are highly conserved, it is necessary to investigate if the *Methylophilus* cytochrome c″ belongs to the SHP family.

1.3.3 Diheme cytochrome *c* (DHC)

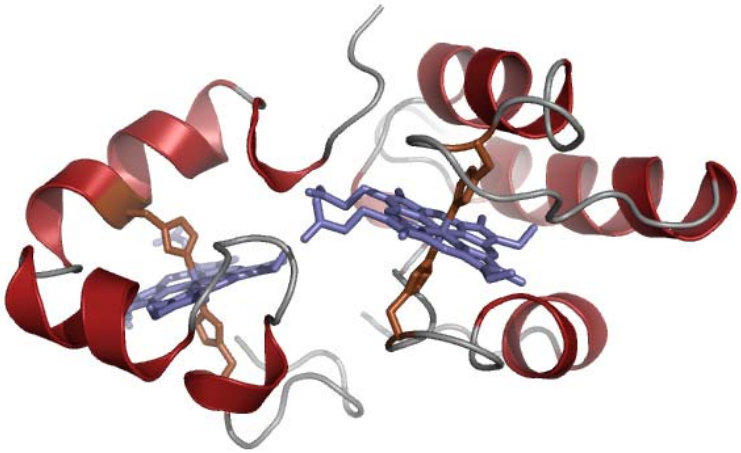

Figure 1.16: The structure of Rhodobacter sphaeroides DHC (2FWT). *The α-helices are shown in red, loops in gray, heme ligands in brown, and heme in purple. This Figure was generated using PyMOL (DeLano Scientific; http://pymol. sourceforge.net/).*

In 1985, a study of the soluble cytochromes of *Rhodobacter sphaeroides* revealed that at least five *c*-type cytochromes and one *b*-type cytochrome are present [86]. One of these is cytochrome $c_{551.5}$ which was later renamed as diheme cytochrome *c* (DHC). According to the gene maps, the genes of SHP, DHC and the other *b*-type

cytochrome are encoded together [1-3]. Thus, they may be functionally linked.

The DHC from *Rhodobacter sphaeroides* is a soluble protein with a mass of 16 kDa and represents a new class of *c*-type cytochrome [1]. The structure was published in 2006 (Figure 1.16) and shows that DHC folds into two distinct domains, each containing one heme, and that both hemes are bis-His coordinated. The shortest edge-to-edge distance between two heme groups is 10.2 Å, and this distance is bridged by Tyr31, thus ensuring fast internal electron transfer. In addition, according to the classifications described before, DHC, with multiple bis-His coordinated hemes, is very close to the class III cytochromes *c*. In addition the redox potentials of the hemes of DHC are -240 mV and -310 mV [1].

Both hemes of DHC are hexa-coordinate in the reduced and oxidized form, and can not bind any ligand. Therefore, DHC does not look likely to have any enzymatic activity, and is more likely to function as an electron transporter.

1.3.4 The SHP/DHC complex

As described above, the genes of SHP and DHC are encoded in the same operon and are proposed to be functionally linked. The tight binding of SHP and DHC in low salt conditions has already been reported, leading to the suggestion that the two proteins may form a complex. Until now, although the structures of SHP and DHC are known, the structure of SHP/DHC complex is still undetermined. In addition to their tight binding it has been established reduced DHC transfers electrons to SHP very efficiently, with a second-order rate constant of $1.85 \pm 0.11 \times 10^7$ $M^{-1}s^{-1}$ (at pH 7.2, 10 °C, and I = 500 mM) [1].

The proposal that SHP, DHC and Cyt-*b* have linked functions is supported by the finding that, in the case of *Shewanella oneidensis* MR-1, mRNA levels for all three cytochromes are up-regulated by nearly 10-fold when grown under anaerobic conditions with nitrate as the electron acceptor [4] (table 1). For this reason it is

supposed that this functional link may be in nitrate metabolism.

1.4 Bacterial nitrate metabolism

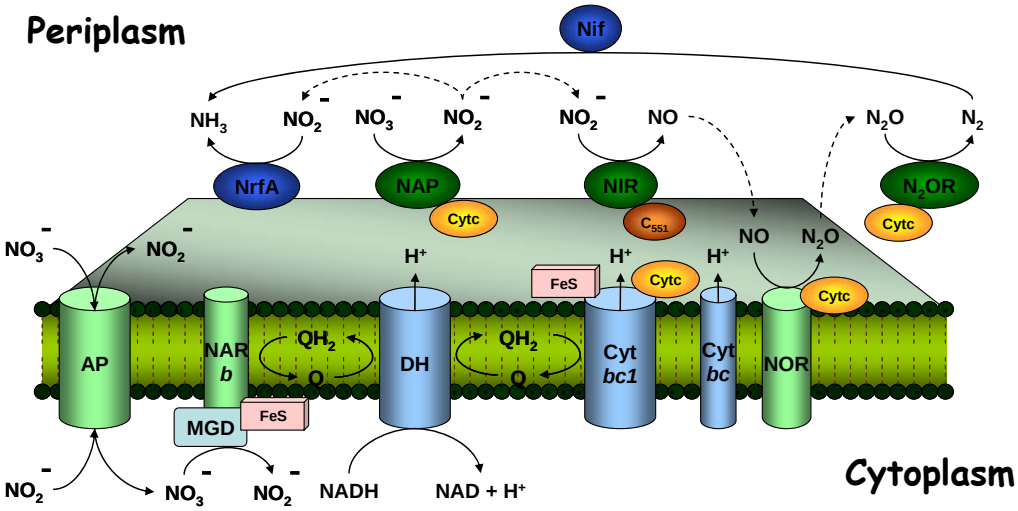

Figure 1.17: A model of nitrate metabolism in bacteria. *The blue areas represent the components of the constitutive aerobic respiratory chain consisting of an NADH dehydrogenase complex (DH), quinone cycle (Q, QH_2), cytochrome bc1 complex (Cyt bc_1), and the cytochrome cb terminal oxidase complex (Cyt cb). The denitrification system comprises respiratory nitrate reductase (NAR), nitrite reductase (NIR), NO reductase (NOR), N_2O reductase (N_2OR) and nitrate reductases (NAP). Enzymes are modeled according to the situation with R. eutropha and Paracoccus denitrificans. Abbreviations: FeS, iron-sulfur centers; b, c, heme b and heme c; cyt c, unspecified c-type cytochromes accepting electrons from the bc1 complex and acting on N_2OR and NOR; cyt c_{551}, cytochrome c_{551}* [87, 88].

SHP and DHC are two bacterial proteins which we studied in this thesis. Both of their genes are up-regulated while using nitrate as the terminal electron acceptor. Therefore we predicted these two proteins are involved in nitrate metabolism.

Aerobic metabolism is very similar in different species, but anaerobic metabolic processes show vast variation in microbes. This is because various inorganic molecules can be used as the terminal electron acceptor. As described in section 1.1, nitrate can be used as a terminal electron acceptor during anaerobic respiration in certain microbes. While some respiratory processes are well-understood, anaerobic

nitrate respiration (or nitrate metabolism) involves multiple periplasmic proteins (Figure 1.17).

Nitrate reduction is catalysed by Nar and Nap (periplasmic nitrate reductase). Nitrate metabolism is term used to describe the diverse number of redox reactions, primarily occurring in bacteria, that interconvert nitrogen species across the range of their oxidation states, from nitrate (+5) to ammonia (-3) [89, 90]. These reactions occur *via* a series of intermediates including dinitrogen, nitrite, nitric oxide, nitrous oxide and hydroxylamine. Nitrate is reduced step-by-step by various metalloenzymes, and finally produces molecular nitrogen or ammonium. There are two typical pathways for nitrate metabolism. One is anaerobic ammonium oxidation (ANAMMOX) [91, 92] and the other is denitrification [93] (Figure 1.18).

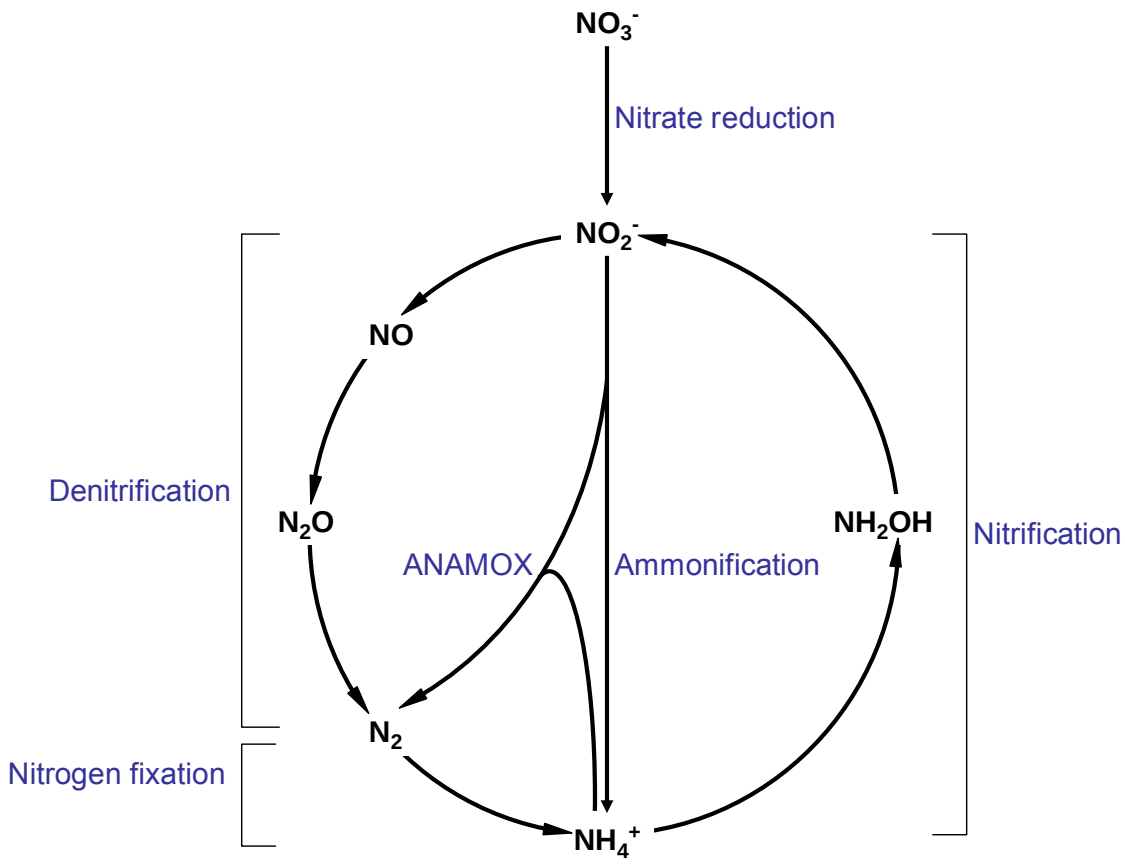

Figure 1.18: The biological nitrogen cycle

1.4.1 Anaerobic ammonium oxidation (ANAMMOX)

Nitrite is a product of nitrate reduction catalyzed by nitrate reductase (Nar) [94, 95]. In the subsequent step some bacteria can directly convert nitrite to ammonium ion (NH_4^+) by the action of nitrite reductase (NrfA) [96, 97]. Ammonia can then react with nitrite to produce nitrogen gas. This process is called (anaerobic ammonium oxidation) [91, 92]. The bacteria involved in this process are able to grow under chemolithoautotrophic conditions, using ammonia as an electron donor and nitrite as an electron acceptor [94, 95]. The reactions are shown below.

$$NO_3^- \rightarrow NO_2^- \quad \text{(Nar catalysis)}$$
$$NO_2^- \rightarrow NH_4^+ \quad \text{(Nrf A catalysis)}$$
$$NH_4^+ + NO_2^- \rightarrow N_2 + 2H_2O \text{ (chemical reaction)}$$

As the scheme shows above, the enzyme involved in the ANAMMOX is Nar and Nrf A.

1.4.1.1 Nrf A (Nitrate reductase)

There are two types of nitrite reductase. Cytochrome cd_1 Nir catalyses the one electron reduction of nitrite to nitric oxide ($NO_2^- + 2H^+ + e^- \rightarrow NO + H_2O$), while NrfA catalyses the reduction of nitrite to ammonium ion ($NO_2^- + 8H^+ + 6e^- \rightarrow NH_4^+ + 2H_2O$). This six-electron reaction occurs without the release of any intermediate products.

The crystal structure of Nrf A has been obtained from various species including *Sulfurospirillum deleyianum*, *wolinella succinogenes* and *Escherichia coli* [98-100], all of which are highly conserved. According to the crystal structure (Figure 1.19) [101], Nrf A is a pentaheme cytochrome *c*, and it is supposed to form a homodimer *in vivo*.

The protein is folded compactly and dominated by three long α-helical segments, two of which are involved in dimer formation through a mainly hydrophobic surface. As Figure 1.20 shows, each monomer contains five hemes which are closely packed in near-parallel and near-perpendicular heme pairs, in a similar manner to that observed in hydroxylamine oxidoreductase [101, 102]. Hemes 2-5 of Nrf A are conventionally bound by the typical cytochrome *c* motif (CXXCH) and are *bis*-histidinyl coordinated. Heme 1 (the active-site heme), however, is coordinated with a novel ligation, lysine. This unusual coordination comes from a CXXCK motif (Lys134 in *W. succinogenes* Nrf A, Lys126 in *E. coli* Nrf A and Lys133 in *S. deleyianum* Nrf A).

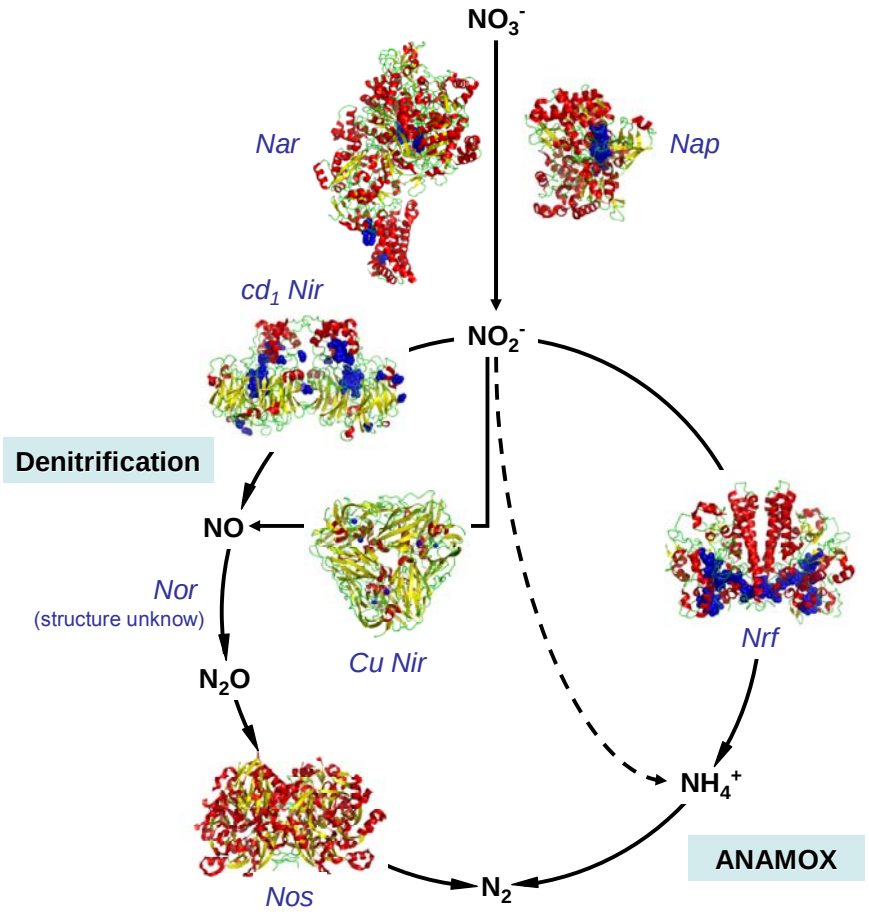

Figure 1.19: X-ray structures of the enzymes of the bacterial nitrogen cycle. *NAR, membrane-bound nitrate reductase; cd1NIR, cytochrome cd1 containing nitrite reductase; CuNIR, copper-containing nitrite reductase; NRF, cytochrome c nitrite reductase; NOS, Nitrous oxide reductase. ANAMMOX (anaerobic ammonium oxidation) This Figure was generated using PyMOL (DeLano Scientific; http://pymol. sourceforge.net/).*

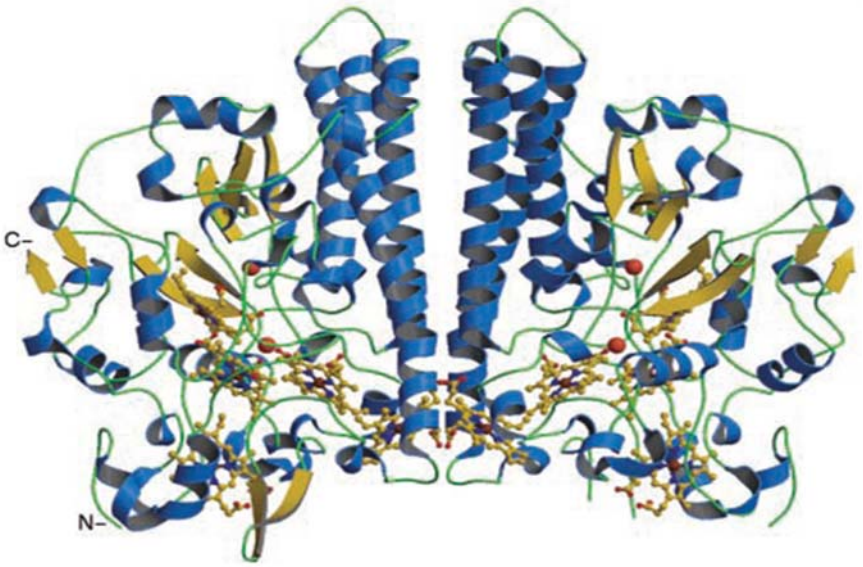

Figure 1.20: The homodimeric structure of cytochrome c nitrite reductase, NrfA, from Desulfovibrio desulfuricans, determined to 2.3 Å [103]***.*** *(Figure from Cunha et al, 2003) The orientation of the heme groups is visible towards the base of the structure, on either side of the dimer interface.*

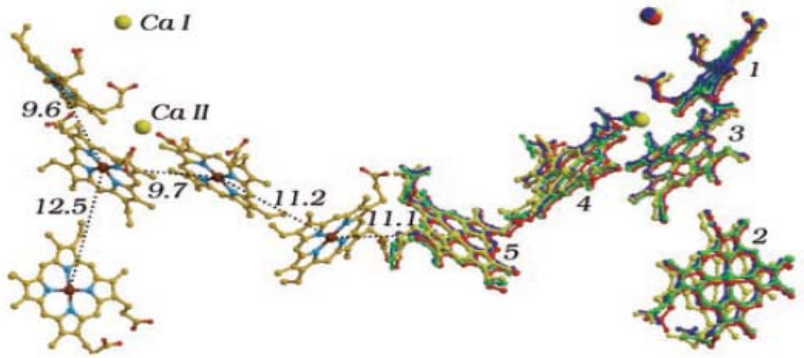

Figure 1.21: The arrangement of the heme groups in the dimeric NrfA enzyme [103]***.*** *The hemes are numbered in their order of occurrence in the protein sequence and the distances between the iron atoms are given in Å. Heme 1 is the active site. The right hand side monomer shows the superposition of the arrangements of hemes in the monomers of NrfA from S. deleyianum (red), W. succinogenes (blue) and E. coli (green)*

The mechanism of the six-electron reduction of nitrite to ammonia by the

cytochrome *c* nitrite reductases has been investigated using structural and density functional theoretical methods (Figure 1.21) [103]. The first step of the reaction is the binding of nitrite to the water-bound resting state of the enzyme, thus initiating the reaction cycle. The first N-O bond is heterolytically cleaved, followed by two one-electron reductions and a protonation, yielding Fe(II)-HNO. This species is readily reduced by two electrons to form Fe(II)-H_2NOH. A further reduction leads to the dissociation of the second water molecule and the product, ammonia, finally dissociates.

1.4.2 Denitrification

Denitrification describes the processes by which nitrate is successively reduced to nitrogen gas. These reactions are carried out almost exclusively by bacteria, although it has been determined that some contribution is made by certain species of fungi [88, 104, 105].

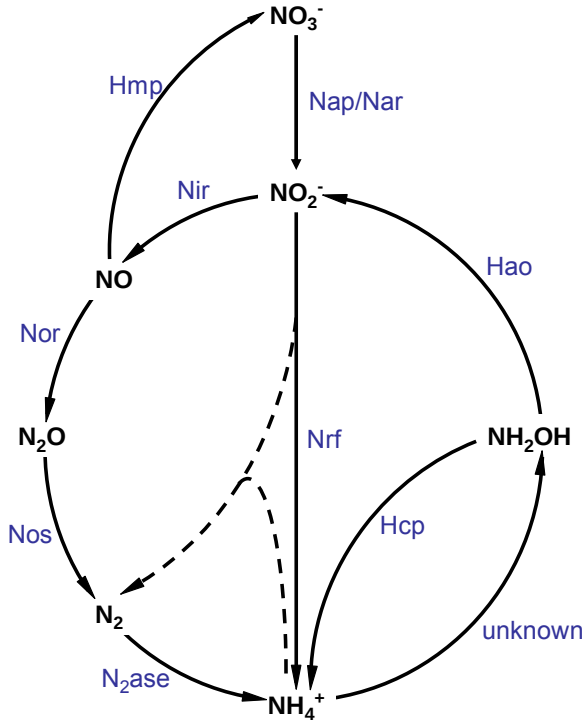

Figure 1.22: The enzymes involved in the biological nitrogen cycle. *The solid line is the enzyme-catalyzed reaction. The dotted line is the chemical reaction.*

Denitrification, a kind of respiration, is a microbial process for nitrate reduction, in which nitrate is reduced via nitrite (NO_2^-), nitric oxide (NO) and nitrous oxide (N_2O), and ultimately produces molecular nitrogen (N_2). Sometimes, several species of bacteria are involved in the complete reduction of nitrate to molecular nitrogen [88, 104, 105]. Thermodynamically speaking, oxygen is a more favourable electron acceptor, and nitrate respiration is not particularly efficient. Therefore, denitrification is a minor process in the high oxygen concentrations. However, in environments where oxygen consumption exceeds the rate of oxygen supply and nitrate is plentiful (such as in some soils, groundwater, or benthonic sediment), nitrate reduction takes place.

Denitrification occurs in the cell membranes and periplasm of nitrate reducing bacteria (Figure 1.17), and the whole metabolic cycle is shown in Figure 1.18. In the first step, nitrite is formed by nitrate reductases (periplasmic dissimilatory Nap), but the following nitrogen cycle steps depend on the species. As Figure 1.18 shows, there are two denitrification pathways. After nitrate is reduced to nitrite by nitrate reductases (Nar/Nap), the reduction process could be producing molecular nitrogen through nitric oxide and nitrous oxide, or directly produce ammonium ion (NH_4^+). As the upper pathway in Figure 1.22 shows, nitrite (NO_2^-) can be subsequently reduced to nitric oxide (NO), nitrous oxide (N_2O) and finally dinitrogen (N_2) using nitrogen oxide reductases NirK, NorB and NosZ. The structures and mechanisms of these metalloenzymes will be discussed below (Figure 1.23).

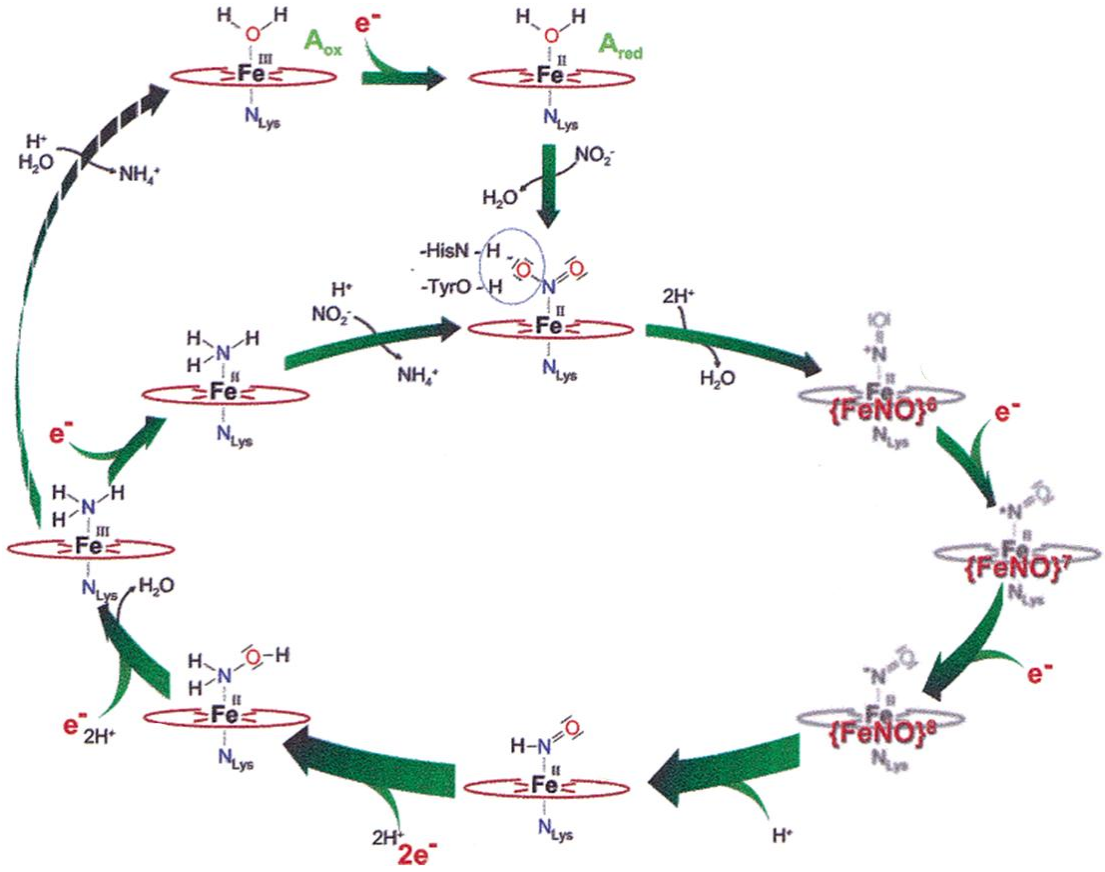

Figure 1.23: Proposed mechanism for the reduction of nitrite to ammonium by cytochrome c nitrite reductase. [106]

1.4.2.1 The Nitrate reductases (Nap/Nar)

There are two kinds of nitrate reductases involved in the nitrogen cycle. Both of them catalyze the reduction of nitrate to nitrite ($NO_3^- + 2H^+ + 2e^- \rightarrow NO_2^- + H_2O$). One of these types of nitrate reductase is located in the periplasm (Nap), and the other is found in the cytoplasmic membrane (Nar).

Nitrate Reductase (Nap) [107-109]**:** The periplasmic nitrate reductase (Nap) system is a large and complex enzyme with multiple subunits (A, B, C, G and H) and a mass of ~800 kDa, which contains bound FAD and a cytochrome$_{557}$, and also binds a [4Fe-4S] cluster and molybdenum. NapA and NapB subunits form a soluble heterodimeric complex located in the periplasm. NapA contains a [4Fe-4S] cluster and

molybdenum (~ 90 kDa); NapB is a small diheme subunit with ~ 16 kDa molecular weight). The structure of NapA/B from *Rhodobacter sphaeroides* has been solved (Figure 1.24) [107].

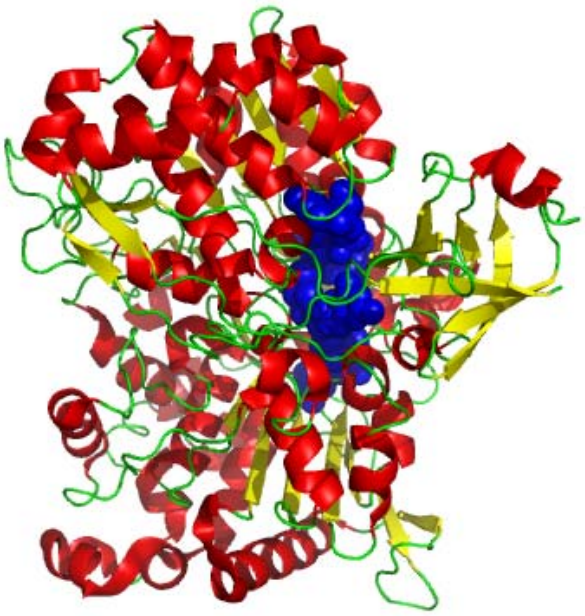

Figure 1.24: The structure of the Nap from Escherichia coli *(2NYA). The α-helices are shown in red, β-sheet in yellow, loops in green, and heme in blue. This Figure was generated using PyMOL (DeLano Scientific; http://pymol.sourceforge.net/).*

Nitrate Reductase (Nar) [110-112]**:** Nar is a membrane-bound nitrate reductase composed of three subunits (NarG, H and I). Two of them (NarG and NarH) are soluble subunits, which are anchored to the cytoplasmic membrane subunit (NarI) by hydrophobic interactions. The structure of NarI subunit contains two *b*-type hemes and a quinol binding site that receives electrons from the quinol pool; NarH contains three [4Fe-4S] and one [3Fe-4S] cluster that form a bioelectronic wire to transport electrons from NarI to NarG. The NarG subunit contains the active site which

unusually contains an [4Fe-4S] cluster and the molybdenum. The structure of NarG/H/I from *E. coli* K12 has been solved and is shown in Figure 1.25 [110].

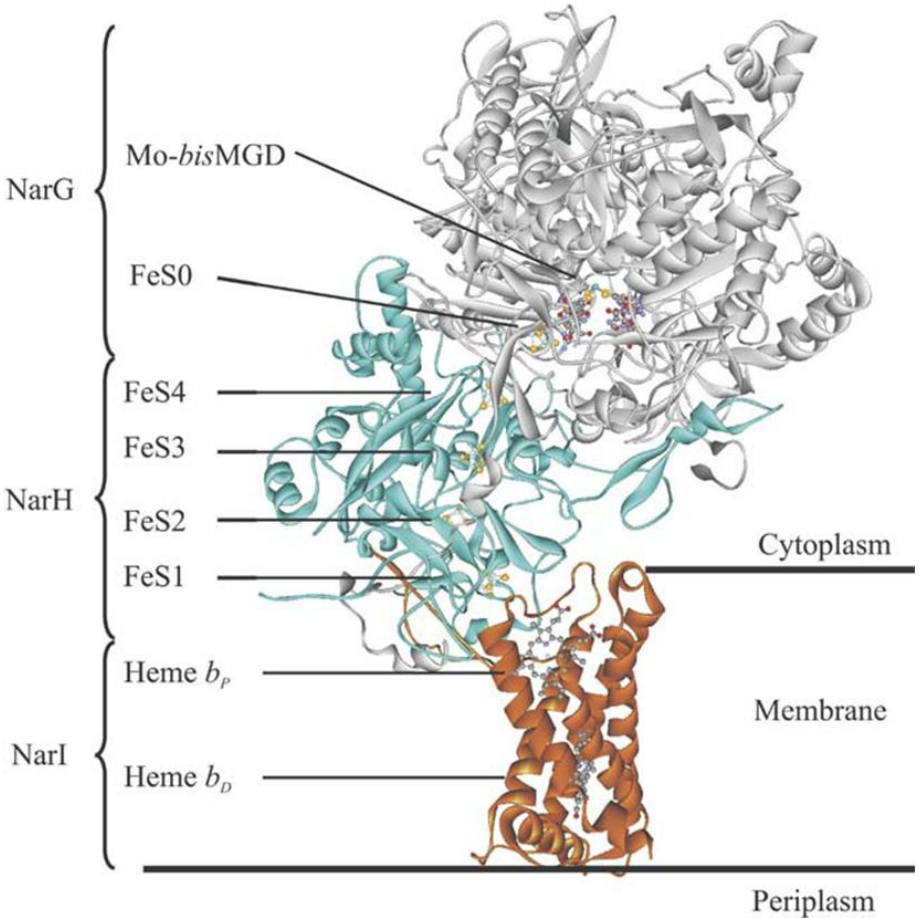

Figure 1.25: The overall three-dimensional structure of the membrane-bound nitrate reductase, Nar GHI, from E. coli K12. *Figure from González et al, 2006. The location of the enzyme in the membrane is shown. Each of the subunits and metal cofactors is identified* [113].

1.4.2.3 The Nitrite Reductases

There are three types of nitrite reductases. One of them is NrfA, which catalyzes the reduction of nitrite to ammonium ($NO_2^- + 8H^+ + 6e^- \rightarrow NH_4^+ + 2H_2O$, described in section 1.5.1.1). The other two (cd_1Nir and CuNir) catalyze the reduction of nitrite to nitric oxide ($NO_2^- + 2H^+ + e^- \rightarrow NO + H_2O$). These nitrite reductases are located in

the periplasm of Gram-negative bacteria.

Cytochrome cd_1 Nitrite Reductase (cd_1Nir) [114-118]**:** As its name implies, cytochrome cd_1 nitrite reductase contains one *c*-type and one d_1-type heme. It catalyzes reduction of nitrite to nitric oxide. Several structures have been solved, including those from *Paracoccus pantotrophus* and *Paracoccus denitrificans* (Figure 1.26) [114]. It exists as a dimer, and the active site of the enzyme is the d_1 heme.

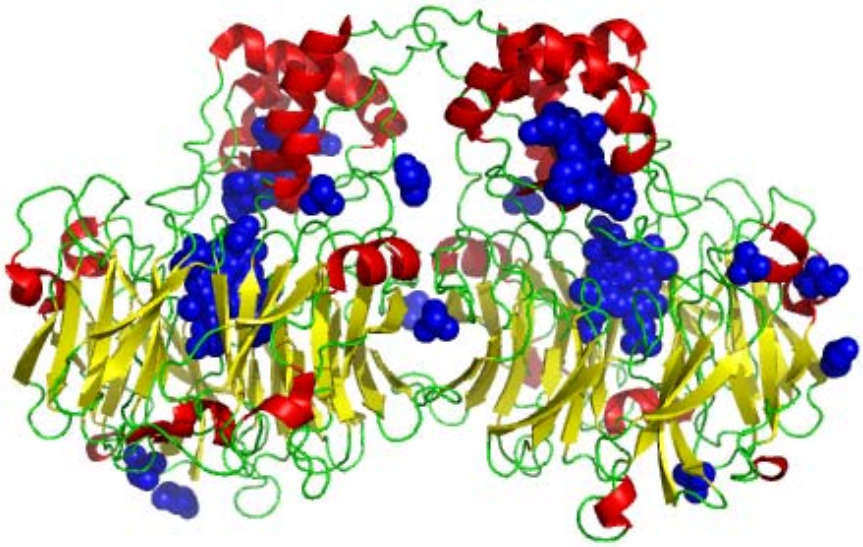

Figure 1.26: The structure of cytochrome cd1 nitrite reductase from Paracoccus denitrificans (1QKS). *The α-helices are shown in red, β-sheet in yellow, loops in green, and electron transfer cofactors (hemes and iron-sulfur centers) in blue. This Figure was generated using PyMOL (DeLano Scientific; http://pymol. sourceforge.net/).*

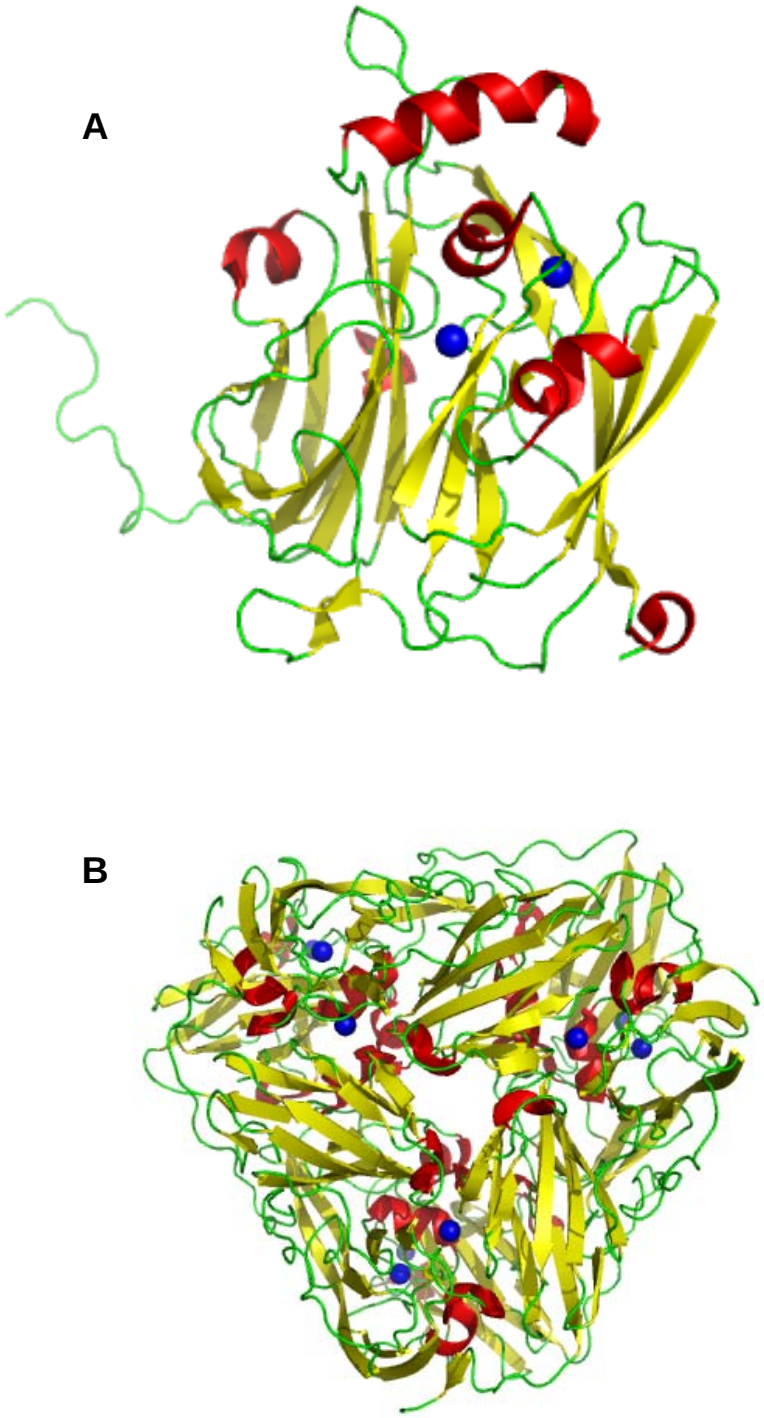

Figure 1.27: The structure of the copper-containing nitrite reductase (CuNir) from Hyphomicrobium denitrificans (2DV6). *Panel A reveals the monomer structure and panel B is the structure of the homotetriameric CuNir. The α-helices are shown in red, β-sheet in yellow, loops in green, and electron transfer cofactor (copper) in blue. This Figure was generated using PyMOL (DeLano Scientific; http://pymol. sourceforge.net/).*

Copper-containing Nitrite Reductase (CuNir) [119-121]**:** The copper-containing nitrite reductase (CuNir) is a homotrimeric enzyme which binds 6 copper centres in total [119]. Again, it is located in the periplasm and catalyzes the reduction of nitrite to nitric oxide. Its structure was solved as shown in (Figure 1.27) [119].

1.4.2.4 The Nitric Oxide Reductase (Nor) [122-125]

Bacterial nitric oxide reductase is a membrane-bound enzyme that catalyses the conversion of nitric oxide to nitrous oxide ($2NO + 2H^+ + 2e^- \rightarrow N_2O + H_2O$) in the periplasm. The cytochrome bc complex isolated from membranes of the model denitrifying soil bacterium *Paracoccus denitrificans* is the best-characterized example of the bacterial respiratory nitric oxide reductases [126]. This enzyme is composed of two subunits, NorC (a monoheme cytochrome *c* of 17kDa molecular weight) and NorB (a 53 kDa subunit containing two *b*-type cytochromes and a non-heme iron). The active site of the enzyme is a dinuclear centre which consists of one of the *b*-type hemes and the non-heme iron. Until now, the structure of the bacterial nitric oxide reductase is still unclear.

The *Pseudomonas stutzeri* cytochrome cbb_3 is an isoenzyme in the family of cytochrome *c* oxidases which sharing structural features with bacterial nitric oxide reductases. This protein slso displays a nitric oxide reductase activity (V_{max} = 100 ± 9 mol NO·mol cbb_3^{-1} ·min^{-1} and K_m = 12 ± 2.5 μM) [127]. Although this NO reductase activity is considerably lower than that typical of NOR, it is much higher than that of the ba_3-type oxidase from *Thermus thermophilus*.

In addition to bacteria, fungi also possess some denitrification ability. The end product of this process is nitrous oxide. Although no structure of bacterial Nor has been solved, a crystal structure has been obtained for the nitric oxide reductase from *Fusarium oxysporum* [122]. However, fungal NOR is a water soluble cytochrome

P450 which is completely different to the bacterial enzyme.

1.4.2.4 The Nitric Oxide Reductase (Nor) [122-125]

Bacterial nitric oxide reductase is a membrane-bound enzyme that catalyses the conversion of nitric oxide to nitrous oxide ($2NO + 2H^+ + 2e^- \rightarrow N_2O + H_2O$) in the periplasm. The cytochrome bc complex isolated from membranes of the model denitrifying soil bacterium *Paracoccus denitrificans* is the best-characterized example of the bacterial respiratory nitric oxide reductases [126]. This enzyme is composed of two subunits, NorC (a monoheme cytochrome *c* of 17kDa molecular weight) and NorB (a 53 kDa subunit containing two *b*-type hemes and a non-heme iron). The active site of the enzyme is a dinuclear centre which consists of one of the *b*-type hemes and the non-heme iron. Until now, the structure of the bacterial nitric oxide reductase is still unclear.

The *Pseudomonas stutzeri* cytochrome cbb_3 is an isoenzyme in the family of cytochrome *c* oxidases which share structural features with bacterial nitric oxide reductases. This protein also displays nitric oxide reductase activity (V_{max} = 100 ± 9 mol NO·mol cbb_3^{-1} ·min^{-1} and K_m = 12 ± 2.5 μM) [127]. Although this NO reductase activity is considerably lower than that typical of NOR, it is much higher than that of the ba_3-type oxidase from *Thermus thermophilus*.

In addition to bacteria, fungi also possess some denitrification ability. The end product of this process is nitrous oxide. Although no structure of bacterial Nor has been solved, a crystal structure has been obtained for the nitric oxide reductase from *Fusarium oxysporum* [122]. However, fungal NOR is a soluble cytochrome P450 which is completely different to the bacterial enzyme.

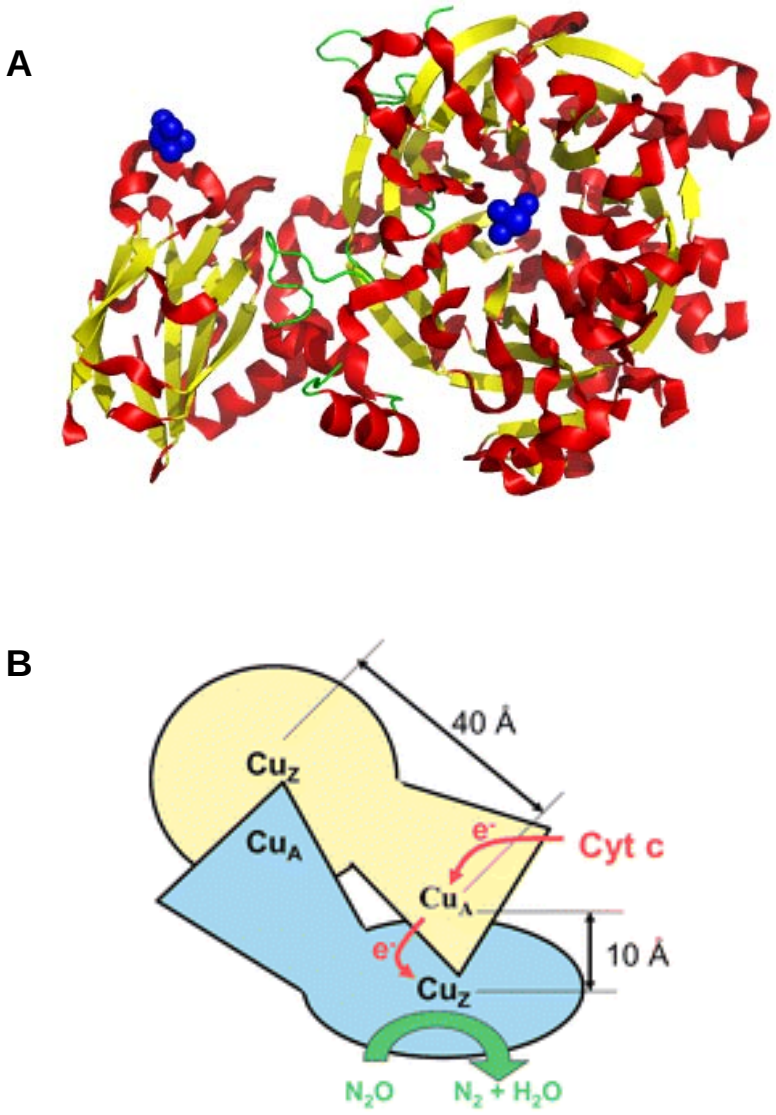

Figure 1.28: Structure of nitrous oxide reductase and its copper clusters. *(A) Structure of one subunit of the homodimeric N_2OR from Paracoccus denitrificans (1FWX)* [129]*. This Figure was generated using PyMOL (DeLano Scientific; http://pymol. sourceforge.net/). (B) The subunit structure of N_2OR showing the head-to-tail arrangement that brings the electron storage centre Cu_A to within ca. 10 Å of the catalytic cluster Cu_Z in the other subunit. Panel A reveals the monomer structure and panel B is the structure of the homotetrameric CuNir. The α-helices are shown in red, β-sheet in yellow, loops in green, and electron transfer cofactors (copper ion) in blue.*

1.5 Nitric oxide detoxification

Previous studies revealed that SHP and DHC are up-regulated while using nitrate as an electron acceptor, however there is no evidence to prove that this up-regulation is directly induced by nitrate or by other nitrogenous species. Therefore, this up-regulation could be induced by any nitrosative stress generated during nitrate metabolism, including nitric oxide.

Compared with other nitrosative stress species, nitric oxide is particularly important due to its unique properties. Nitric oxide is a water-soluble diatomic molecule which is able to react with a variety of cellular targets, especially thiol groups and transition metal centres in proteins. For this reason, a nitric oxide detoxification system is important for bacterial survival in the environment. In mammals, nitric oxide is involved in the innate immune response to infection, including direct bacterial killing and up- or down-regulation of genes involved in innate immunity and inflammatory responses to microbes [130]. Thus, bacteria need some enzyme to deplete nitric oxide levels, and SHP and DHC may be involved in nitric oxide detoxification.

There are two types of enzyme that can be used to deplete nitric oxide, NO reductase and nitric oxide dioxygenase. NO reductase is described in section 1.4.2.4, while the following section introduces the most widely-studied nitric oxide dioxygenase, flavohemoglobin (HMP).

1.5.1 Nitric oxide dioxygenase (Nod)

In addition to uptake from the environment, NO is also generated endogenously in microbes. This happens in bacteria which are able to use nitrite as an electron acceptor for anaerobic respiration. For example, *E. coli* reduces nitrite to ammonia under anaerobic growth conditions, but traces of NO are apparently formed as a by-product of this metabolism [93]. For this reason, various microbes appear to have evolved strategies for NO detoxification, including using nitric oxide dioxygenase.

Unlike the other enzymes involve in denitrification, which are all reductases, Nod is a dioxygenase. It is indirectly involved in denitrification by catalyzing conversion of nitric oxide to nitrate. (Figure 1.22).

Flavohemoglobin (HMP) is the most studied nitric oxide dioxygenase. It rapidly catalyzes the reaction of heme-bound O_2 with NO to form nitrate (HMP-Fe(II)-O_2 + NO → HMP-Fe(III) + NO_3^-) [131, 132]. However, it has been alternatively suggested that HMP activity is inhibited by NO at low O_2 concentrations because the nitrosyl form of HMP is relatively inactive (k_{off}/k_{on} for NO (0.008 nM) $\ll$ k_{off}/k_{on} for O_2 (0.012 μM)) [7]. Other anaerobic studies reveal that HMP slowly reduces NO to NO^-, which is followed by the formation of N_2O [132]. Therefore, HMP is proposed to protect organisms from NO-mediated damage under aerobic conditions.

The overall fold of HMP (Figure 1.29) is composed of three different domains, namely the C-terminal NADH-binding, the FAD-binding and the N-terminal globin domains. In HMP, electrons are transported from NADH to FAD, and subsequently to the heme iron in the globin domain.

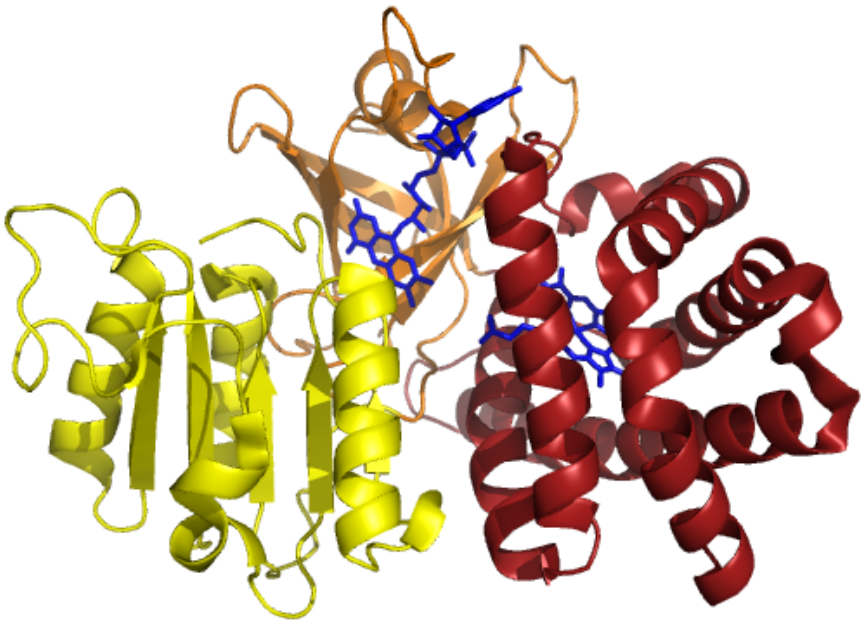

Figure 1.29: Flavohemoglobin from Alcaligenes eutrophus (1CQX). *The figure shows the overall three-dimensional structure of flavohemoglobin (Hmp). In red is the N-terminal globin; orange is the FAD-binding domain; yellow is the C-terminal NADH-binding domain; electron transfer cofactors (heme and FAD) in blue. This Figure was generated using PyMOL (DeLano Scientific; http://pymol. sourceforge.net/).*

1.6 Aims of this thesis

The aims of this thesis are to answer some of the questions surrounding SHP. Firstly, although the crystal structures of SHP and its electron-transfer partner, DHC, have been solved, the structure of SHP/DHC complex is still unknown. Therefore, chapter 3 details the characterization of the interaction of SHP and DHC, which has helped to characterize the SHP/DHC complex and was used to optimize the conditions for growth of co-crystals. Secondly, previous studies have established that ferrous SHP has O_2 and NO binding ability. However the function of SHP is still unclear. Chapter 4 and 5 describe the *in vitro* functions of SHP under aerobic and anaerobic conditions by spectroscopic, thermodynamic and kinetic techniques. Thirdly, chapter 6 discusses

phenotypic studies with an SHP knockout strain of *Shewanella*, which were used to confirm the *in vitro* functions and to elucidate the physiological role of SHP *in vivo*. Lastly, SHP utilizes a unique heme ligand, asparagine. For this reason it may be assumed that the asparagine plays a special role. Thus chapter 7 attempts to address the role of this special sixth heme residue through the employment of biochemical studies.

Chapter II

MATERIALS AND METHODS

2 MATERIALS AND METHODS

2.1 Strains and Plasmids

All SHP and DHC constructs were created by Dr. Katrien Backers, Laboratory of Protein Biochemistry and Protein Engineering, Department of Biochemistry, Physiology and Microbiology, Gent, Belgium. All SHP mutant constructs were created by Dr. Caroline S. Miles, Institute of Structural and Molecular Biology, University of Edinburgh, UK. Strains and plasmids used are listed in table 2.1 and table 2.2.

Table 2.1 Bacterial plasmids and strains

Original species	Expression gene	mutation	vector	Co-vector	Host strain
Rhodobacter sphaeroides	SHP	Wild type N88A N88H N88D N88M N88K C89A C97A	pMC519 (Car^r, Ch^r)	PEC86 (Kan^r)	MC1061 & BL21 (DE3)
Rhodobacter sphaeroides	DHC	Wild type	PLPPsOmpAc551.5 (Car^r)	PEC86 (Ch^r)	MC1061 & BL21 (DE3)

(Car^r): Carbenicillin resistant; (Ch^r): Chloramphenicol resistant; (Kan^r): Kanamycin resistant

MC1061 genotype: (*hsdR, mcrB, araD*139, Δ (*araABC-leu*) 7679, Δ*lacX*74, *galU, galK, rpsL, thi*); BL21 genotype: (F^-, *ompT*, $hsdS_B$ ($r_B^- m_B^-$) , gal (λ *c I* 857, *ind*1, *Sam*7, *nin*5, *lac*UV5-T7*gene*1) , *dcm* (DE3)); JM109 genotype: (*recA*1, *endA*1, *gyrA*96, *thi, hsdR*17, *supE*44, *relA*1, Δ *(lac-proAB*) /F' [*traD*36, $proAB^+$, *lac* I^q, *lacZ*ΔM15])

Table 2.2 Shewanella knockout strain

strain	Genotype	reference
Shewanella oneidensis MR-1 (WT)	Wild type	Gift from Prf. G. Reid, Mutant was created by Dr. L. Cooper
Shewanella oneidensis MR-1 (Δ1)	shp knockout	
Shewanella oneidensis MR-1 (Δ3)	Shp, dhc and cyt b knock out	

All strain used here is Rifampicin resistant

2.2 Culture Media and Buffers

2.2.1 Antibiotics

Table 2.3 Antibiotics used in this study

Antibotic	**Stock solution**	**Working concentration in bacterial media**
Carbenicillin	25 mg/ml (in dH_2O)	25 μg/ml
Chloramphenicol	25 mg/ml (in EtOH)	25 μg/ml
Kanamycin	25 mg/ml (in dH_2O)	25 μg/ml
Rifampicin	10 mg/ml (in MeOH)	10 μg/ml

2.2.2 Buffers

Table 2.4 Buffers used for protein purification.

	Components	Usage
Buffer A	10 mM Tris-HCl 1 mM EDTA pH 7.2	used in ion exchange purification of SHP
Buffer B	10 mM Tris-HCl 1 mM EDTA pH 7.8	used in ion exchange purification of DHC
Buffer C	20 mM Tris-HCl 300 mM KCl 1mM EDTA pH 7.0	used in gel filtration
Buffer D	10 mM HEPES pH 7.2	for protein storage
Sample buffer	4 ml glycerol (5.04 g) 0.8 g SDS 2.5 ml 1M Tris-HCl 80 µl bromophenol blue slurry (5 mg/ml in water; vortex well before using.) H2O to 8 ml Addβ-mercaptoethanol to 20% (for example 0.2 ml bME to 0.8 ml 4X SB) before using.	For preparing SDS page sample

All buffers were prepared using dH_2O, and the pH was adjusted with 8 M NaOH and 8 M HCl.

2.2.3 Culture media and agar plates

Table 2.5 Culture media

Luria-Bertani Broth (1L)	
Bacto-tryptone	10 g
Yeast extract	5 g
NaCl	5 g
SOC medium (1L)	
Bacto-tryptone	25 g
Bacto-yeast extract	5 g
NaCl	0.5 g
1M KCl	2.5 ml
ddH2O to	1 L
	pH 7.0
Shewanella MR-1 minimal medium (1L)	
$(NH_4)_2SO_4$	0.225 g
K_2HPO_4	0.225 g
KH_2PO_4	0.225g
$NaHCO_3$	1.9 g
g of $MgSO_4 \cdot 7H_2O$	0.117g
$CaCl_2 \cdot 2H_2O$	0.1g
20× Trace elements	50 ml
1000× Amino acids	1 ml
Electron donors	15 ml
Electron acceptors	20 ml
	pH 7.2
20× Trace element solution (1L)	
Na_2 EDTA	500 mg
H_3BO_3	70 mg
NaCl	11.7 mg
$FeSP_4.H_2O$	30 mg
$CoCl.6H_2O$	25 mg
$NaMoO_4$	25 mg
$SeS_2(S_2O_2)$	20 mg
$ZnSo_4.7H_2O$	5 mg
$CuSO_4.5H_2O$	10 mg
$MnSo_4.4H_2O$	1 mg
	pH 7.4

Amino acid solution (1L)	
Arginine	20 g
Glutamate	20 g
Serine	20 g
Electron donors and acceptors	
Succinate (donor)	1 M
$NaNO_3$ (acceptor)	100 mM
LB plates (1L)	
Bacto-tryptone	10 g
Yeast extract	5 g
NaCl	5 g
Agar	14 g
	pH 7.2

2.3 Growth and maintenance of bacterial strains for protein expression

2.3.1 Cell transformation

30 µl of PEC86 plismid contained competent cells BL21 *E. coli* were gently defrosted on ice before 5 to 10 ng of expression plasmids DNA in a volume of 1 to 5 µl were added and mixed. The mixture was incubated for 20 minutes on ice and then heat shocked at 42°C for exactly 45 seconds in a water bath before being quickly placed on ice again for 2 minutes. Pre-warmed SOC medium (see table 2.1) (250 µl) was added before transferring the vial to 37°C for 1 hour in a shaker at 225 rpm. Subsequently, different aliquots (10 to 100 µl) of the transformation mix were plated onto two LB plates containing the appropriate antibiotic concentration. A flame-sterilised loop was dragged across the surface of the culture and used to streak out the agar plate. The plates were incubated overnight at 37 °C in order to promote the growth of bacterial colonies.

2.3.2 DMSO stocks

Small stocks for future use were prepared by adding 77 µl DMSO to 1 ml of Bacteria growthed in LB form single colony (7% DMSO by volume). DMSO stocks were then stored at – 80 ^{o}C until required and kept on ice while in use. The DMSO stocks were replaced periodically using colonies from freshly prepared LB agar plates.

2.3.3 Growth of bacterial cultures

Liquid cultures of bacteria were grown in the appropriate broth by inoculating with a single colony using a sterile inoculating loop. Cultures of the bacterial strains were grown at the appropriate temperature.

2.4 Protein purification

2.4.1 SHP purification

Cell lysis

The frozen cell pellet was re-suspended in ice cold buffer **A** (10 mM Tris, 1 mM EDTA, pH 7.2) allowing approximately 50 ml buffer for 25 g of wet cell pellet. PMSF (final concentration 200 µM) was added to this to prevent proteolysis, and cell membranes were lysed by sonication. In order to prevent overheating, the beakers containing the cell suspension were kept on ice and cooled for 30 seconds between each burst of sonication. Total cell lysate was centrifuged at 20000 rpm for 1 hour. The supernatant containing SHP protein was pooled and kept on ice prior to purification.

DE-52 weak anion exchange column

The supernatant was smoothly loaded to the top of a pre-equilibrated DE-52 column. The column was washed with 2 column volumes of buffer **A**. The semi-purified SHP was eluted by a linear gradient of 0-300mM KCl in buffer A over 5 column volumes. Typically, SHP was eluted at 100 mM KCl. The collected sample was then dialysed against 100 sample volumes of buffer **A** at 4 ˚C overnight.

Q-sepharose strong anion exchange column

The dialysed protein sample was loaded onto the top of a Q-sepharose column, which was also pre-equilibrated with buffer **A**. The column was washed with 2 column volumes of buffer **A**. a linear gradient of 0-300mM KCl in buffer A over 5 column volumes. was used to separate the contaminating proteins. SHP was eluted at around 120 mM KCl. The collected fractions were then concentrated to 1 ml by centrifugation (Amicon Centripep, 10 kDa cut-off) at 2500 rpm.

Superdex G75 gel filtration column (FPLC)

A size extraction column (Superdex G75, 10/300 GL) connected to an ÄKTA-purifier™ system (Amersham Biosciences), was equilibrated using buffer **C** (20 mM Tris-HCl, 300 mM KCl, pH 7.2). A 1 ml sample was auto-injected to the column. The SHP was eluted at around 12 ml.

2.4.2 DHC purification

Cell lysis

The frozen cell pellet was re-suspended in ice cold buffer **B** (10 mM Tris, 1 mM EDTA, pH 7.8) and lysed as described in section 2.4.1.

DE-52 weak anion exchange column

The supernatant was loaded onto the top of a DE-52 column pre-equilibrated with buffer **B**. The column was washed with 2 column volumes of buffer **B**. The semi-purified DHC was eluted by a linear gradient of 0-500mM KCl in buffer B over 5 column volumes. Typically, DHC was eluted at 250 mM KCl. The collected sample was then dialysed against 100 sample volumes of buffer **B** at 4 ℃ overnight.

Q-sepharose strong anion exchange column

The dialysed protein sample was loaded onto the top of a Q-sepharose column which was also pre-equilibrated with buffer **B**. The column was washed with 2 column

volumes of buffer **B**. A linear gradient of 0-300mM KCl in buffer B over 5 column volumes was used to separate the contaminating proteins. DHC was eluted at around 200 mM KCl. The collected fractions were then concentrated to 1 ml by centrifuge (AmicoCentripep, 10 kDa cut-off) at 2500 rpm.

Superdex G75 gel filtration column (FPLC)

A size extraction column (Superdex G75, 10/300 GL), connected to an ÄKTA-purifier™ system (Amersham Biosciences), was equilibrated using buffer **C** (20 mM Tris-HCl, 300 mM KCl, pH 7.2). A 1 ml sample was auto-injected onto the column. DHC was eluted at around 11 ml.

2.5 Gel electrophoresis

2.5.1 NuPAGE

SDS-PAGE was performed using NuPAGE® Novex 4-12 % Bis-Tris pre-cast polyacrylamide gels in combination with SeeBlue Plus 2® molecular weight markers. Assessment of the purity and integrity of the proteins was carried out through gel electrophoresis at various stages of the expression/purification. The protein samples were diluted using buffer as described in table 2.2 and boiled for 3 minutes to denature the protein and allow SDS binding. SDS binds with a constant ratio to the proteins as a function of their mass (1.4 g SDS: 1g protein) and shields their charges, the different distance to which each protein migrates depending only on its mass.

The central reservoir was filled with running buffer ensuring that the buffer level was beyond the sample loading wells. Aliquots of each sample (ranging from 5 to 15 µl) were loaded into the wells, reserving one well for SeeBlue Plus 2® molecular weight markers (5 µl). A potential difference (150 V, 120 mA and 60 W) was applied to the gel for the time necessary for the dye front to reach the bottom of the gel (approximately 1 hour). The voltage was then removed and the polyacrylamide gel was stained in Coomassie blue (Table 2.2) for approximately 15 minutes and

destained for at least 1 hour to remove excess of stain. Coomassie blue binds to the protein, forming a band, and the comparison between the positions of the blots with the markers give an indication about the presence of proteins and their size.

2.5.2 Coomassie stain

The gel was stained for 20 minitues with 0.1% Coomassie blue (R-250) in fixative (40 % methanol, 10 % acetic acid, 50 % H_2O). The gel was then destained with destain buffer (40 % methanol, 10 % acetic acid, 50 % H_2O).

2.5.3 Heme stain

Heme staining is a method of detecting all *c*-type cytochromes present in a protein sample (Goodhew, 1984). The gel was equilibrated in the buffer containing 30 % methanol and 250 mM NaOAc (pH 5.2) for 5 minutes, and then it was transferred to TMBZ buffer (400 μg/ml 3,3-5,5-tetranethylbenzidine, 30 % methanol and 250 mM NaOAc, pH 5.2) and incubated in the dark for 15 minutes. 100 μl H_2O_2 was added to develop heme bands.

2.5.4 Concentration and storage

Pure and concentrated protein was divided into aliquots, flash frozen in liquid nitrogen and stored at -80^{o}C until required.

2.5.5 Purity determination

The purity of the protein was measured at several stages by both analysis of UV/vis peak ratios and by SDS-PAGE (Sodium Dodecyl Sulfate-Poly Acrylamide Gel Electrophoresis).

2.5.6 Heme Content

Clearly, the mutant constructs used in these experiments are all centred around the heme group at the active site of the enzyme. This creates sufficient concern as to the integrity of the heme itself. The failure to incorporate heme could result in altered activities and as such, heme content must be assessed via the pyridine hemeochrome

assay.

Table 2.6: Heme Content

Buffer D	20 mM Tris, 100 mM KCl, pH 7.5
Reagent A	0.2 ml % M NaOH, 2.5 ml pyridine, 2.3 ml H_2O
Prepared using MilliQ ultrapure water (of resistivity 18 Ω cm^{-1}) and pH adjusted using HCl	

Each enzyme sample (~5 µM) in assay buffer D (20 mM Tris, 100 mM KCl pH 7.5) was diluted with an equal volume of the pyridine hemeochrome reagent A (Table 2.5). The resulting solution was mixed thoroughly and reduced through the addition of the minimum amount of sodium dithionite (10 µl of 5 mg/ml^{-1} $Na_2S_2O_4$). A spectrum of the reduced pyridine-bound structure was recorded and heme concentrations were calculated using $\Delta\xi_{556\text{-}540}$ = 22100 $M^{-1}cm^{-1}$. Comparison of the SHP concentration calculated from the ferric and ferrous species with the heme concentration calculated from the pyridine hemeochrome assay [133, 134] gives an indication of heme incorporation.

2.6 Protein-protein binding

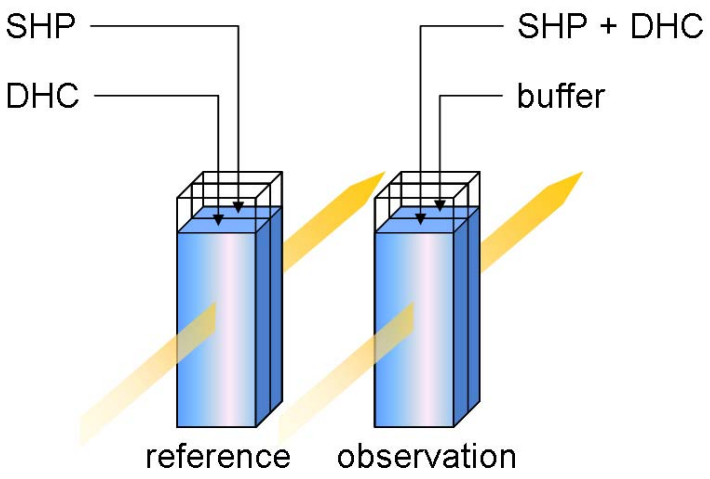

Figure 2.1: Double cuvettes installation used for dissociation constant detection.

Two double compartment cuvettes (2 × 1.5 ml capacity) and a double beam UV/Vis spectrophotometer (Shimadzu 2101) were used to measure the K_d of SHP and DHC binding. In the reference cell, DHC solution (5 ~ 10 μM) was added into one compartment, and to the other compartment, filled with buffer, was added small aliquots of SHP (~1 μM). This resulted in a spectroscopic change, but no physical change. In the observation cell, buffer was added into one compartment. In the other compartment small aliquots of SHP (~1 μM) were added to DHC solution (5 ~ 10 μM). This resulted in a physical change as well as a spectroscopic change. Thus, the difference in absorption could be plotted against SHP concentration and fitted by equation to determine the dissociation constant. The experimental setup is shown in Figure 2.1

2.7 OTTLE Potentiometric Titrations

All OTTLE (**O**ptically **T**ransparent **T**hin **L**ayer **E**lectrode) potentiometric titrations were carried out at 25 ^{o}C using a Cary UV/vis spectrophotometer and an Autolab PGSTAT10 potentiostat. A list of buffers and mediators are shown in tables 2.6 and 2.7.

All samples for OTTLE titration were prepared in a Belle Technology glove box under a nitrogen atmosphere, with O_2 levels maintained at < 5 ppm. All buffers were degassed prior to use by bubbling with nitrogen gas for >1 hour. Enzyme samples were introduced to the box and allowed to degas under the nitrogen atmosphere for at least 1 hour prior to use. The protein was mixed with apropos mediators (Table 2.5), depending on the expected midpoint potential, in high salt buffer (500 mM NaCl, 0.1 M Tris, pH 7.5, 10 % glycerol). The mixed sample was introduced into a quartz UV/Vis cell and covered with the overlay buffer (500 mM NaCl, 0.1 M Tris, pH 7.5). After adding the three electrodes, the holes were plugged. All steps were in anaerobic conditions.

A specially constructed cell comprised (Figure 2.2) of a modified quartz UV/Vis cell with a path length of 0.3 mm, Pt/Rh (95/5) gauze working electrode (wire diameter 0.06 mm, mesh size 1024 cm^{-1}, Engelhardt, UK), platinum wire counter electrode and a Ag/AgCl reference electrode (model MF2052, Bioanalytical Systems, IN 47906, USA) was used. Enzyme samples were injected into the lower part of the cell using a Hamilton 0.1 mm leur lock syringe. The remainder of the cell was filled with OTTLE upper buffer. Special care was taken to ensure that the interface between the enzyme sample (10 % glycerol) and non glycerol buffer did not undergo any mixing. The lower part on the cell was placed into a carry 50 Probe spectrophotometer so that changes in the spectra could be observed. The potential was applied using a Autolab PGSTAT potentiostat via a Pt/Rh (95/5) (wire diameter 0.06 mm, mesh size 1024 cm^{-1}, Engelhardt, UK) gauze working electrode, platinum wire counter electrode and Ag/AgCl reference electrode (model MF2052, Bioanalytical Systems, IN 47906, USA). The enzyme samples were allowed to equilibrate before the potential was

changed and spectra were recorded at each applied potential. Oxidation was achieved by raising the potential in 50 mV steps, offset by 25 mV relative to the reductive trace. Difference spectra were calculated and the maximum absorbance changes associated with a change in the redox state were plotted against applied potential (vs SHE). E_m values were determined by fitting the data to the Nernst equation (Microcal Origin 7.0) (Figure 2.3).

The Ag/AgCl reference electrode employed in the OTTLE cell was calibrated against indigotrisulfonic acid (E_m = -99 mV vs SHE) and FMN (E_m = -220 mV vs SHE) in the same conditions. Applied potentials were corrected relative to the standard hydrogen electrode. All detected electrode potentials were corrected to comespond to the standard hydrogen electrode.

Table 2.7: OTTLE Titration Buffers

Up layer buffer	50 mM Tris, 500 mM KCl
Down layer buffer	50 mM Tris, 500 mM KCl, 10 % glycerol
Prepared using MilliQ ultrapure water (of resistivity 18 Ω cm^{-1}) and pH adjusted using HCl	

Mediators (Table 2.7) were introduced into the anaerobic box as powder samples and dissolved in degassed down layer buffer to a concentration of ~2 mM. An appropriate selection of mediators spanning the estimated midpoint potential for each titration were chosen and added to a concentration of ~2 μM.

Table 2.8: Mediators for Redox Potentiometry

Electrochemical mediator	E_0 (mV vs SHP)
Potassium ferricyanide	430
2,3,5,6-tetramethyl phenylenediamine (DAD)	260
1,2-napthoquinone (12NQ)	135
N-methyl-1-hydroxyphenazonium methosulfate (PYO)	80
N-ethyl phenazonium ethosulfate (PES)	55
5-hydroxy-1,4-napthoquinone (5H14NQ)	-3
2-hydroxy-1,4-napthoquinone (2H14NQ)	-50
Flavin mononucleotide (FMN)	-200
N, N'-dibenzyl-4,4-bipyridinium (BV)	-311
N, N'-dimethyl-4,4-bipyridinium (BV)	-430

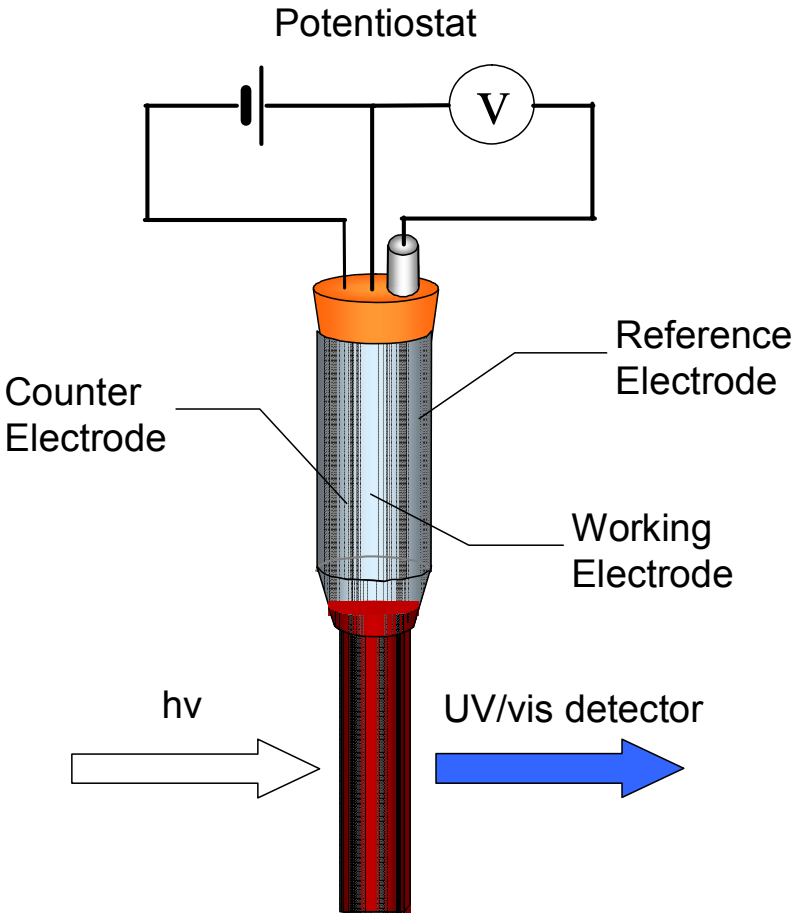

Figure 2.2: OTTLE system. *OTTLE cell showing a diagrammatic representation of the potentiostat and electrodes.*

A

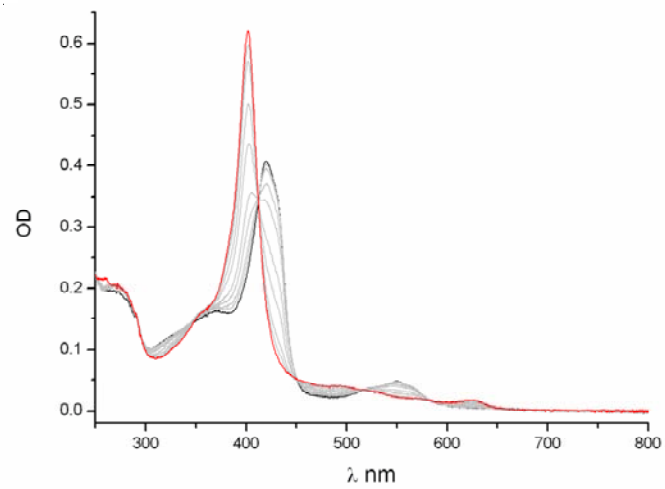

B

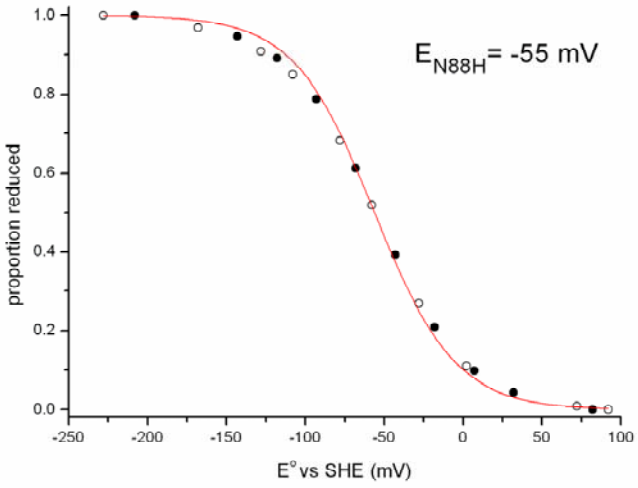

C

$$E = E_m - \frac{-RT}{nF} * \ln \frac{[red]}{[ox]}$$

Figure 2.3: OTTLE Potentiometric Titrations. *Panel **A** shows the changes in spectra observed during reduction and reoxidation of SHP (N88H). Panel **B** shows a plot of proportion reduced vs applied potential and the 1e- Nernst plot fit for this data. Panel **C** shows the Nernst equation.*

2.8 Protein crystallization

Crystals were growth by the hanging drop vapour diffusion method, using 24 well Linbro® plates (from Hampton Research). Initial crystallization screens were carried out using Hampton Crystal Screen™, Crystal Screen 2™ and a PEG/glycerol/pH Screen. Hanging drops of 4 µl were prepared by adding 2 µl of 200 µM protein (in 10 µM HEPES, pH 7.2) to 2ml of well solution. In such screens, a number of different conditions for crystallization were tested. When crystal nucleation was achieved, optimization of the condition was carried out varying protein concentration, pH, buffers and precipitant concentration.

2.8 Enzyme Kinetics

2.8.1 Anaerobic stopped-flow spectrophotometry

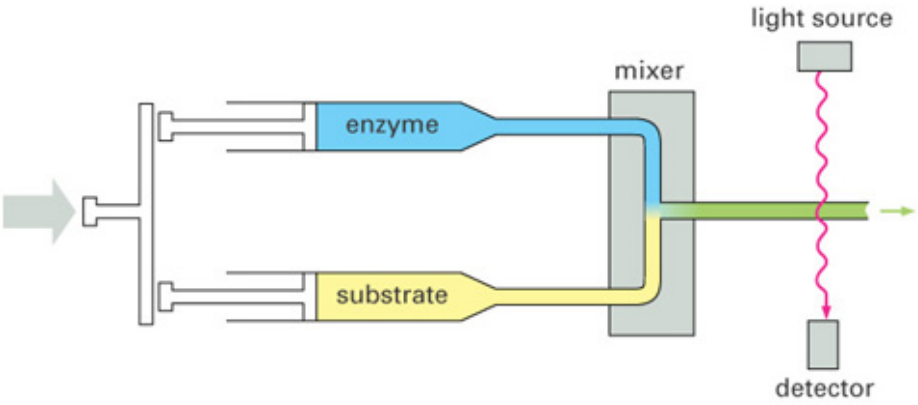

Figure 2.4: Stopped-flow spectrophotometry

A stopped flow instrument is a rapid mixing device used to study the chemical kinetics of a reaction in solution (Figure 2.4). The usual dead time of a stopped flow apparatus is 1-2 milliseconds. Pre-steady-state kinetic measurements shown in this thesis were all carried out at 10°C using an Applied-Photophysics stopped-flow spectrophotometer (SX.17MV) in conjunction with either a single wavelength or diode-array detector. The stopped flow apparatus was housed within an anaerobic

glovebox (Belle Technology; [O_2] < 10 ppm).

2.8.2 Preparation of NO saturated buffer of known concentration

20 ml buffer was prepared in sealed containers followed by bubbling N_2 (O_2 free) gas for 15 minutes. Then this buffer was bubbled with NO gas for 1 minute. Aliquots of NO-saturated buffer were removed via a rubber septum and syringe to ensure the [NO] remained relatively constant. NO concentration was determined by the Griess method [135]. Firstly, 1µl NO saturated solution was injected into O_2 rich buffer to form a nitrite solution. Then sulfanilamide and NED (N-1-napthylethylenediamine dihydrochloride) solutions were mixed with the sample. Through the chemical reactions shown in Figure 2.5, an azo compound was produced and revealed a 520 nm absorption peak. By comparison with representative nitrite standard reference curves, the concentration of NO could be determined.

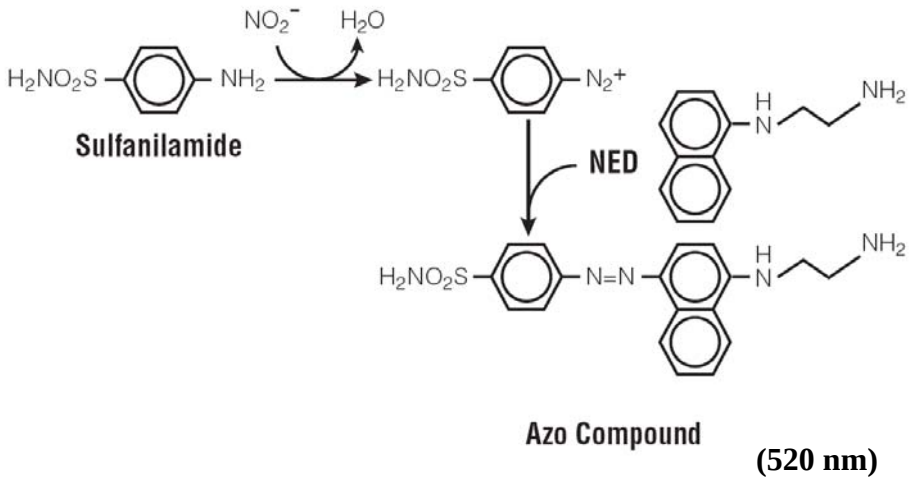

Figure 2.5: Griess Reaction. *The figure shows the chemical reactions involved in the measurement of NO_2^- using the Griess Reagent System.*

2.8.3 Preparation of O_2 saturation buffer of known concentration

O_2 saturated buffers were generated by bubbling sealed containers with O_2 gas for 10 minutes. Aliquots of O_2 saturated buffer were removed via a rubber septum and syringe to ensure the [O_2] remained relatively constant. The concentration of O_2 in

O_2-saturated buffers was detected by reaction with the colourless reduced methyl viologen (MV) to form the blue oxidized form. MV concentrations were calculated using a Cary 50 UV/vis spectrophotometer with a 1cm quartz cuvette contained within an anaerobic glove box. The appropriate concentration of methyl viologen was achieved by dilution of an electrochemically-reduced stock solution (3 M). Absolute concentrations were calculated using the extinction coefficient ε_{600}= 13000 $M^{-1}cm^{-1}$. Oxygen concentrations were assessed from the difference between the two spectra at 600 nm (using ε_{600} = 13000 $M^{-1}cm^{-1}$) assuming that 4 methyl viologen molecules are required to provide the 4 electrons necessary to reduce oxygen to water.

2.8.4 Oxygen and nitric oxide binding to SHP

Reduced SHP (excess dithionite removed via gel filtration on a G-25) was mixed with various concentrations of gaseous molecules (O_2 and NO) by the stopped-flow method. The reactions were monitored at 421 nm over various time scales. Under pseudo first order conditions the reaction progress traces for each concentration can be fitted to a single exponential function. From this k_{obs} (the observed rate constant) can be obtained. The different k_{obs} values are then plotted versus gas concentration. The gradient provides the second order bimolecular rate constant (k_{on}) for the reaction and the Y intercept the dissociation rate constant (k_{off}). k_{obs} is defined by this equation:

$$k_{obs} = k_{off} + k_{on} \times [c]$$

Therefore, if we perform association rate experiments at various concentrations of gaseous molecules (O_2 and NO); the results should look like the Figure 2.6 below.

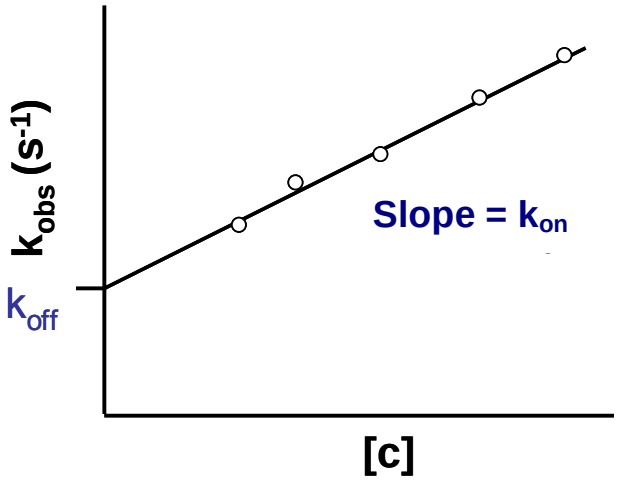

Figure 2.6: Observed rates against concentration of gaseous molecules. *The figure shows a plot of observed rates against concentration of gaseous molecules allowing the calculation of k_{on} and k_{off}.*

Furthermore, the ratio of k_{off} to k_{on} is the K_d for gas binding:

$$K_d = \frac{k_{off}}{k_{on}}$$

Finally, the values of k_{on}, k_{off} and K_d can be obtained.

2.8.5 Electron transfer from ferrous DHC to ferric SHP and mutants

10 μM reduced DHC (excess dithionite removed) was mixed with 1 μM ferric SHP and its mutants (N88A, D, H, M and K) by the stopped-flow spectrophotometer. The reaction was monitored at 431 nm.

2.8.6 Auto-oxidation of oxy-ferrous SHP complex

Rate constants for the decay of the oxy-ferrous complex to the ferric form were evaluated using the stopped-flow apparatus. Pre-reduced SHP (excess dithionite removed via gel filtration on a G-25) was mixed with oxygen saturated buffer ($[O_2]$ ~ 500 μM) and the formation and subsequent decay of the oxy-ferrous species were monitored over the range 250-800 nm using a diode-array detector. Typically the

formation of the oxy-ferrous species in such high oxygen concentrations was so rapid that it was completed within the dead time of the stopped-flow apparatus. Absorbance changes at 419 nm associated with oxy-ferrous decay were plotted against time and fitted to single exponential using Origin 7 software.

2.8.7 Nitric oxide dioxygenase activity assay

Pre-reduced SHP (excess dithionite removed via gel filtration on a G-25 size exclusion column) was mixed with oxygenated buffer (final $[O_2]$ = ~ 100 μM) to form an oxy-ferrous species at 10^{o}C. This was then mixed with 200 μM nitric oxide using the stopped-flow method. Absorbance changes at 407 nm associated with oxy-ferrous decay were plotted against time and fitted to single exponential using Origin 7 software.

Under anaerobic conditions, 500 μl pre-reduced SHP (excess dithionite removed via gel filtration on a G-25 size exclusion column, [SHP] = ~ 50 μM, in 100 mM sodium phosphate buffer pH 7.5) was mixed with oxygenated buffer (final $[O_2]$ = ~ 50 μM) to form an oxy-ferrous species at 10^{o}C. Nitric oxide was then added (to a concentration of 50 μM), and SHP was removed from the solution by filtration using a Vivaspin concentrator (5 kDa MWCO PES) (Figure 2.7). Following this the filtered, protein-free, solution was used as a spectral baseline. NADPH was then added and a spectrum obtained. The NADPH-dependent nitrate reductase (from Aspergillus species, *Sigma*. final conc. 5 U/l) was then added to this solution and incubated at 25 ^{o}C for 20 min. After incubation another spectrum was collected. NADPH has an absorption peak at 340 nm (ε_{340} = 6.22 $mM^{-1}cm^{-1}$). After addition of nitrate reductase the NADPH concentration is decreased substantially.

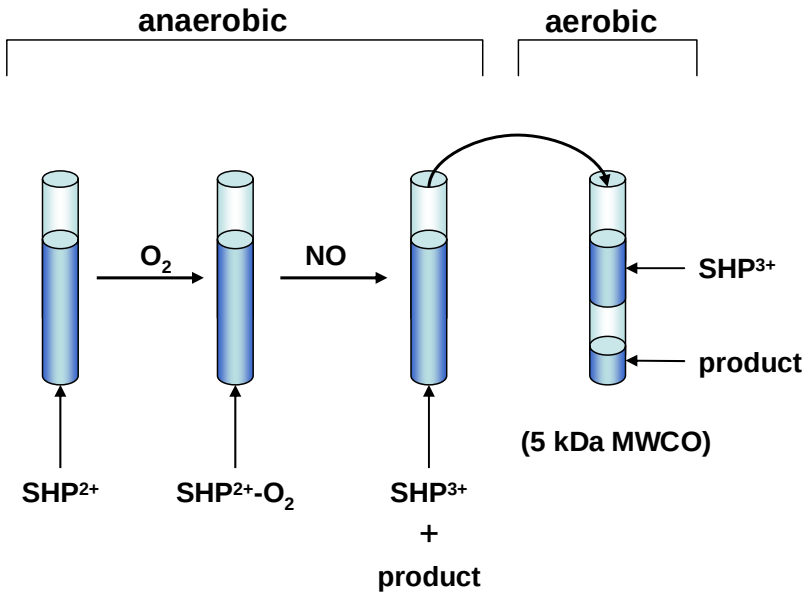

Figure 2.7: Preparation of the product sample for the nitric oxide dioxygenase assay.

2.8.8 Nitrite reductase activity assay

The test for nitrite reductase activity of SHP is carried out by steady-state kinetic experiments at 25°C. 1ml assay buffer (20 mM Tris, pH 7.0) was prepared with reduced MV (added to about OD_{520} = 1.0) and varying concentrations of nitrite ([nitrite] = 0 to 1000 μM). SHP (concentration is about 200 nM) was then added to the MV and nitrite mixed solution. The reaction was monitored using the decrease in absorbance at 520 nm corresponding to MV oxidation. The rate constant k_{cat} and Michaelis constant K_m were determined by fitting the data to the Michaelis-Menten equation (Microcal Origin 7.0) (Figure 2.8). The observed rate constants at saturating concentrations were determined in an analogous method to that described above. Initial rates of MV oxidation were measured in the presence of saturating concentrations of nitrite and converted to activity units.

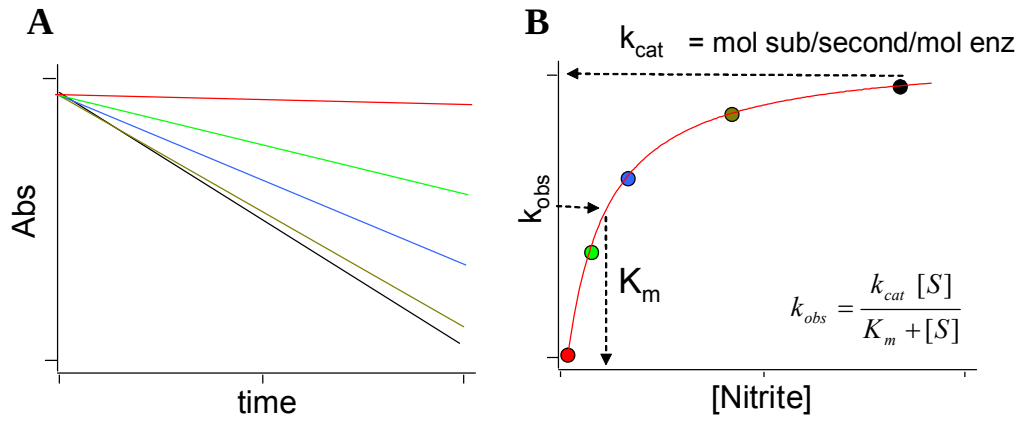

Figure 2.8: Steady-state kinetic analysis. *Panel A shows the decreasing absorbance at 520 nm associated with MV oxidation at different concentrations of nitrite. Panel B shows a standard Michaelis-Menten plot of observed rates against concentration of substrate allowing the calculation of the rate constant (k_{cat}) and Michaelis constant (K_m).*

2.9 Phenotype studies

2.9.1 Growth curves in LB liquid culture

20 ml starter liquid cultures of bacteria (*Shewanella* wild type and knockout strain) were grown in the LB broth (with 10 µg/ml Rifampicin) at 30 ^{o}C for 16 hours by inoculating with a single colony using a sterile inoculating loop. Then 50 µl of starter cultures was transferred to 0.95 ml fresh LB broth (added Rifampicin to 10 µg/ml). Cultures were than incubated at 30 ^{o}C, 100 rpm. OD_{600} values were recorded by the UV/vis spectrophotometer every 30 minutes. The appropriate volume of NO-saturated buffer (~ 1 mM NO in 100 mM Tris buffer, pH 7.0) was added during log phase growth; the same volume of the buffer (100 mM Tris buffer, pH 7.0) was added to control cultures.

2.9.2 The phenotypic assay on bacterial lawns

20 ml starter liquid cultures of bacteria (*Shewanella* wild type and knockout strain) were grown in the LB broth (added with 10 µg/ml Rifampicin) at 30 ^{o}C for 16 hours

by inoculating with a single colony using a sterile inoculating loop. Then 1 ml of starter cultures were transferred to 20 ml fresh LB broth (added Rifampicin to 10 μg/ml) and incubated at 30 ^{o}C and 100 rpm for 3 hours. Then 100 μl of the cultures were spread evenly on the LB agar plates and the agar dried. A sterile filter paper was then placed on the top of the gel following the addition of 7 μl of 200 mM sodium nitroprusside (SNP) (in 100 mM Tris buffer, pH 7.0). The preparation process is shown as Figure 2.9.

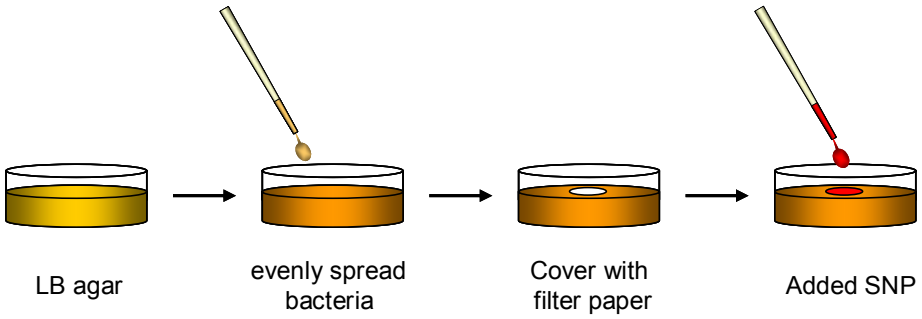

Figure 2.9: Bacterial lawns preparation. *The figure shows the method of the phenotypic assay on bacterial lawns.*

Chapter III

THE INTERACTION OF SHP AND DHC

3 The interaction of SHP and DHC

3.1 Introduction and Aims

As described in chapter 1, there are some biological hints revealing the relationship between SHP and DHC. Firstly, the genes encoding both proteins and that encoding the Cyt-*b* are all found in the same chromosome region in different species [1-3]. Secondly, in the case of *Shewanella oneidensis* MR-1, mRNA levels of SHP, DHC, and Cyt-*b* are up-regulated by nearly 10-fold when grown under anaerobic conditions using nitrate as the electron acceptor [4]. Thus it seems likely that SHP and DHC have some functional link in the cell, perhaps as redox partners.

The reduction potential of SHP has been found to be about -100 mV [1] while the redox potentials of the two hemes of DHC are -240 mV and -310 mV [1]. Thus, if SHP and DHC are electron transfer partners, the thermodynamically favorable direction of electron transfer is from DHC to SHP. Indeed, our previous studies have shown that electron transfer from reduced DHC to oxidized SHP proceeds very rapidly (k_{et} = 1.85 ± 0.11 × 10^7 $M^{-1}s^{-1}$), even at 500 mM KCl and at 10 °C [1].

For inter-protein electron transfer to occur the proteins must come into close contact. In this chapter the nature of the SHP/DHC interaction is investigated. Although the structures of SHP and DHC are known, there is as yet no structure of the SHP/DHC complex. Therefore, ionic strength and pH effects on SHP/DHC complex formation are investigated, with the ultimate aim of obtaining the SHP/DHC complex crystal structure.

3.2 Results

3.2.1 Purification of SHP and DHC

Wild-type SHP and DHC from *Rhodobacter sphaeroides* were purified from *E. coli* (MC1061 and BL21) as described in Chapter 2. The protein validity was confirmed by SDS PAGE and heme staining, and purity was confirmed by Coomassie blue staining and UV-visible spectroscopy. The final yield of purified SHP (wild-type) is about 0.3 mgl^{-1} of cell culture from MC1061, and 1 mgl^{-1} from BL21. The yield of purified DHC is only 0.1 mgl^{-1} from MC1061, but increased to 3 mgl^{-1} from BL21.

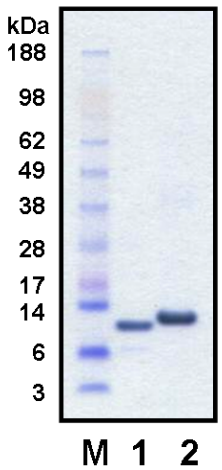

Figure 3.1: Coomassie blue stained gel of SHP and DHC. *(NuPAGE 4-12% Bis-Tris gels, Invitrogen). M is protein marker (See Blue Plus 2, Invitrogen), lane 1 is purified SHP (wild type), and lane 2 is purified DHC.*

On SDS PAGE the protein migrates slightly further than would be predicted from its molecular weight (12kDa). This is due to its α-helical nature, making it more compact than may be expected for a protein of its molecular weight. Thus, it can pass through the gel matrix easier than the standard marker proteins. The same situation is also found for DHC, which has a predominantly α-helical structure. Therefore, the protein band also runs 'lighter' than other proteins with the same molecular weight, 16 kDa.

During purification SHP forms an oxy-ferrous species in the cell-free extract, but this has a half life of less than 30 minutes at room temperature. Thus, in the purifying process, SHP will release O_2 molecule as superoxide (will be described in chapter 4) and be oxidized to the ferric form. The oxy-ferrous SHP is red while the colour of

concentrated ferric SHP is deep green.

In addition to *Rhodobacter sphaeroides* SHP, the *Shewanella oneidensis* MR-1 SHP was also sub-cloned into the *E. coli* over-expression system fused with a C-terminal his_6-tag. Unfortunately, although the protein is successfully over-produced, it is not folded correctly and heme is not incorporated.

3.2.2 SHP and DHC binding

3.2.2.1 The binding between SHP and DHC is specific

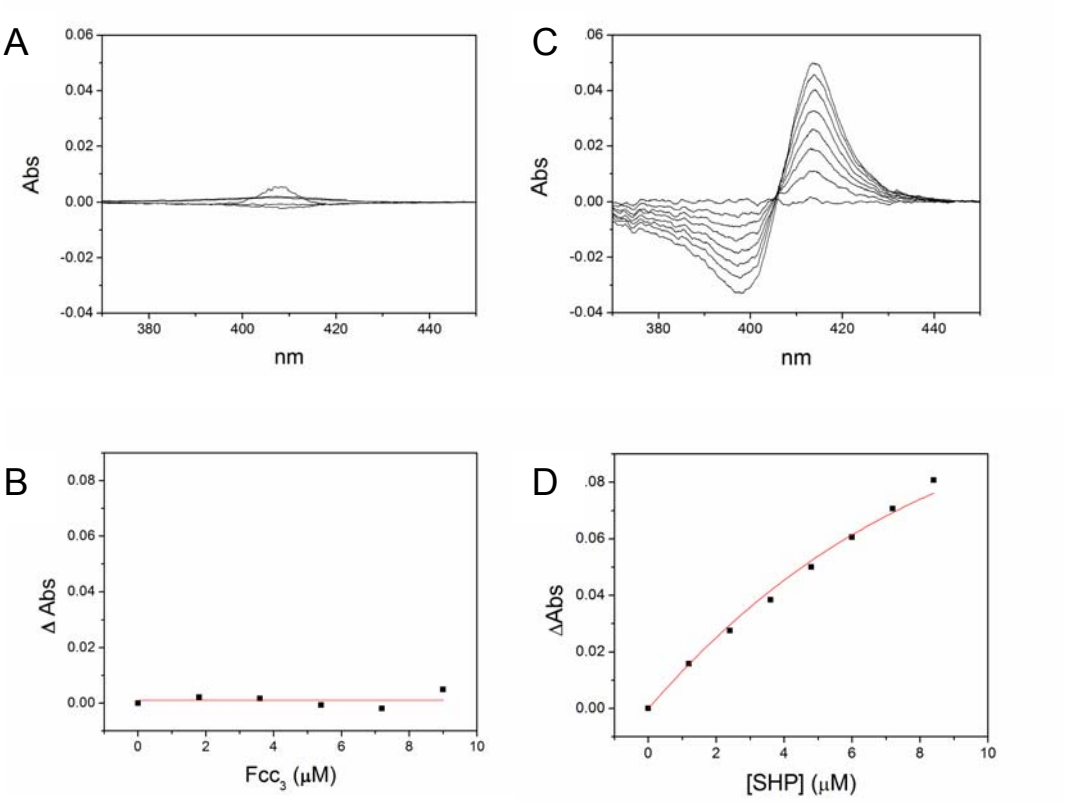

Figure 3.2: Spectral perturbations. *Panel A shows the spectral perturbations induced upon Fcc_3 binding to DHC (in 25 mM Tris-HCl, pH 8.0). Panel B shows the relationship between maximal absorbance changes (ΔOD_{407}) versus concentration of DHC. Panel C shows the spectral perturbations induced upon SHP binding to DHC (in 25 mM Tris-HCl, pH 8.0). Panel D shows the relationship between maximal absorbance changes ($\Delta OD_{413-396}$) versus concentration of DHC. The data is fitted to the equation 3.1, see appendix I, from which the dissociation constant (K_d) can be evaluated.*

A comparison of the genomes of various bacteria shows that SHP and DHC are always found on the same operon. Previous research also revealed that they function as electron transport proteins and these two cytochromes were proven to bind to each other *in vitro* conditions (the K_d value is approximately 230 nM, 10mM HEPES, pH 7.5, 25°C) [1].

The binding assay is described in chapter 2, and involves two double cuvettes and a double beam UV/Vis spectrophotometer. In this way a spectroscopic change is observed when SHP and DHC bind to each other. As a control, DHC was replaced with a non-physiological protein (F*cc*$_3$) [136] under the same conditions, and no spectroscopic change was observed (Figure 3.1). This indicates no binding between F*cc*$_3$ and DHC under the same ionic strength conditions.

3.2.2.2 Ionic strength effects on SHP and DHC binding

The affinity of SHP and DHC for one another is highly dependent on the salt concentration of the solution. UV/Vis spectrophotometry can be used to measure the affinity of SHP for DHC at different salt concentrations (Figure 3.3, table 3.1). From Figure 3.3 it is clear that the K_d value for the interaction of SHP and DHC increases with ionic strength.

I (mM)	K_d (μM)
6 mM	0.23
36 mM	1.20
66 mM	6.21
96 mM	9.32
126 mM	20.99
206 mM	-

Table 3.1: Dissociation constants for the SHP/DHC complex with varying ionic strength. *I is ionic strength (mM), and K_d is the dissociation constant (μM). The buffers used are 10 mM HEPES, pH 7.5, and different KCl concentrations (0 mM, 30 mM, 60 mM, 90 mM, 120 mM).*

In low salt conditions (10mM HEPES, pH 7.5, 25°C) the K_d value is approximately 230 nM, indicating very tight binding. However, in high salt conditions (10mM HEPES, 120 mM KCl, pH 7.5, 25°C) the K_d is greater than 20 μM. Furthermore, if the salt concentration is higher than 200 mM (10mM HEPES, 200mM KCl, pH 7.5, 25°C) then no binding of SHP to DHC can be detected.

$$A = \varepsilon \times l \times C$$

$$A = \varepsilon_{\Delta 413-396} \times \frac{1}{2} \times \frac{(E_o + S_o + K_d) - \sqrt{(E_o + S_o + K_d)^2 - 4E_oS_o}}{2} \qquad \textit{Equation 3.1}$$

$$\therefore \varepsilon_{\Delta 413-396} = \frac{0.02686}{0.5} = 0.05372(\mu M^{-1}cm^{-1})$$

$$= 53.72 \pm 4.14(mM^{-1}cm^{-1}) \qquad \textit{Equation 3.2}$$

We can also use the above equation to calculate the absorption coefficient of SHP/DHC complex. According to equation 3.1 and table 3.2.1, we can average the absorption coefficient as 53 ± 4 $mM^{-1}cm^{-1}$.

Results in this section shows that the SHP/DHC formation is ionic strength dependent. It indicates that the binding between SHP and DHC is an electrostatic interaction.

3.2.2.3 pH effects on SHP and DHC binding

SHP and DHC binding is also affected by pH. By measuring the SHP/DHC K_d value in different pH solutions a graph of 1/ K_d against pH can be drawn. In figure 3.3 it can be seen that the value of reciprocal K_d is higher at pH 7.5 ~ 8.5, indicating higher affinity of SHP for DHC within that pH region.

To summarize, SHP and DHC bind tightly under low-salt conditions (K_d = 230 nM in

10 mM HEPES, pH 7.2), and the complex is more stable at pH 7.5 to pH 8.5.

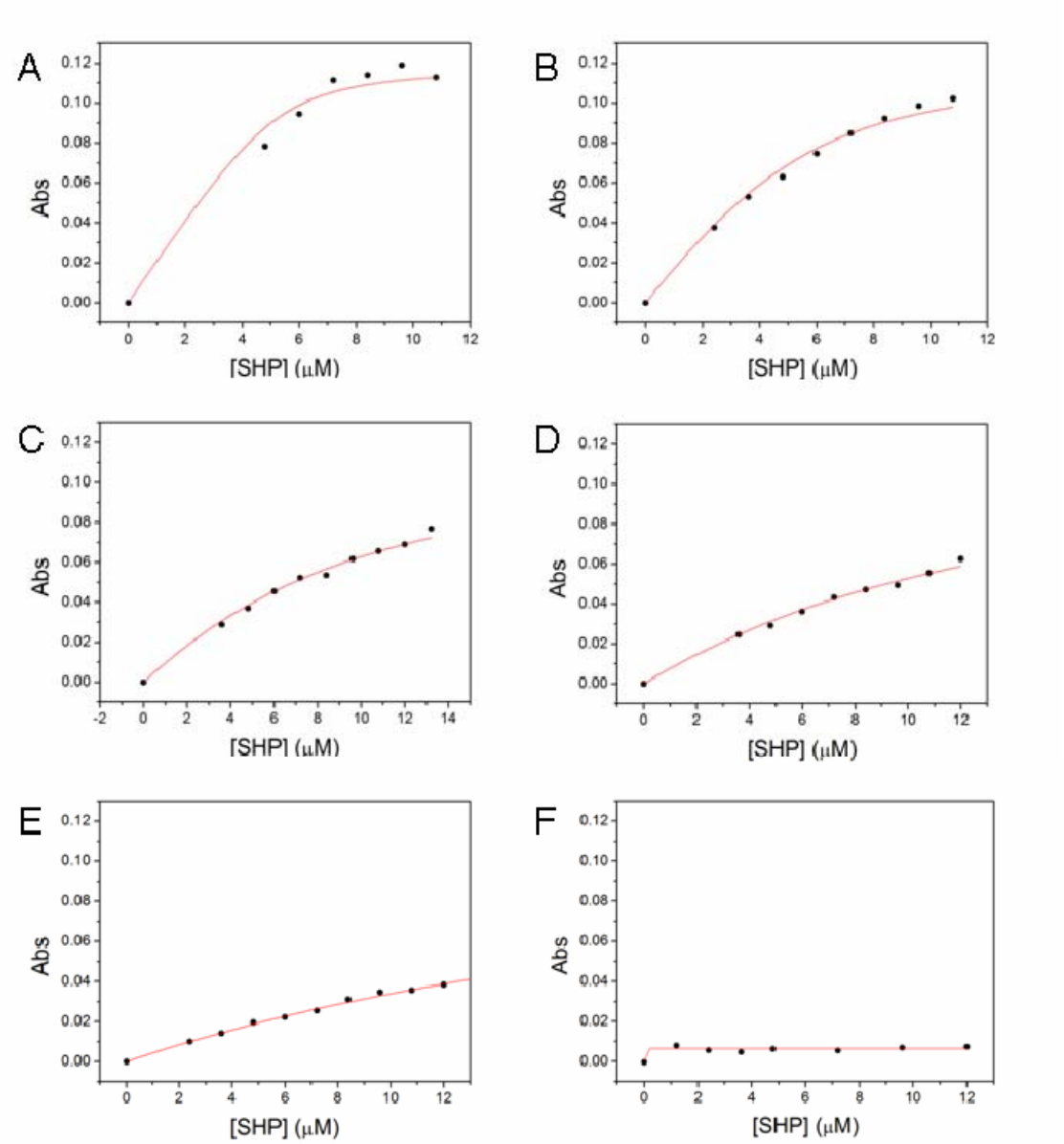

Figure 3.3: Difference in maximal absorbance changes (ΔOD413-396) in varying salt conditions, plotted against concentration of SHP. *Fitted to equation, see appendix I, from which the dissociation constant can be obtained. (A). 10mM HEPES, pH 7.5, 25 ℃. (B). 10mM HEPES, 30mM KCl, pH 7.5, 25 ℃. (C). 10mM HEPES, 30mM KCl, pH 7.5, 25 ℃. (D). 10mM HEPES, 60mM KCl, pH 7.5, 25 ℃. (E). 10mM HEPES, 120mM KCl, pH 7.5, 25 ℃. (F). 10mM HEPES, 200mM KCl, pH 7.5, 25 ℃.*

3.2.3 Co-crystallisation of SHP and DHC (with Dr. C. Mowat and Miss L. Campbell)

Given the high affinity SHP and DHC have for each other under certain conditions, it was decided to attempt to obtain the crystal structure of the proteins in complex. The aim of this is to visualize the docking site and to determine the amino acid residues involved upon binding, and the distances between the hemes. This was initiated by screening for co-crystallisation conditions.

Single crystals of both SHP and DHC were obtained by the hanging drop vapour diffusion method. In both cases these crystals grew from a 1:1 SHP:DHC mixture. The SHP crystal was obtained using 4 μl drops, containing 2 μl of 5mg/ml SHP:DHC (1:1) and 2 μl of the well solution. The well solution was 30 % w/v PEG 20K, 10 mM sodium acetate pH 4.7. The DHC crystal was obtained with 4 μl drops containing 2 μl of 5mg/ml SHP:DHC (1:1) and 2 μl of the well solution. In this case the well solution was 25% w/v PEG 20K, 10% v/v glycerol and 10 mM sodium acetate pH 4.8.

3.3 Discussion

Attempted growth of SHP/DHC co-crystals

SHP and DHC form a complex only in low salt conditions. This necessity for low ionic strength severely limits the range of conditions that would be typically used for crystal screening. For this reason the precipitant choice was limited to organics such as PEGs (12 ~ 50 % w/v, with or without 10% glycerol at 4 ^{o}C and 18 ^{o}C), with pH as the other variable (using 10 mM sodium acetate or TrisHCl buffer, and covering the pH range 4.7 - 9.0). As the results in section 3.2.3 show, only SHP or DHC alone will crystallize (at low pH, ~3.0 – 5.0). Unfortunately, while the optimum pH for complex formation is between pH 7.5 and 8.5, no crystals were obtained under those conditions as yet.

Work is ongoing to find conditions for crystallization at the optimum pH for complex formation.

The physiological function of SHP and DHC

The genes encoding SHP and DHC are located on the same operon, and both of their mRNA levels are up-regulated 10-fold during anaerobic growth using nitrate as the electron acceptor [4]. Therefore, it is probable that SHP and DHC have some shared biological function as redox partners.

The redox potential of the heme of SHP is -100 mV, higher than the redox potentials of DHC (-310 and -240 mV). Thus the thermodynamics are poised for favourable electron transfer from DHC to SHP, which proceeds with a second order rate constant of $1.85 \pm 0.11 \times 10^7$ $M^{-1}s^{-1}$ at 500 mM KCl and 10 ^oC [1]. If compared with recognised physiological partners such as cytochrome *c* and cytochrome *c* peroxidase [137, 138], the rate of SHP reduction by DHC is great enough to be a potentially important process *in vivo*.

As the data show in section 3.2.2, SHP and DHC tightly bind to each other in low salt conditions (K_d = 260 nM in 10 mM HEPES, pH 7.2, and 25 ^oC). However, in the same conditions, DHC does not reveal an obvious affinity with the control protein F*cc*$_3$. This indicates that the binding between SHP and DHC is selective, and therefore DHC may be the specific electron donor to SHP. At higher salt conditions (200 mM KCl, 10 mM HEPES, pH 7.5, and 25 ^oC), the binding between SHP and DHC becomes much weaker. This raises the question of whether this binding is physiologically relevant, because a typical cellular total ion concentration is around 137 mM.

3.4 Conclusions

It is proposed that SHP and DHC could be physiological redox partners. Ferrous DHC can reduce ferric SHP with the second order rate constant of $1.85 \pm 0.11 \times 10^7$

$M^{-1}s^{-1}$ [1]and the two proteins form a dynamic complex. Reduced SHP was suggested to have enzyme activity without DHC binding.

Chapter IV

AN AEROBIC FUNCTION FOR SHP

4 An aerobic function for SHP: Nitric oxide dioxygenase activity

4.1 Introduction and Aims

Due to steric hindrance around heme iron, ferrous SHP can only bind with small diatomic gases e.g. O2 and NO [2]. The dissociation constant (K_d) for O_2 binding to ferrous SHP has been calculated to be 26 ± 3 μM [1]. Like other ferrous heme proteins, SHP has a greater affinity for nitric oxide than oxygen (the K_d for NO binding to ferrous SHP is around 10 nM) [1, 5]. However, due to the activity site being too crowded, ferrous SHP does not bind well with larger molecules. For example, nitrate and imidazole are too big to stable bond to the heme iron, both K_d for nitrate and imidazole are over 1M (data not shown).

As described in the chapter 1, the mRNA levels of SHP, DHC and cyt *b* are up-regulated 10-fold in *Shewanella oneidensis* MR-1 grown using nitrate as the terminal respiratory electron acceptor [4], thus it is possible that the physiological roles of SHP may be in nitrate metabolism. However, the size of nitrate is too big to be a candidate of substrate for SHP, and some nitrification steps need more than one electron transfer (SHP is a monoheme cytochrome). Therefore this study focused on testing for nitrite reductase, nitric oxide reductase and nitric oxide dioxygenase.

In this chapter, we conclusively show that SHP can catalyse the reaction between oxygen and nitric oxide to give the nitrate ion as the final product. Thus we propose a possible function for SHP as a nitric oxide dioxygenase. Generally speaking, the reaction of NO dioxygenase is through the oxy-ferrous complex reacting with nitric oxide to generate nitrate [7, 139-141]. Here we also describe a mechanism for the catalytic reaction with ferrous-NO complex.

4.2 Results

4.2.1 SHP^{2+}-O_2 reacts with nitric oxide to produce nitrate

Protein	Fe^{2+}/O_2			Fe^{2+}/NO			Reference
	k_{on} ($\mu M^{-1} s^{-1}$)	k_{off} (s^{-1})	K_d (μM)	k_{on} ($\mu M^{-1} s^{-1}$)	k_{off} ($10^{-4} s^{-1}$)	K_d ($10^{-6} \mu M$)	
Mb	13 ± 0.03	11 ± 3	0.85 ± 0.23	21 ± 1	1.1 ± 0.3	5.3 ± 1.6	[142]
HMP	38	0.44	0.01	26	2	8	[6, 7, 142]
SHP	0.17 ± 0.01	3.2 ± 0.6	18.8 ± 3.5	0.13 ± 0.01	36 ± 7	280 ± 76	This work

Table 4.1: Comparison of the kinetic parameters for O_2 and NO binding to ferrous SHP, Flavohemoglobin and Myoglobin. *Kinetic parameters for the binding of O_2 and NO binding to Rhodobactor sphaeroides SHP, E. coli flavohemoglobin (HMP) and sperm whale myoglobin (Mb). HMP and Mb parameters were measured at 20 °C, pH 7.0. SHP parameters were measured at 10 °C, pH 7.5.*

Up-regulation of SHP mRNA levels in the presence of nitrate as the electron accepter indicates a possible role for the protein in nitrate metabolism (Table 1.1). Reduced SHP can bind oxygen or nitric oxide to form complexes (Table 4.1), and SHP could therefore function as a nitric oxide dioxygenase, catalysing the reaction between oxygen and nitric oxide. A mechanism for nitric oxide dioxygenation has been proposed in the case of flavohemoglobin (HMP) and neuroglobin (Ngb), and involves reaction of the oxy-ferrous complex with nitric oxide to generate nitrate. Thus it must be determined whether SHP^{2+}-O_2 can react with NO.

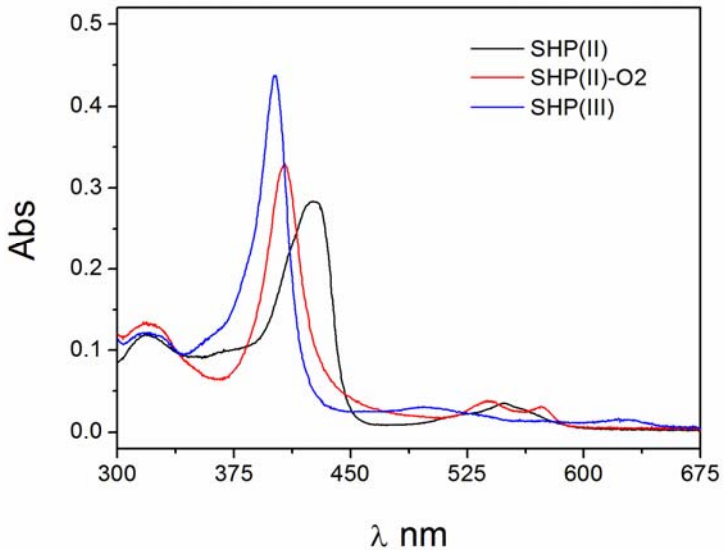

Figure 4.1: UV/vis absorption spectra of SHP. *The figure shows UV/vis absorption spectra of oxidized (blue), reduced (black), and oxy-ferrous (red) forms of SHP.*

In stopped-flow experiments the spectrum obtained by mixing SHP^{2+}-O_2 with NO is different from the spectrum of SHP^{2+}-O_2 alone. The initial position of the Soret peak is 407 nm (SHP^{2+}-O_2) and the final one is 401 nm (SHP^{3+}) (Figure 4.1). In addition, the α and β peaks (572 nm and 540 nm) of SHP^{2+}-O_2 are also decreased, suggesting that SHP^{2+}-O_2 has reacted with NO to produce ferric SHP (SHP^{3+}). This result is in accordance with the detoxification mechanism, in which SHP^{2+}-O_2 reacts with NO to form a SHP^{3+}-peroxynitrite intermediate that finally decays to yield nitrate and ferric SHP. A time course study of the reaction of SHP^{2+}-O_2 with NO reveals an observed rate constant (k_{obs}) of 230 s^{-1} at 10 ^{o}C. This is shown in Figure 4.2. However, this reaction is either too fast or the spectrum of the intermediate is too similar to SHP^{3+} to be able to distinguish it.

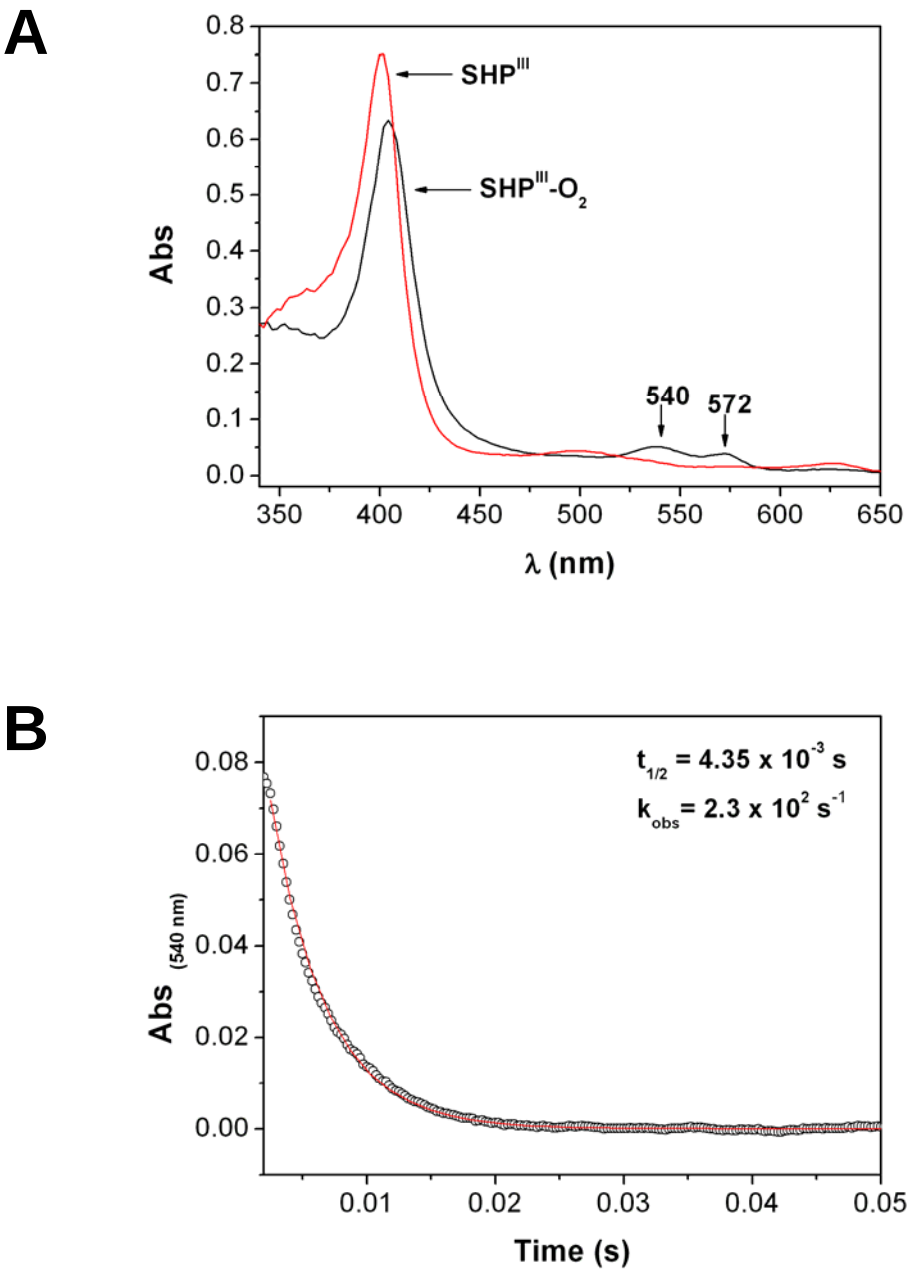

Figure 4.2: Reaction of SHP^{2+}-O_2 with NO. *(A) The black trace is the spectrum of the SHP^{II}-O_2 complex prior to mixing with NO. Upon reaction with NO, nitrate and ferric SHP (red trace) are produced. (B) The time course trace for the reaction. Decrease in absorbance at 540 nm was used to monitor decay of SHP^{2+}-O_2.*

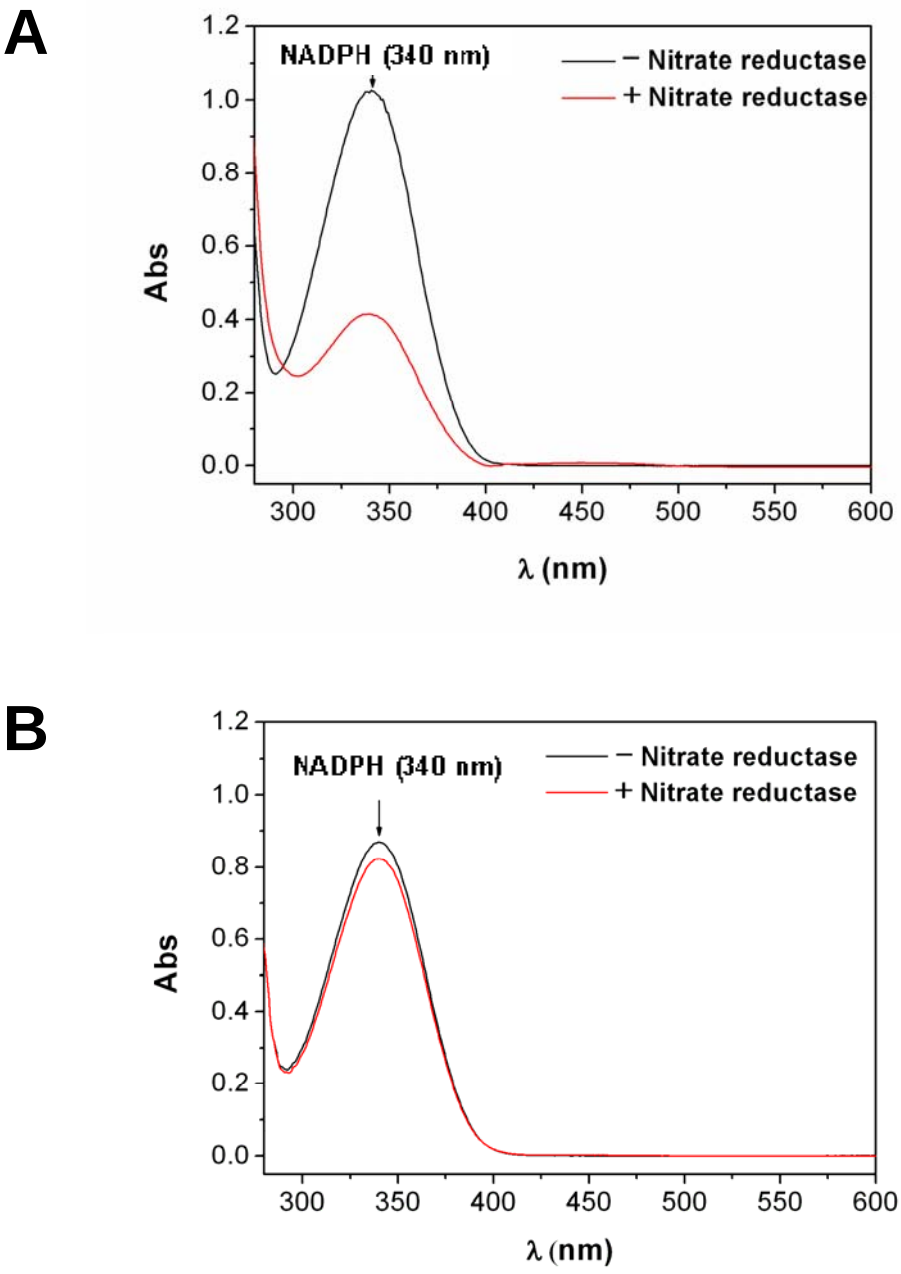

Figure 4.3: Nitrate is produced by the reaction of SHP^{2+}-O_2 with NO. *(A) After reaction of SHP^{2+}-O_2 with NO, NADPH was added and SHP removed by filtration. The spectrum of the solution containing product was collected (black trace). Upon addition of NADPH-dependent nitrate reductase the red trace was obtained, indicating consumption of nitrate (the product of the reaction). (B) The control experiment carried out in the absence of SHP. The black trace was obtained prior to addition of nitrate reductase and the red trace after its addition. This indicates no production of nitrate in the absence of SHP.*

In order to demonstrate the production of nitrate, reduced SHP (in 100 mM sodium phosphate buffer pH 7.5) was mixed with buffer 100 μM in O_2 to form SHP^{2+}-O_2. Nitric oxide was then added (to a concentration of 50 μM), and SHP was removed from the solution by filtration using a Vivaspin concentrator (5 kDa MWCO PES). The filtered, protein-free, solution was used as a spectral baseline. NADPH was then added and a spectrum obtained (this is shown in Figure 4.3). NADPH-dependent nitrate reductase was then added to this solution and incubated at 25 ^{o}C for 20 min. After incubation another spectrum was collected (Figure 4.3). NADPH has an absorption peak at 340 nm (ε_{340} = 6.22 $mM^{-1}cm^{-1}$), and it can be seen from Figure 4.3 that after addition of nitrate reductase the NADPH concentration is decreased substantially. The control experiment carried out in the absence of SHP shows that addition of nitrate reductase causes a decrease in NADPH concentration of less than 5 % (Figure 4.3). This consumption of NADPH indicates the presence of 0.01 mM nitrate in the solution as a result of NO dioxygenation.

4.2.2 The rates of O_2 and NO binding to reduced SHP are similar

Generally speaking, in the ferrous form oxygen binding heme proteins will also bind nitric oxide. For example, myoglobin (Mb), flavohemoglobin (HMP), and neuroglobin (Ngb) can bind both O_2 and NO, and all of them have higher NO affinity than O_2. For instance, the oxygen dissociation constant (K_d) of sperm whale myoglobin is 0.85 ± 0.23 μM, while its nitric oxide K_d is 5.3 ± 1.6 × 10^{-6} μM. In all three cases the ferrous-NO complex is very stable, and may be regarded as a dead-end complex. Nitric oxide dioxygenase activity involves the ferrous-O_2 complex reacting with NO. This implies that the heme protein should bind oxygen first and then react with nitric oxide. However, if nitric oxide binds first, then the ferrous-NO dead-end complex will be formed. It must therefore be determined whether oxygen can compete with NO to bind to the heme iron.

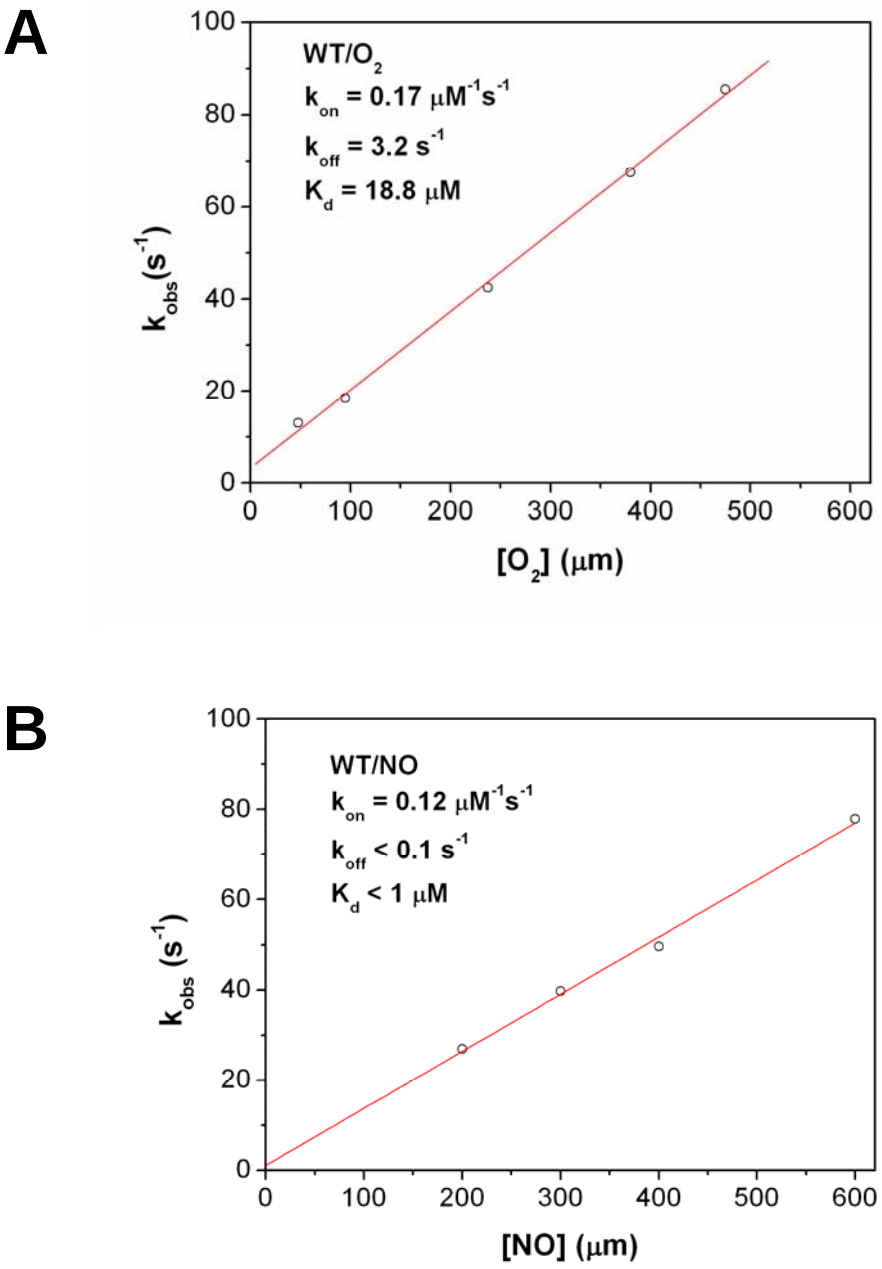

Figure 4.4: Oxygen and nitric oxide binding to reduced SHP. *(A) Reaction of SHP^{II} with O_2 at varying [O_2]. (B) Reaction of SHP^{II} with NO at varying [NO].*

Binding of O_2 or NO to reduced SHP can be monitored in a stopped-flow experiment by observing the change in the Soret peak position upon their binding (426 nm to 408 nm or 413 nm respectively). For O_2 binding, the second order rate constant (k_{on}) is

found to be 0.17 $\mu M^{-1} s^{-1}$, and this is of similar magnitude to that obtained for NO binding to ferrous SHP (k_{on} = 0.12 $\mu M^{-1} s^{-1}$). Plots of k_{obs} *vs* ligand concentration are shown in Figure 4.4. However, the rate constant for ligand dissociation for SHP-O_2 (k_{off} = 3.2 s^{-1}) is much greater than that for SHP-NO (k_{off} < 0.1 s^{-1}) (Figure 4.4). In addition, the dissociation constant for NO with ferrous SHP is significantly lower (K_d < 1 μM) than that for O_2 (K_d = 18.8 μM). Consequently NO binding to ferrous SHP may be considered almost irreversible. This result is similar to those observed for the other oxygen binding cytochromes [6, 7, 142] (Table 4.1).

4.2.3 SHP-NO can react with superoxide but not O_2

In the previous section it was confirmed that SHP has nitric oxide dioxygenase activity, and that its mechanism is *via* the oxy-ferrous complex reacting with nitric oxide. However, it was also discovered that ferrous SHP binds oxygen and nitric oxide with similar rates. This implies that a proportion of ferrous-NO SHP can be formed in an environment containing both oxygen and nitric oxide.

Time course spectra for the addition of SHP^{2+}-NO to 1 mM O_2 are shown in Figure 4.5, and show that the initial spectrum is the same as the final spectrum and that this spectrum is consistent with the presence of SHP^{2+}-NO. This indicates that SHP^{2+}-NO does not react with O_2 over 20 minutes, and this is similar to observations made in the cases of Ngb^{2+}-NO and HMP^{2+}-NO [7, 143-145].

SHP^{2+}-O_2 is not as stable as SHP^{2+}-NO. The SHP^{2+}-O_2 complex does not only have a greater k_{off} value (3.2 s^{-1}) than that for SHP^{2+}-NO (k_{off} < 0.1 s^{-1}) (Figure 4.5), but also can auto-oxidize with rate constant of 2.8 x 10^{-4} s^{-1} at 10 °C (Figure 4.5). SHP^{2+}-O_2 decay is shown by the build-up of SHP^{3+} (Figure 4.5) and the generation of superoxide. This auto-oxidization behavior is also reported for most oxygen binding heme proteins, including hemoglobin and flavohemoglobin [146, 147].

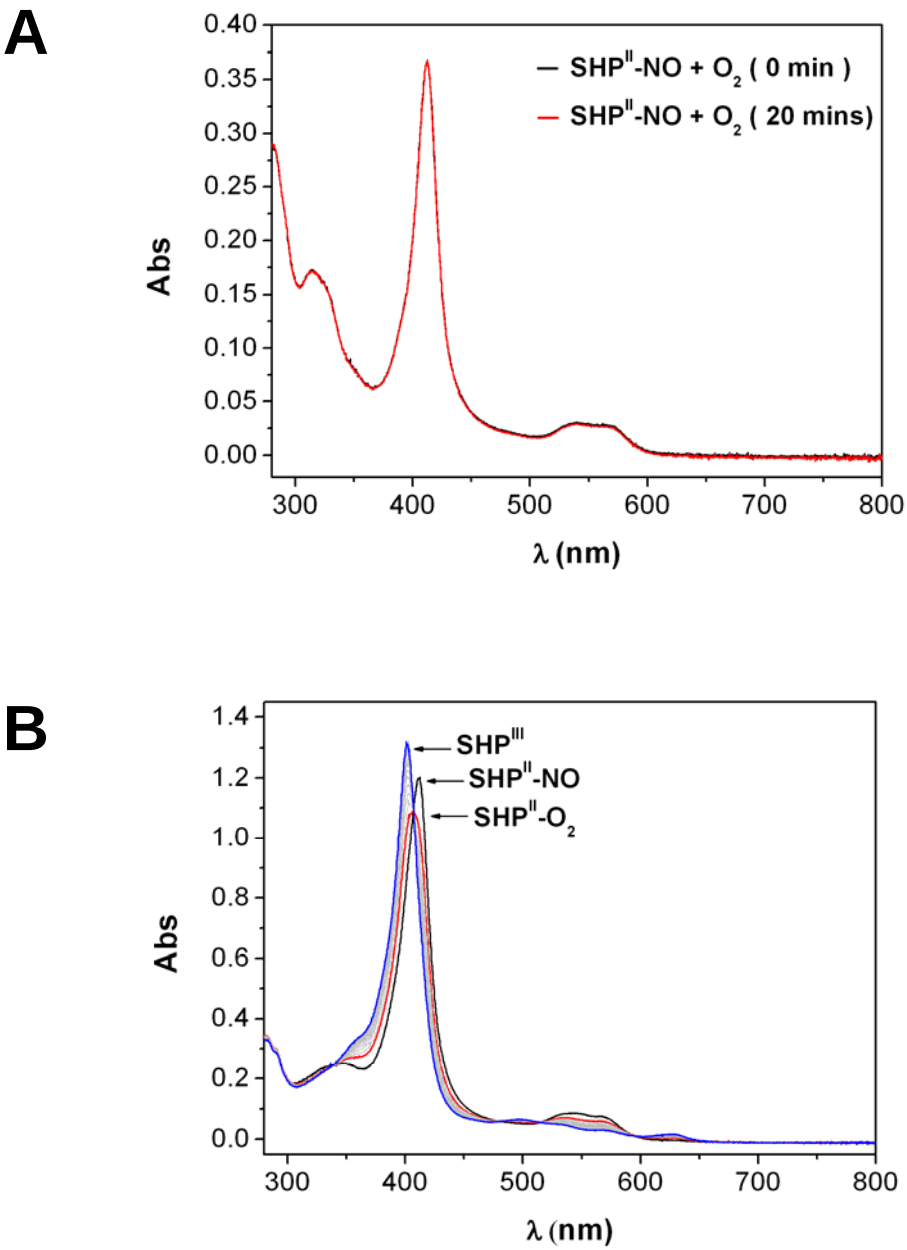

Figure 4.5: SHP^{2+}-NO incubated with oxygen and superoxide. *(A) Spectra of SHP^{2+}-NO in the presence of 1 mM O_2 at t = 0 and t = 20 minutes. (B) Addition of superoxide to SHP^{2+}-NO. The spectrum is seen to change rapidly from the SHP^{2+}-NO species (black) to SHP^{2+}-O_2 (red). This then slowly decays to SHP^{3+} (blue).*

The stability of SHP^{2+}-NO to auto-oxidation, even at high O_2 concentrations ([O_2] = 1 mM), led to the hypothesis that SHP^{2+}-NO might instead react with superoxide. To ascertain this an aliquot of superoxide was added to a solution of SHP^{2+}-NO and the UV/vis spectrum collected every 10 min. In contrast to O_2 addition, the spectrum of SHP^{2+}-NO in the presence of superoxide is conspicuously changed, with a shift in the Soret peak from 412 nm to 408 nm. This is shown in Figure 4.5. This spectral shift is consistent with the formation of SHP^{2+}-O_2. After further incubation the spectrum is again altered, with a shift in the Soret peak to 401 nm indicating the slow formation of SHP^{3+}. The supposed mechanism is shown in Scheme 4.1. Monitoring of the initial reaction by stopped-flow methods was impossible due to the presence of methanol which is necessary for the stabilization of superoxide in solution. This was found to cause precipitation of SHP.

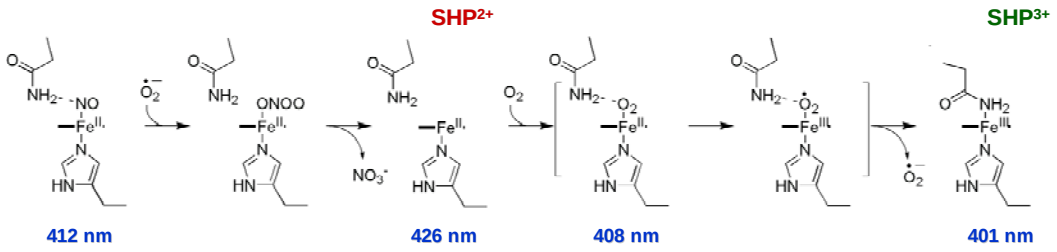

Scheme 4.1

4.2.4 Oxidized SHP is the final product of mixing SHP^{2+}-NO and SHP^{2+}-O_2

The time course of the decay of the SHP^{2+}-O_2 to SHP^{3+} was studied. Oxygen-bound SHP is unstable, with a half-life of approximately 1 hr at room temperature. This suggests that the ferrous heme iron can transfer an electron to iron-bound O_2 to form the SHP^{3+}-O_2^- complex. Dissociation of superoxide will then yield SHP^{3+} and superoxide [5]. Ngb-O_2 and HMP-O_2 also can auto-oxidize [5].

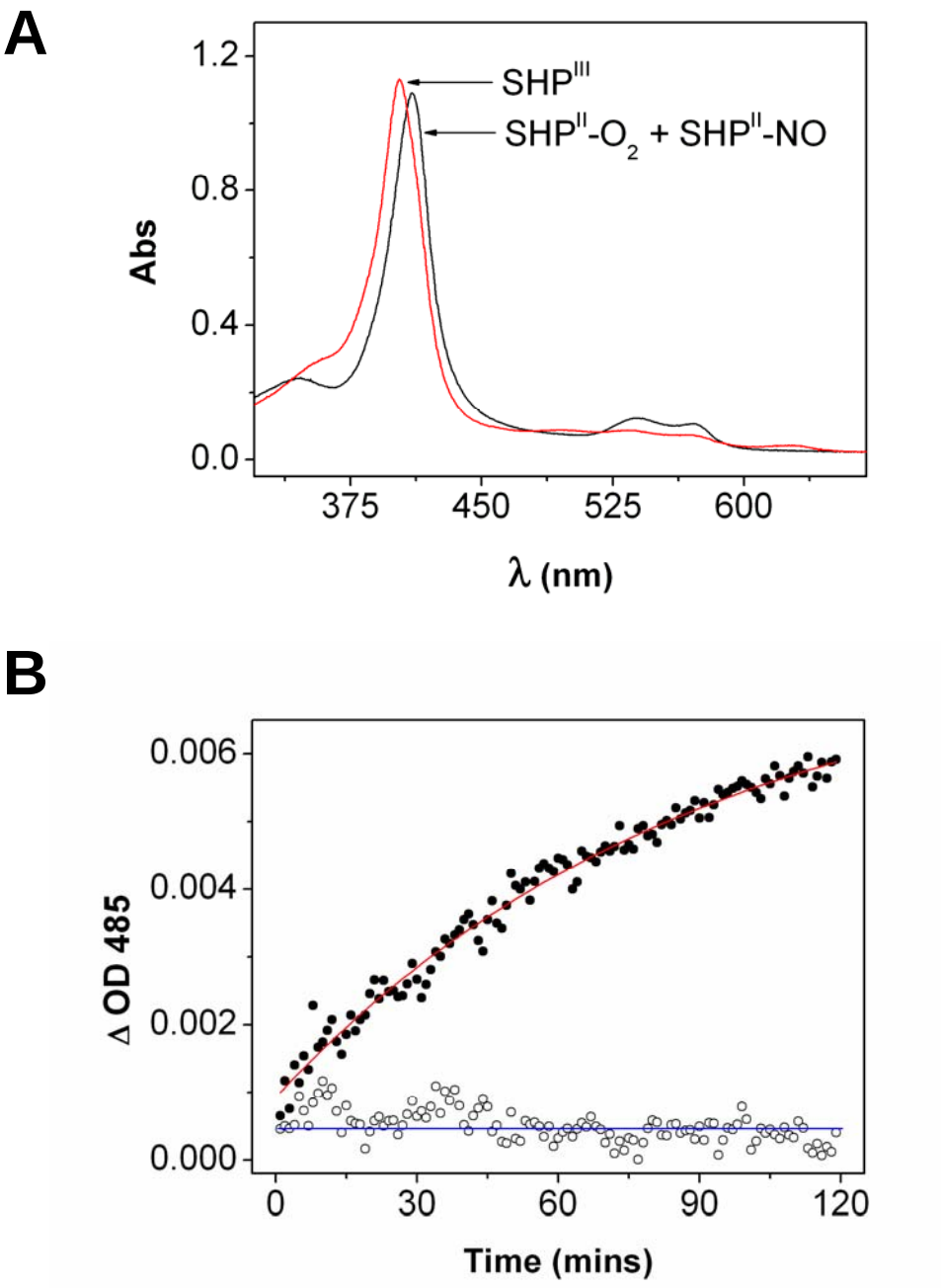

Figure 4.6: Reaction of SHP^{2+}-O$_2$ with NO. *(A) The spectrum shown in black is that for an equimolar mixture of SHP^{2+}-NO and SHP^{2+}-O$_2$. Over time this converts to the spectrum of SHP^{3+}, shown in red, and nitrate is produced. (B) The red fitted trace (closed circles) represents the decay of SHP^{2+}-NO in the SHP^{2+}-NO/SHP^{2+}-O$_2$ mixture in the absence of superoxide dismutase and catalase. The blue fitted trace (open circles) is for the same process in the presence of superoxide dismutase and catalase and shows no decay of*

SHP^{2+}-NO.

In the light of this result, an important question is whether SHP^{2+}-O_2 can act as a source of superoxide. SHP^{2+}-O_2 was mixed with SHP^{2+}-NO to ascertain whether SHP^{2+}-NO can react with superoxide produced by the decay of SHP^{2+}-O_2. The rate of this reaction depends on the rate of superoxide liberation from SHP^{2+}-O_2. The initial spectrum obtained on mixing an equal amount of SHP^{2+}-O_2 (Soret peak is 408 nm) and SHP^{2+}-NO (Soret peak is 412 nm) is shown in Figure 4.6 (black trace). UV/vis spectra were collected every minute, and the result reveals the slow formation of SHP^{3+} (Figure 4.6 red trace). In order to confirm that SHP^{2+}-NO reacts with superoxide released from SHP^{2+}-O_2 and not with the complex directly we carried out a control experiment using superoxide dismutase and catalase (Figure 4.6). With these two enzymes present in the reaction mix there was no decay of the SHP^{2+}-NO thus confirming that the reaction is mediated by the release of superoxide.

4.3 Discussion

Why is nitric oxide dioxygenase necessary?

Nitric oxide is an important signalling molecule, but also a ubiquitous poison. At concentrations below 100 nM, nitric oxide inactivates [4Fe–4S]-containing hydratases, and competes with O_2 binding to metalloproteins such as hemoglobin (Hb) and myoglobin (Mb). For this reason all organisms require an NO-metabolizing enzyme such as nitric oxide dioxygenase and/or nitric oxide reductase, to defend against nitric oxide poisoning [131, 148].

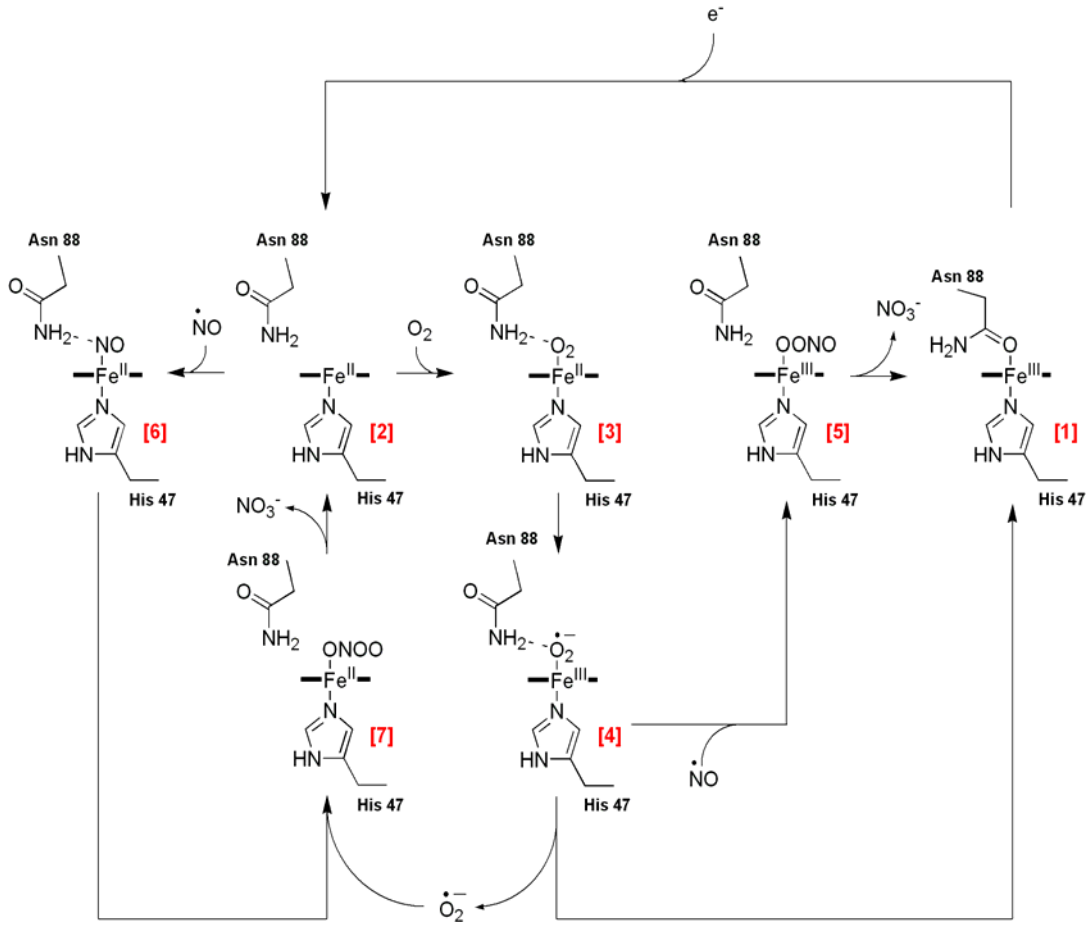

Figure 4.7: The nitric oxide detoxification cycle mediated by the SHP/ DHC/ cyt b system.

SHP may function as a nitric oxide dioxygenase.

SHP and DHC have been demonstrated to be redox partners. In *in vitro* studies, ferric SHP can be reduced by ferrous DHC, and then ferrous SHP can react with oxygen to form the oxy-ferrous complex [1]. In our study we found that, like neuroglobin (Ngb) [6, 149] and flavohemoglobin (HMP) [7, 131, 139, 148], oxy-ferrous SHP can react with nitric oxide rapidly to produce nitrate and ferric SHP (Figure 4.7). It has also been shown that in *Shewanella* MR-1 the mRNA levels for SHP and other related proteins are up-regulated by growth under nitrate conditions. This is summarised in Figure 4.7 [5]. This evidence suggests the involvement of SHP in nitrate metabolism.

Although we have been unable to identify the spectrum of the peroxynitrite-bound intermediate in the stopped-flow experiments, we have shown the product of this reaction to be nitrate (Figure 4.7). Therefore SHP may function as a nitric oxide dioxygenase.

Some similarities between flavohemoglobin and the SHP/DHC complex

Flavohemoglobin (HMP) is a well known nitric oxide dioxygenase, found in prokaryotic and eukaryotic organisms [131]. Its localization in microbes is in the periplasm and cytoplasm. Unlike SHP, HMP includes two domains: a globin domain and a FAD-binding domain with an NAD binding site (Figure 4.8). Through oxidation of NAD(P)H to receive electrons, it can combine nitric oxide and oxygen to form nitrate [7, 131, 139-141, 148]. Compared to HMP, SHP has similar nitric oxide dioxygenase activity. However, while HMP uses intra-molecular electron transfer to get electrons from NAD(P)H to the heme, SHP receives electrons from its binding partner, DHC, through an inter-molecular electron transfer. The mechanism of nitric oxide detoxification is *via* ferrous HMP binding oxygen and then reacting with nitric oxide to produce nitrate. In the process of nitric oxide dioxygenation, only one electron is needed. However, DHC or FAD is able to donate two electrons. The reason why a one-electron reaction uses a reductant with a two-electron capacity is not clear. One possible reason is that the flavin domain or DHC acts as a transducer, coupling the two-electron oxidation of NADPH or quinols to a one-electron process. The other possibility is that a different two-electron reaction occurs under aerobic conditions.

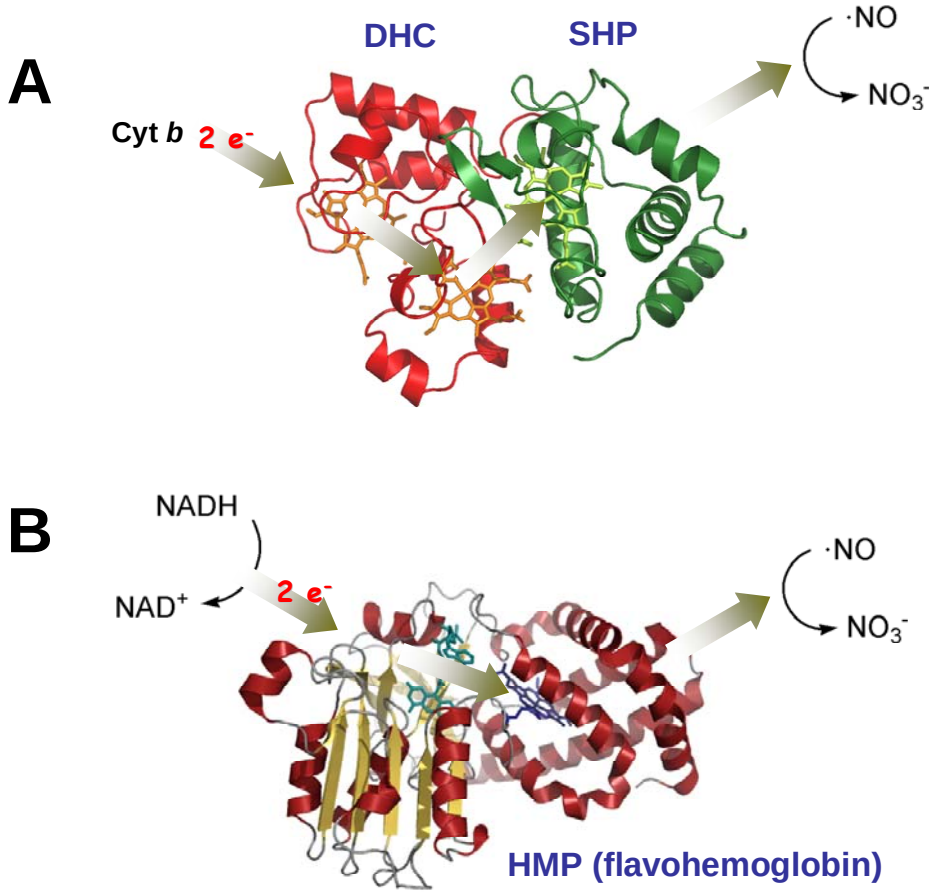

Figure 4.8: A model for electron transfer in SHP/DHC and HMP. *(A) 2 electrons are transferred from Cyt b to DHC (red, PDB: SFWT), followed by transfer to SHP (green, PDB: !DW3). Ferrous SHP catalyzes nitric oxide dioxygenation. (B) 2 electrons are transferred from NADH to FAD, followed by transfer to heme (blue). Reduced HMP (1CQX) also catalyzes nitric oxide dioxygenation. This Figure was generated using PyMOL (DeLano Scientific; http://pymol. sourceforge.net/).*

Structural homology between neuroglobin and SHP

(Ngb) is also a mono heme protein [8, 150]. It is localized to cerebral neurons of vertebrates, and the ferrous form can bind oxygen, nitric oxide, and carbon monoxide. A recent study shows that HMP also has nitric oxide dioxygenase activity, and its mechanism is similar to that which operates in flavohemoglobin. The structure of Ngb shows some similarities with SHP. Both of them reveal oxygen and nitric oxide binding ability, and contain basket structure around the heme group with one heme

edge exposed to the solvend. These two cytochromes show hexa-coordination of heme iron in the ferric form and penta-coordination in the ferrous form. Like HMP, ferrous neuroglobin also binds nitric oxide rapidly and irreversibly. The nitric oxide-bound complex can react with oxygen, but this is very slow [6]. Thus the NO-bound form is considered a "frozen" form, without activity. In Wakasugi's studies [144, 151], oxidized human neuroglobin (Ngb) was proposed to act as a guanine nucleotide dissociation inhibitor (GDI) for the GDP-bound form of the heterotrimeric G protein alpha-subunit. But at present, scavenging nitric oxide is still considered as the main function of neuroglobin, functioning as an oxygen-dependent nitric oxide dioxygenase, physically protecting neuronal cells from nitric oxide damage [152]. Superoxide-generating ability has not been reported, but its structure is similar to other cytochromes that can generate superoxide.

SHP^{2+}-NO reacts rapidly with superoxide that can be generated from SHP^{2+}-O_2

Until now, the mechanism of nitric oxide dioxygenase has been understood to involve the oxy-ferrous (SHP^{2+}-O_2) complex reacting with nitric oxide to produce nitrate and the ferric cytochrome, while the nitric oxide-bound ferrous complex (SHP^{2+}-NO) was considered an inactive form. In this study we have shown that oxy-ferrous SHP, like other nitric oxide dioxygenases, can react with nitric oxide. We have also shown that SHP^{2+}-NO reacts rapidly with superoxide to form ferric SHP, *via* the formation of SHP^{2+}-O_2 as a long-lived intermediate. This is proposed to occur as shown in Scheme 4.1. The SHP^{2+}-NO form reacts with superoxide to produce nitrate and ferrous SHP, which subsequently binds O_2 to produce the oxy-ferrous form. The oxy-ferrous SHP can then slowly release superoxide ($t_{1/2}$ = 1 hour) [1]. Thus, upon mixing of SHP^{2+}-NO and SHP^{2+}-O_2, both species decay to form ferric SHP and nitrate.

The full nitric oxide dioxygenation cycle for SHP

An overall mechanism for NO dioxygenation is shown in Figure 4.7. This mechanism shows that SHP^{3+} (*1*) receives one electron from a donor (believed to be DHC/Cyt *b* in the physiological situation) to form SHP^{2+} (*2*). Upon reduction of SHP

asparagine 88 moves from its position as a ligand to the heme iron, thus allowing the binding of small molecules. SHP^{2+} can then bind oxygen or NO with similar rates. The SHP^{2+}-O_2 form (*3*) would auto-convert to the superoxy-ferric, SHP^{3+}-O_2^-, complex (*4*), that would react with NO to form the ferric peroxynitrite intermediate (*5*). This intermediate would then release nitrate to regenerate SHP^{3+} (*1*). In the other half-pathway, SHP^{2+} reacts with NO to form the SHP^{2+}-NO complex (*6*). This species can then react with the superoxide produced by the decay of the SHP^{3+}-O_2^- complex (*4*) to form the ferrous peroxynitrite intermediate (*7*). This can then release nitrate and rejoin the cycle.

The mechanism of SHP probably also operates in other nitric oxide dioxygenases.

A similar mechanism probably also operates in other nitric oxide dioxygenases such as Ngb and HMP [6, 7, 150]; both bind nitric oxide rapidly and almost irreversibly. Flavohemoglobin catalyzes reaction of nitric oxide and oxygen to produce nitrite and the rate constants, k_{on}, for oxygen or nitric oxide binding to ferrous flavohemoglobin are similar. This similarity in NO and O_2 binding rates can, however, cause inhibition of NO dioxygenase activity in flavohemoglobins [7]. Previous studies suggested that such inhibition of the nitric oxide dioxygenase activity is apparent only at NO/O_2 concentration ratios of > 1:100. Therefore, at a NO/O_2 molar ratio of approximately 1:1500 under aerobic conditions, NO inhibition can essentially be ignored [7, 131, 132]. Unfortunately, because nitric oxide is generated during nitrate metabolism (normally under micro-aerobic conditions) the NO/O_2 concentration ratio will be high enough to inhibit NO dioxygenase activity. In 2001 it was hypothesised that NO-bound ferrous HMP can directly react with oxygen to produce nitrate [7, 131, 132]. However, this reaction is quite slow even under high oxygen pressure *in vitro*, and there may be another pathway *in vivo*. Similarly to SHP, HMP can also generate superoxide [7, 131, 132]. The possibility therefore exists that NO-bound HMP can react with superoxide through a mechanism similar to that proposed here for SHP. This is shown in Scheme 4.2. Some previous studies show that the nitric oxide-bound complex of Ngb can react with oxygen, but the reaction is very slow [6, 150]. Therefore, NO-bound

neuroglobin may, like SHP and possibly flavohemoglobin, react with endogenously-produced superoxide and follow the mechanism proposed in this study.

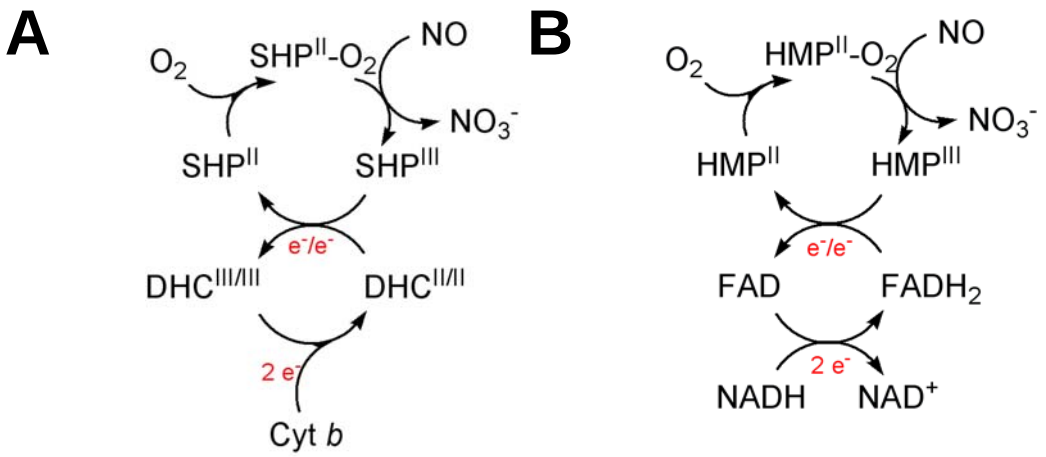

Scheme 4.2: *A scheme for electron transfer in the SHP/DHC/Cyt b (A) and HMP/FAD/NADH (B) systems.*

4.4 Conclusions

SHP has nitric oxide dioxygenase activity. Its mechanism is described in section 4.2.1, and this is likely to be similar to the one that operates in other nitric oxide dioxygenases such as flavohemoglobin and neuroglobin. The NO-bound form of SHP is inactive with O_2 but rapidly reacts with superoxide which could be endogenously produced.

Flavohemoglobin, which is found in unicellular prokaryotic and eukaryotic organisms, is the most studied nitric oxide dioxygenase. Its activity is inhibited by nitric oxide and it generates superoxide by auto-oxidation. Flavohemoglobin has been reported to avoid NO inhibition by binding O_2 with high affinity or by slowly reducing NO to nitroxyl (NO^-) [7, 131, 132, 141, 142, 153, 154].

Previous work has also shown that neuroglobin has nitric oxide dioxygenase activity [6, 150, 152]. Like flavohemoglobin, ferrous neuroglobin also binds NO rapidly and irreversibly. The NO-bound form is able to react with O_2, but does so slowly. For this reason the NO-bound form is considered a 'frozen' form, without activity. The main function of neuroglobin is thought to be in scavenging NO. Although no superoxide generation has been reported for neuroglobin, it is structurally similar to other cytochromes that are able to generate superoxide. It is therefore conceivable that NO-bound neuroglobin may, like SHP and possibly flavohemoglobin, react with endogenous superoxide via the mechanism proposed in Figure 4.7.

The discovery of nitric oxide dioxygenase activity in SHP represents the initial characterization of this system, and there is much work to be done to understand further the physiological relevance of these findings. To this end, several knockout mutants are being studied to determine their phenotypes.

Chapter V

THE ANAEROBIC FUNCTION OF SHP

5 The anaerobic function of SHP

5.1 Introduction and Aims

As discussed in chapter 4, SHP (*sphaeroides* heme protein) is proposed to be a nitric oxide dioxygenase [5] which utilizes the same mechanism as other NO dioxygenases, flavohemoglobin (HMP) and neuroglobin (Ngb) [6-8]. This mechanism is proposed to proceed via an oxy-ferrous complex (SHP^{2+}-O_2) which reacts with nitric oxide. This process is oxygen-dependent. However, according to micro array studies [4], SHP mRNA levels are up-regulated nearly 10-fold when *Shewanella oneidensis* MR-1 is grown with nitrate under anaerobic conditions. This indicates that SHP could also perform some anaerobic function and may possibly be involved in nitrate metabolism.

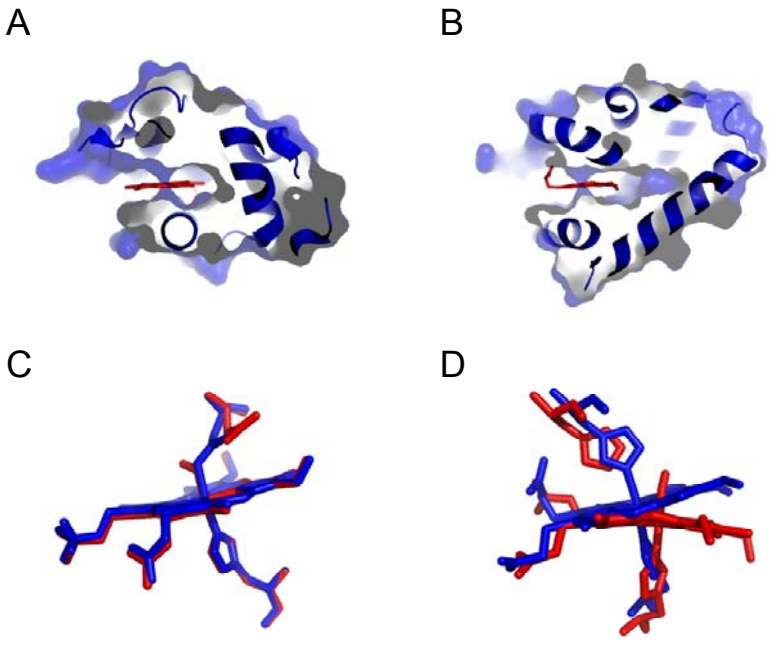

Figure 5.1 Comparison of the structures of SHP and Ngb. *Cartoon structures and surfaces of SHP(1DW0, 1DW2) (A) and Ngb (1QJ6, 1W92) (B) are shown in blue, hemes in red. (C) The relative position of the hemes and two axial ligands of SHP and Ngb were shown in panel C and panel D respectively. Oxidized forms in blue; reduced forms in red. This Figure was generated using PyMOL (DeLano Scientific; http://pymol. sourceforge.net/).*

Although SHP and Ngb are not homologous in terms of their amino acid sequences, the 3-dimensional structures of both monoheme proteins are like a basket around the heme group with one heme edge exposed to the solvent (Figure 5.1) [3, 155]. In the ferric state both SHP and Ngb contain hexa-coordinate iron which becomes penta-coordinate upon reduction. In addition, SHP and Ngb have similar redox potentials. The redox potential of Hgb is about -129 mV [156], slightly lower than that of SHP (-110 mV) [1]. A recent study reveals that ferrous Ngb not only has oxygen-dependent NO dioxygenase activity, but can also react with nitrite and produce NO under anaerobic conditions [157]. Therefore, we wished to know if SHP also has anaerobic nitrite reductase activity.

Microbiologically, NO is important as an intermediate in denitrification and as a substrate for nitric oxide reductases which convert it to nitrous oxide (N_2O) under anaerobic conditions. Unfortunately, NO may inactivate some metalloproteins by binding tightly. Ferrous SHP binds NO with a K_d of less than 1 μM, and does not auto-oxidise [1]. Therefore, even in low NO concentrations, SHP^{2+}-NO would be formed. In aerobic conditions SHP^{2+}-NO could be quickly converted back to ferrous SHP by reacting with superoxide liberated by SHP^{2+}-O_2 or from another source [5]. However, this mechanism cann't happens in anaerobic conditions. Therefore, under anaerobic conditions SHP^{2+}-NO must be processed by some other mechanism. HMP, designated as an NO dioxygenase, was reported to have NO reductase function in anaerobic conditions [141]. Although the structures of SHP and HMP are different, the SHP/DHC complex and HMP are somewhat similar in character. As Figure 1.29 shows, HMP contains a FAD domain (2-electron transfer capacity and analogous to DHC in the SHP/DHC complex) and a heme domain (containing the active site, analogous to SHP in the SHP/DHC complex and with the capacity to transfer a single electron). Thus, since HMP was reported to have NO reductase activity under anaerobic conditions, it is possible that the SHP/DHC complex has the same anaerobic function.

5.2 Results

5.2.1 SHP^{2+} reduces NO_2^- to NO

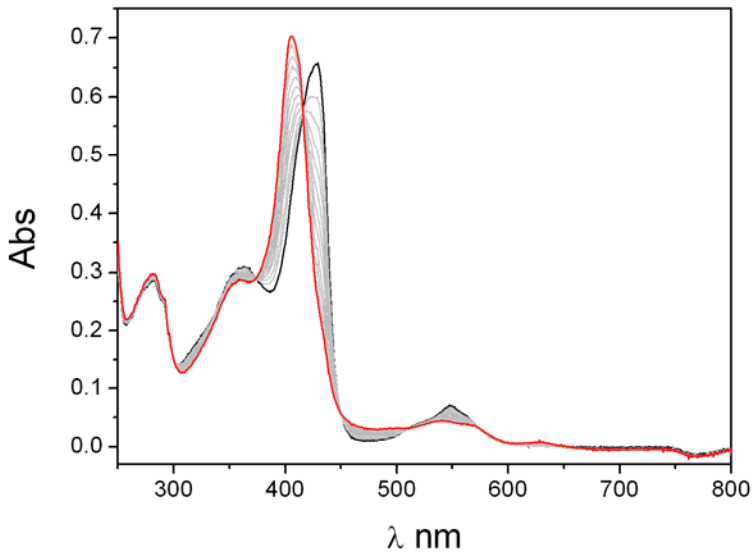

Figure 5.2 The shift in the UV/vis spectrum upon mixing reduced SHP with nitrite. *5 μM ferrous SHP was assayed by adding 2 mM nitrite under anaerobic conditions at pH 7.5. The initial absorption spectrum (black line) migrated to the final spectrum (red line) over time (15 minutes).*

Scheme 5.1

$$SHP^{2+} + NO_2^- + H^+ \rightleftharpoons SHP^{3+}\text{-}NO + OH^-$$

$$SHP^{3+}\text{-}NO \longrightarrow SHP^{3+} + NO$$

$$SHP^{2+} + NO \longrightarrow SHP^{2+}\text{-}NO$$

$$2\ SHP^{2+} + NO_2^- + H^+ \longrightarrow SHP^{3+} + SHP^{2+}\text{-}NO + OH^-$$

The nitrite reductase activity of SHP was assayed by adding 2 mM nitrite

to 5 μM ferrous SHP under anaerobic conditions at pH 7.5. The supposed mechanism is shown in Scheme 5.1 above. As shown in Figure 5.2, when nitrite was added the spectrum of SHP changed over time from the pure ferrous SHP to a mixture of species. This is illustrated by the spectrum shown in Figure 5.2. It can be seen that between 475 nm and 650 nm, four peaks are present in the final spectrum (Figure 5.3). These include the typical α and β peaks of SHP^{3+} (627 nm and 497 nm) and SHP^{2+}-NO (566 nm and 542 nm) (Figure 5.4). This therefore indicates a decrease in the amount of ferrous SHP which is replaced by ferric SHP and SHP^{2+}-NO. According to the general scheme for anaerobic nitrite reduction by heme proteins, the ferrous form reacts with nitrite to form a ferric-NO complex, followed by release of NO and production of the ferric form. The NO produced may then quickly and tightly bind to ferrous heme iron, resulting in a mixture of SHP^{3+} and SHP^{2+}-NO.

These results indicate that SHP may have nitrite reductase activity *in vitro*. Measurement of this activity was then carried out by using of MV assaysas, described in section 2.9.8, and the kinetic parameters found to be K_m = 28 μM, k_{cat} = 0.3 s^{-1}, and $k_{cat}/K_m = 1.1 \times 10^4$ $M^{-1}s^{-1}$.

Besides the steady-state kinetic studies, pre-steady-state kinetics were also investigated by the stopped-flow method. In addition to wild-type SHP, the N88A mutant has been studied. As shown in Figure 5.5, when 5 μM ferrous wild-type SHP or N88A SHP were mixed with 10 mM nitrite (at pH 7.5 under anaerobic conditions) the reactions could be monitored by the absorbance change at 400 nm. The black line in Figure 5.5 is the absorbance change upon wild type SHP reaction with nitrite and is fitted to a double exponential function, while the red trace indicates the N88A mutant's reaction. As the graph shows, the reaction of ferrous N88A with nitrite is much quicker than the same reaction in wild type SHP. This indicates that steric hindrance, due to the presence of the asparagine heme ligand, could be one reason for its low nitrite reductase activity.

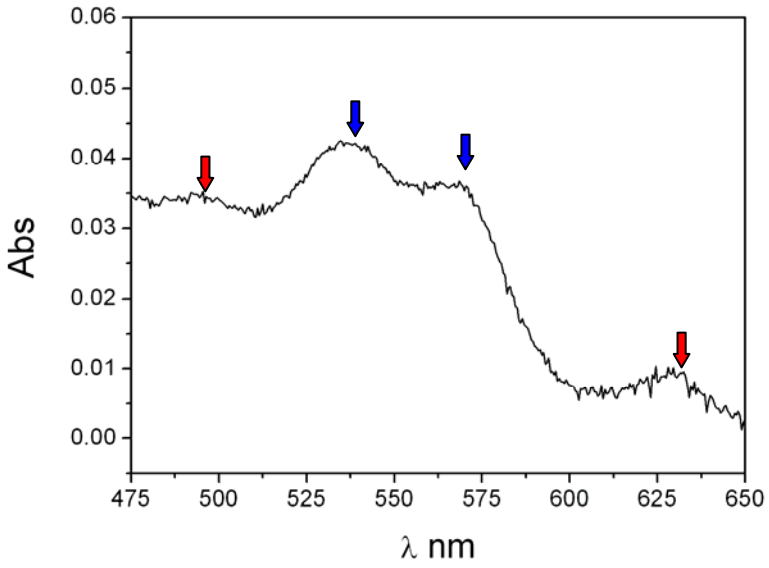

Figure 5.3 Final UV/vis spectrum upon mixing reduced SHP with nitrate. *Figure shows the final spectrum of mixing pure ferrous SHP with 20 mM nitrate with 10 mM nitrite (at 100 mM KCl and 50 mM Tris pH 7.5 under anaerobic conditions). These include the typical α and β peaks of SHP^{3+} (627 nm and 497 nm) indicated by red arrow and SHP^{2+}-NO (566 nm and 542 nm) indicated by blue arrow.*

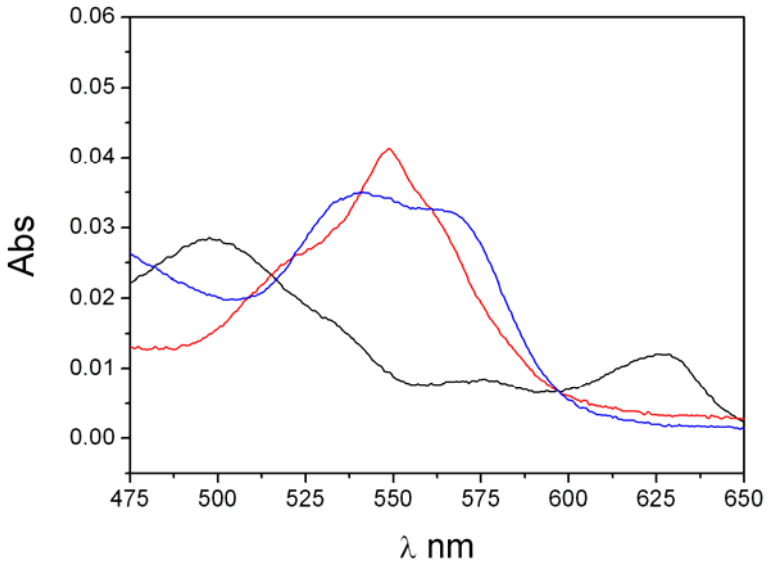

Figure 5.4 UV/vis spectra of various SHP forms. *Ferric SHP is shown in black; ferrous SHP is shown in red; ferrous-NO SHP is shown in blue.*

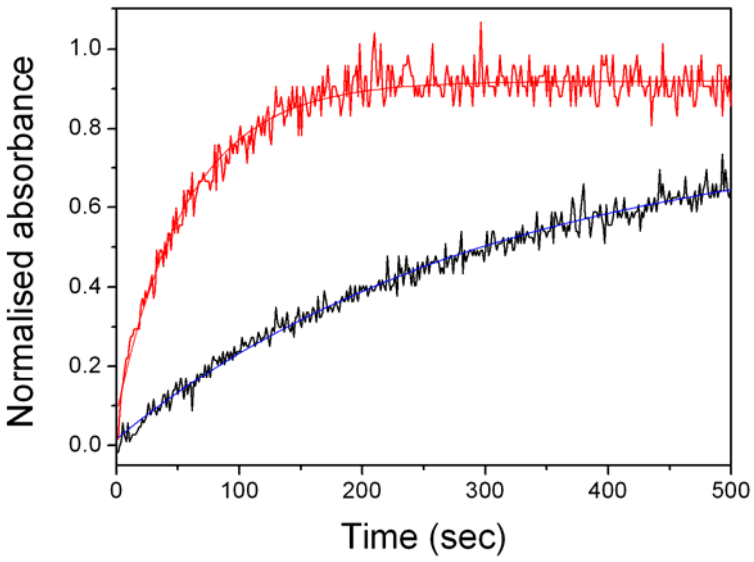

Figure 5.5: Reaction of SHP and N88A mutant SHP with nitrate. *Ferrous wild-type SHP or N88A SHP were mixed with 10 mM nitrite (at pH 7.5 under anaerobic conditions) and reactions were monitored at 400 nm. The reaction of wild-type is shown in black and that of N88A is shown in red.*

Comparing the results of the steady-state and pre-steady-state studies there are a couple of points of interest. Firstly, the values of both K_m and k_{cat} are small (28 μM and 0.3 s^{-1}). This implies that while nitrite has high affinity for SHP, the process of catalyzing conversion of nitrite to nitric oxide is slow. Secondly, results obtained with the N88A mutant reveal that steric hindrance may slow the whole reaction, Thus, compared with other nitrite reductases (e.g. *Pseudomonas* nitrite reductase which has a value for k_{cat}/K_m of $10^7 \sim 10^8$ $M^{-1}s^{-1}$) [158], SHP is less efficient ($k_{cat}/K_m = 1.1 \times 10^4$ $M^{-1}s^{-1}$). For this reason, SHP is unlikely to function physiologically as a nitrite reductase.

5.2.2 SHP^{2+}-NO can be converted to SHP^{2+} by ferrous DHC (NO reductase activity)

The results in Chapter 4 reveal that in aerobic conditions, ferrous SHP will react with

O_2 and subsequently with NO as an NO dioxygenase. However, in the absence of O_2, this is clearly impossible. As discussed in Chapter 3, SHP binds NO tightly and essentially irreversibly, so under anaerobic conditions SHP^{2+}-NO must be processed by some other mechanism.

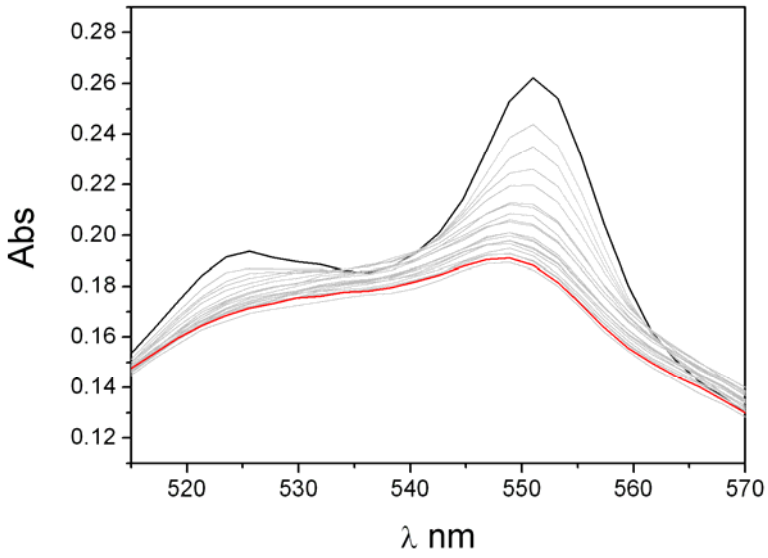

Figure 5.6: The shift in UV/vis spectrum shift upon mixing SHP^{2+}-NO with ferrous DHC under anaerobic conditions. *2μM SHP^{2+}-NO and 2μM DHC^{2+} were mixed in high salt conditions (10 mM Tris pH 7.0, 500 mM KCl). The initial absorption spectrum (black line) migrated to final spectrum (red line) over time (1 minute).*

The function of DHC is suggested to be as an electron donor to SHP [1]. Previous studies show that these two cytochromes form a tight complex in low salt conditions (K_d = 0.2 μM at 10 mM HEPES, pH 7.5, 25°C) and that ferric SHP can be reduced quickly (k_{et}=1.85 ± 0.11 × 10^7 $M^{-1}s^{-1}$, 500 mM KCl, 20 mM Tris, pH 7.2 and 10°C) by ferrous DHC. Since DHC is a potential 2-electron donor it is possible that the SHP^{2+}-NO complex can receive an extra electron from DHC. To measure this SHP^{2+}-NO was mixed with 5 μM DHC^{red} under anaerobic stopped-flow conditions as described in section 2.9.1, and the reaction monitored spectrophotometrically. Figure 5.6 shows the spectral changes over time. This indicates that an electron was transferred from fully-reduced DHC to SHP^{2+}-NO. Because NO is the only potential

electron acceptor in this reaction, it is possible that this process represents NO reduction *via* SHP. As Scheme 5.2 shows, the process is proposed to involve the formation of an SHP^{2+}-NO^- complex, followed by NO^- release. Subsequent reaction of two NO^- molecules with two protons would then generate N_2O and a water molecule.

Scheme 5.2 the model of SHP/DHC system reduce NO

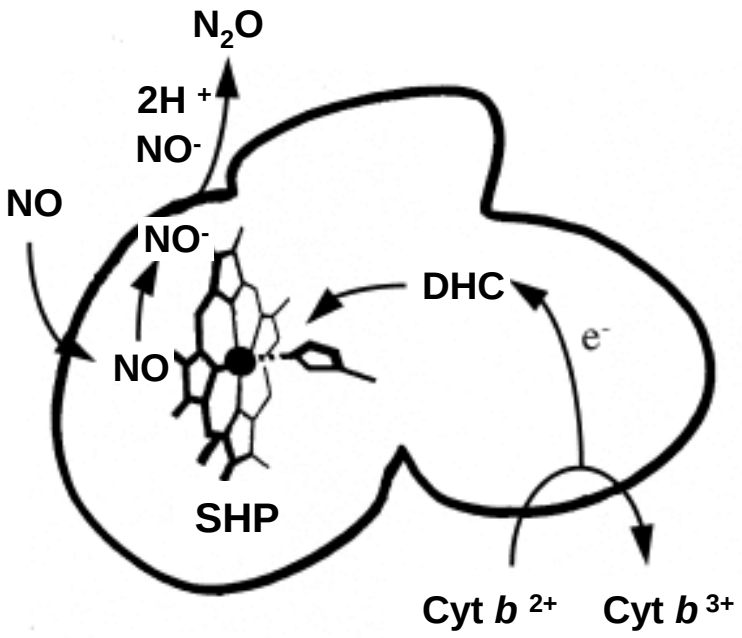

DHC displays an isosbestic point (between oxidized and reduced forms) at 431 nm in the UV/vis spectrum. Thus, this wavelength was used to monitor the reaction of SHP^{2+}-NO. As shown in Figure 5.7, the absorbance increases rapidly and then slowly decreases. When this change in absorbance over time is plotted, the curve reveals a double exponential trace with $k_1 = 0.17\ s^{-1}$ and $k_2 = 1.5 \times 10^{-3}\ s^{-1}$. This indicates that SHP^{2+}-NO quickly receives an electron from ferrous DHC to form the SHP^{2+}- NO^- complex (the fast phase), and then releases NO^- (the slow phase).

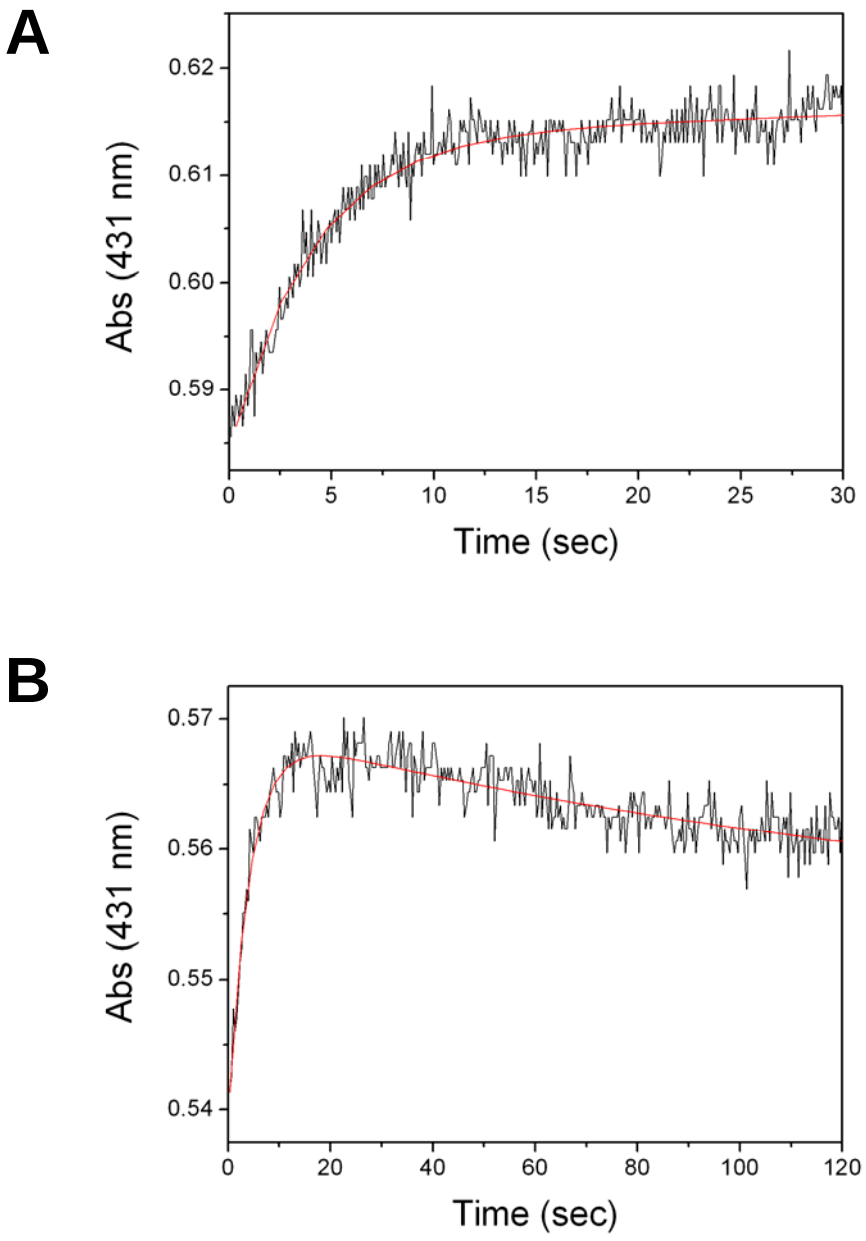

Figure 5.7: Reaction of SHP^{2+}-NO with ferrous DHC. *The reaction of SHP^{2+}-NO with ferrous DHC was monitored at 431 nm (black line). The trace was fitted to a double exponential function (red line).*

5.3 Discussion

Why is the anaerobic function of SHP important?

Some bacteria can respire and survive in both aerobic and anaerobic conditions. These bacteria can utilise not only oxygen as a terminal respiratory electron acceptor but also other species such as Fe(III), Mn(IV), sulfate, fumarate, DMSO and nitrate. According to the results of a micro-array study, mRNA levels of SHP were found to be significantly up-regulated (10-fold) under anaerobic conditions and using nitrate as the electron acceptor [4]. It has therefore been proposed that SHP may be be involved in nitrate metabolism.

Is SHP a nitrite reductase?

Microbiologically, nitrate can be reduced to nitrite by nitrate reductase. The nitrite formed can then subsequently be reduced by nitrite reductase, of which there are several classes. One of these, the pentaheme *c*-type cytochrome NrfA, can reduce nitrite to ammonia in a 6-electron process [159]. In contrast, the cytochrome cd_1 nitrite reductase can convert nitrite to NO or N_2O [82]. Furthermore, some nitrite reductases can only convert nitrite to nitric oxide in a single-electron process. Examples of these are NIR (a copper containing enzyme) or neuroglobin (a monoheme protein).

If SHP is involved in nitrate metabolism then nitrate, nitrite or nitric oxide could possibly be a substrate. Although it has been demonstrated that SHP is able to catalyse the reaction of O_2 with nitric oxide to form nitrate, this cannot occur under anaerobic conditions [5]. SHP up-regulation under anaerobic conditions with nitrate [4] indicates that SHP is likely to have some oxygen-independent function. As the results in this chapter show, ferrous SHP is able to reduce nitrite to nitric oxide (Figure 5.3). The catalytic efficiency of SHP (k_{cat}/K_m) is considerably lower than other nitrite reductases. This infers that although SHP can reduce nitrite *in vitro*, it is unlikely to function as a nitrite reductase *in vivo*. Further to this low catalytic activity, the fact that the product of nitrite reduction, nitric oxide, binds to ferrous SHP tightly and irreversibly inhibits its enzyme activity. For these reasons, SHP is not a good

candidate as a physiological nitrite reductase.

Could SHP be a nitric oxide reductase?

The high affinity of SHP for nitric oxide leads to the question of whether SHP can catalyse any reaction of nitric oxide. It is reported in Chapter 4 that SHP has NO dioxygenase activity. The flavohemoglobin, HMP, which functions as an NO dioxygenase, is also reported to function anaerobically as a nitric oxide reductase. In this process HMP^{2+}-NO releases NO^- which reacts with another NO^- and two H^+ to yield N_2O and H_2O [160-162]. Therefore, it is possible that SHP has the same anaerobic function as HMP.

SHP^{2+}-NO is a stable complex which does not auto-oxidise to SHP^{3+} and NO^-. Therefore, SHP alone cannot function as a nitric oxide reductase, but it is conceivable that the DHC/SHP system could carry out NO reduction. In section 5.2.2 it was found that SHP^{2+}-NO can get an extra electron from reduced DHC to form the SHP^{2+}-NO^- complex. Furthermore, the SHP^{2+}-NO^- complex is unstable and releases NO^- readily. Although the final product of this reaction has not been identified, the released NO^- is suggested to react with the other NO^- and $2H^+$ and finally become N_2O. Thus, although SHP is not a nitric oxide reductase, the SHP/DHC complex could be.

Is SHP a nitric oxide signaling protein?

Neuroglobin, like SHP, demonstrates poor nitrite reductase activity. Furthermore, reduced Ngb tends to react with NO to form the inactive Ngb^{2+}-NO complex. Therefore, Ngb is not thought of as a nitrite reductase. However, although there is no strong evidence yet, Ngb was suggested to generate NO as a signaling molecule *in vivo* [163]. Due to the high affinity of reduced Ngb for NO it is possible that this process involves association of Ngb^{2+}-NO with some other protein in a way not observed for the NO-free neuroglobin. In this event it may not be necessary for Ngb to have high nitrite reductase efficiency.

As the results show in this study, SHP can generate NO by reducing nitrite, although the reaction is very slow. Therefore it is unlikely to be a nitrite reductase, but may be a nitric oxide signalling protein. According to the gene map, *shp* is neighboured by *dhc*, *cyt b*, and a histidine kinase. This situation is similar to another *Shewanella* monoheme protein, H-NOX (Heme-Nitric oxide/OXygen binding) [164], which regulates the auto-phosphorylation activity of the histidine kinase encoded alongside H-NOX. Thus, if SHP is also a NO signalling protein and regulates the histidine kinase activity, it does not need good nitrite reductase activity. However, more studies are needed to support this hypothesis.

5.4 Conclusions

SHP can reduce nitrite to generate NO *in vitro*, but its catalytic efficiency is perhaps too low to be considered a nitrite reductase *in vivo*. Although this nitrite reductase activity cannot compete with NIR or NrfA, it is still possible to reduce nitrite to generate NO that might be involved in NO signaling. Furthermore, ferrous SHP can bind but not reduce nitric oxide. Instead, the SHP/DHC complex reveals NO reduction ability. Thus, the SHP/DHC system may function as a means of NO elimination in anaerobic conditions.

Chapter VI

Phenotype studies of SHP

6 Phenotype studies of SHP

6.1 Introduction and Aims

Homologues of SHP have been identified in 38 bacterial species including *Shewanella oneidensis* and *Rhodobacter sphaeroides*. In addition to the conservation of SHP primary structure in *Shewanella oneidensis* and *Rhodobacter sphaeroides*, in both bacteria the encoding genes are on operons which also encode DHC and a cytochrome *b* (supplementary). Thus, it is possible that the function of SHP could be the same in these two bacteria.

The upregulation of mRNA levels for these three proteins in *Shewanella* oneidensis grown with nitrate as the terminal electron acceptor [4] leads to the possibility of their involvement in nitrate metabolism. Investigations of this potential role using biochemical methods are described in Chapters 4 and 5. Due to the availability of crystal structures for *Rhodobacter* SHP (in the ferric, ferrous, and ferrous NO-bound forms) [3] and DHC [1], these proteins were chosen as the subjects of biochemical studies.

The finding that SHP has NO dioxygenase activity is reported in Chapter 4. If this nitric oxide dioxygenase activity is physiologically-relevant, rather than an *in vitro* artificial function, an SHP knock-out strain should reveal an NO-sensitive phenotype. Due to existing expertise in working with *Shewanella* MR-1 and the fact that the previous microarray study was carried out using *Shewanella* MR-1 [4], it seemed suitable to use knockouts in this bacterium to carry out these phenotypic studies. Therefore, a *Shewanella* MR-1 knockout strain was created by Dr. L. Cooper (section 2.1), in which the gene encoding SHP was disrupted. In this chapter, the use of this knockout strain and *Shewanella* WT to ascertain a physiological role for SHP is reported.

6.2 Results

6.2.1 Growth in LB liquid culture

The mRNA level of SHP is markedly up-regulated by growth in the presence of nitrate [4], and SHP has been proposed to be an NO dioxygenase (chapter 4). To assess the physiological relevance of this finding nitrate, nitrite, or NO saturated buffer were added to the culture media of *Shewanella* WT and its knockout strain during log phase growth.

6.2.1.1 Nitrate and nitrite addition under aerobic conditions

Various concentrations of nitrate and nitrite were added to *Shewanella* WT and SHP knockout strain cultures during log phase growth, as described in section 2.11. The highest concentrations used were 100 mM for nitrate and 1 mM for nitrite The OD_{600} was used to monitor growth. All aerobic samples grew with similar growth curves. No significant difference could be found between wild type and knockout strains.

6.2.1.2 Nitric oxide addition under aerobic conditions

As Figure 6.1 shows, the growth curves of *Shewanella* WT and SHP knockout strain are very similar when they are cultured in LB medium at 30^{o}C. Under these conditions NO was added to both culture media (WT and knockout) to a concentration of 100 μM. Compared with wild type, growth of the SHP knockout strain is obviously slower in the first 30 minutes (Figure 6.1).

In the same culture conditions, 1/1000 culture medium volume ratio of 4 mM NO-saturated buffer was added per 1 hour into wild type and SHP knockout culture mediums. As the results show (Figure 6.2), growth of both NO-supplemented cultures are slower than the control groups (buffer added only), with the SHP knockout strain growing more slowly than the wild type.

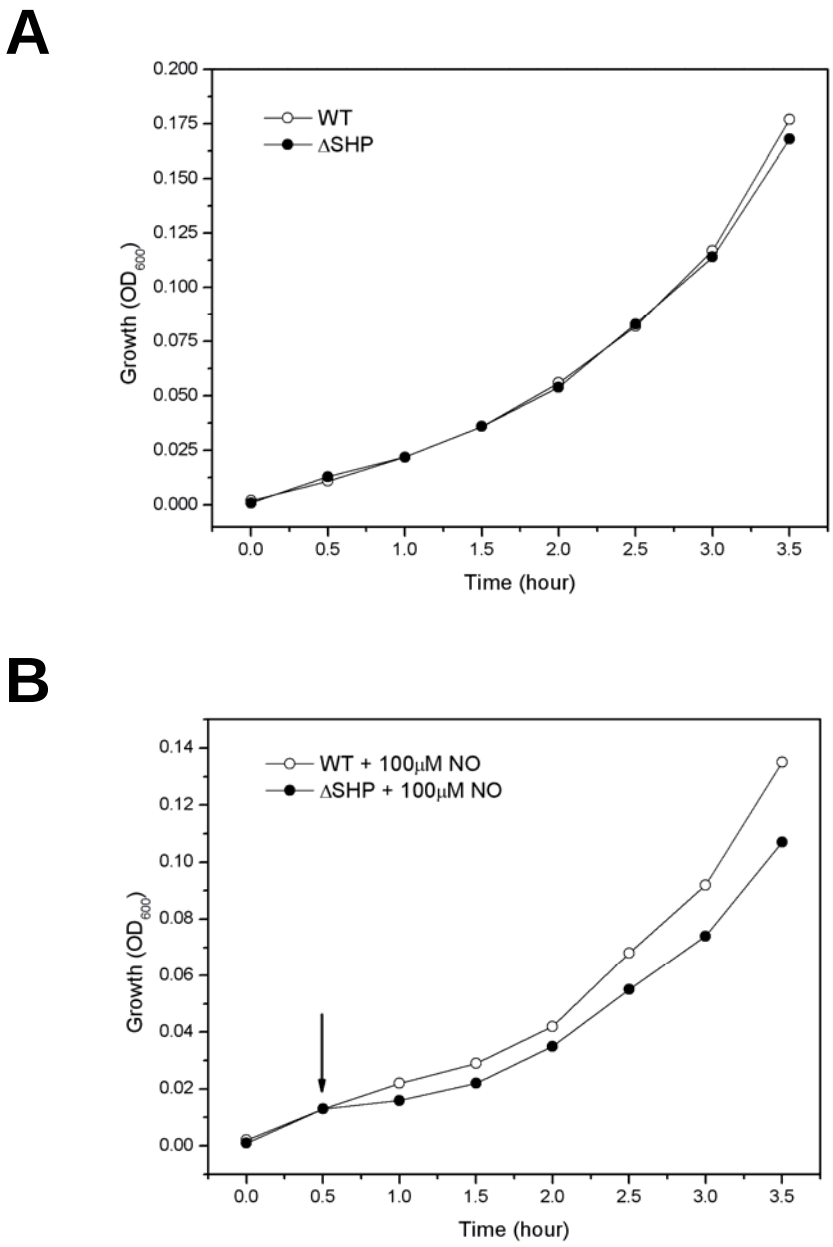

Figure 6.1 Response of Shewanella wild type and SHP knockout strains to nitric oxide in LB media. *(A) Shewanella MR-1 and SHP knockout strains were aerobically grown in LB medium. Growth curves were monitored at 600 nm per 30 minutes. (B) NO saturated buffer was added into cultures to final 100 μM (indicated by the arrow).*

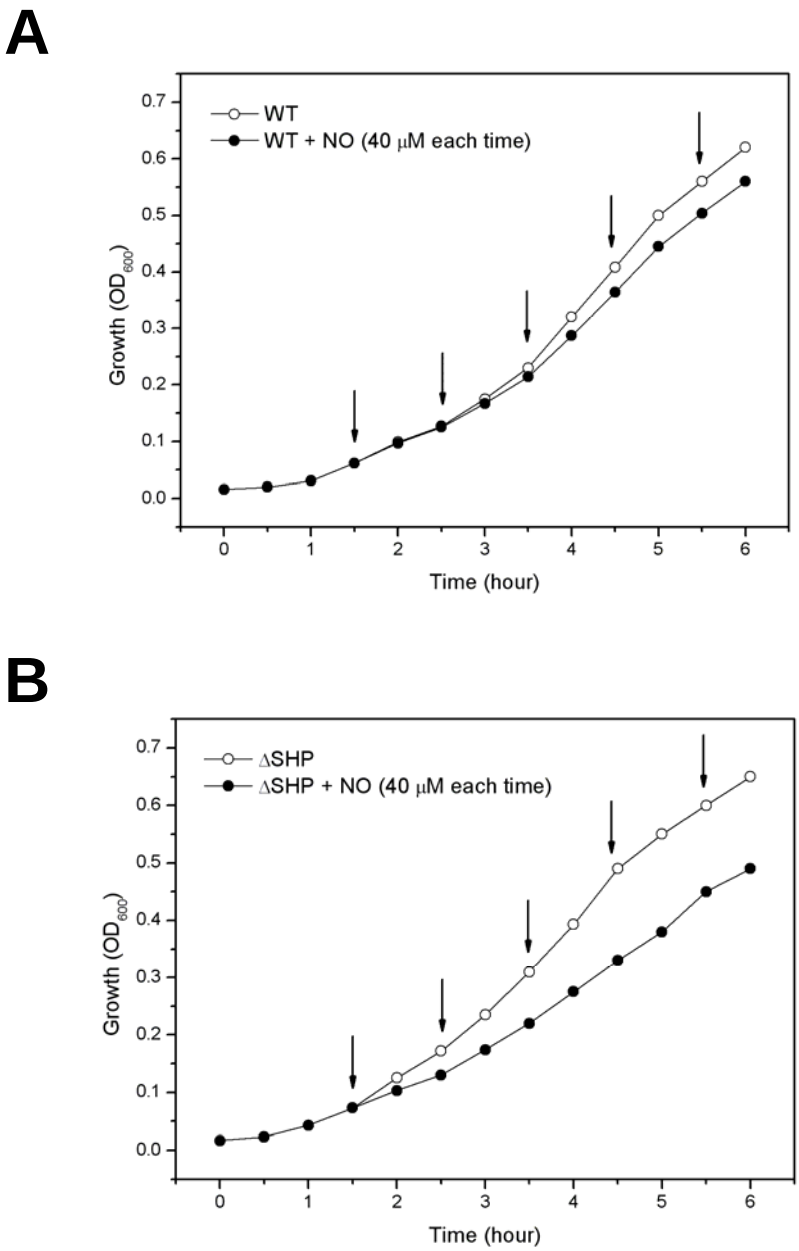

Figure 6.2 Response of Shewanella wild type and SHP knockout to nitric oxide. Shewanella MR1 wild type *(A) and SHP knockout (B) strains were aerobically grown in LB medium. 40 μM NO (final solution concentrate) was added into cultures at one hour intervals (as indicated by the arrows). Growth curves were monitored at 600 nm every 30 minutes.*

6.2.2 Phenotype testing

The results in section 6.2.1 show that in liquid cultures *Shewanella* WT reveals a higher NO tolerance ability than the SHP knockout mutant. Therefore a further experiment was carried out to confirm whether the SHP knockout strain is more NO-sensitive.

Bacterial lawns of *Shewanella* WT and SHP knockout strains were prepared as described in chapter 2.11. As Figure 6.3 shows, after 36 hours culture under aerobic conditions a clear zone appeared on the lawn of the SHP knockout plate. In the case of the wild type strain it can be seen that there is more bacterial growth further away from the source of NO, and compared with the knockout strain wild type does not form an obvious clear zone.

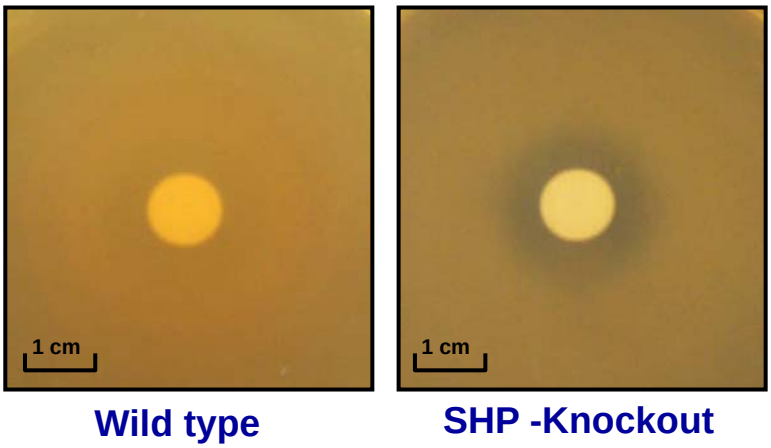

Figure 6.3 Response of Shewanella wild type and SHP knockout to nitric oxide on LB agar plates. *Bacteria lawns of Shewanella wild type and SHP knockout were prepared on LB agar plates. Central white circles are sterilized filter paper soaked with sodium nitroprusside. The bacteria appear yellow-brown, and clear zone surrounding the filter paper indicates no bacterial growth.*

The same experiment was carried out under anaerobic conditions. In this experiment, 50 mM fumarate is added to the LB agar plates. The bacterial lawn plates were

prepared under aerobic conditions and then placed in anaerobic conditions. After 60 hours in the presence of sodium nitroprusside, both the *Shewanella* WT and SHP knockout strains had a clear zone in the centre with similar size. Unfortunately, the bacteria lawns are too thin to be observable in a photograph (Figure 6.4).

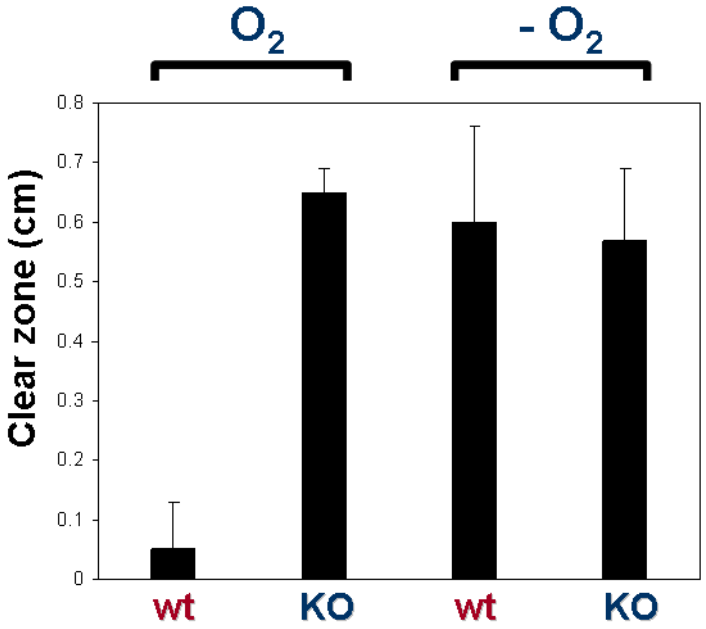

Figure 6.4 Aerobic and anaerobic response of Shewanella wild type and SHP knockout to nitric oxide. *Bacterial lawns of Shewanella wild type and SHP knockout were prepared on LB agar plates. Pieces of sodium nitroprusside-soaked filter paper were used to cover the central area of the bacterial lawn. After incubation at 30 °C, clear zones appeared around the filter papers indicating that bacteria had been killed. This indicates that the clear zone appeared on the bacterial lawns during both aerobic and anaerobic incubation. Error bar here is standard deviation.*

6.3 Discussion

Is SHP an NO dioxygenase?

As the results in this chapter show, whether in liquid culture or in bacterial lawn experiments, *Shewanella* WT reveals higher NO tolerance than the SHP knockout strain under aerobic conditions. This suggests that in the absence of SHP, *Shewanella*

is more susceptible to NO damage. This evidence supports a role for SHP in NO detoxification. Under anaerobic conditions, the bacterial lawn experiments show that *Shewanella* WT and SHP knockout are not obviously different. Both are very sensitive to NO (released by sodium nitroprusside). Therefore, it is possible that the NO detoxification ability is oxygen-dependent. Thus, SHP could be a NO dioxygenase, using the mechanism described in the chapter 4.

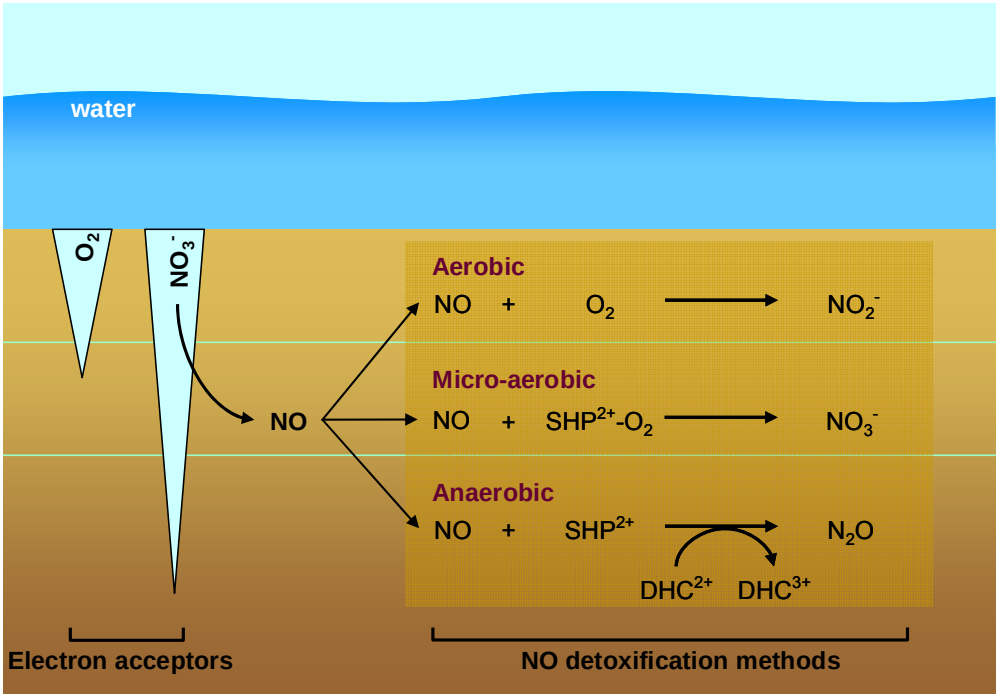

Figure 6.5 Model for NO detoxification in various oxygen concentration conditions. *Electron acceptors oxygen and nitrate are available to the symbionts in the sediment layer* [165].

Furthermore, in the aerobic bacterial lawn experiments, different phenotypes are only observed when culture plates were sealed. If the culture plates were not sealed, no clear zone could be found on lawns of both wild type and SHP knockout strains. This finding indicates that NO detoxification is optimized under micro-aerobic conditions. When the oxygen concentration is too high, NO may directly react with oxygen before it can damage the cell [166]. Therefore NO-mediated cell damage is most likely

under micro-aerobic conditions. This result makes sense because *Shewanella* species are generally found in freshwater or deep-sea sediments. As Figure 6.5 shows, the environment of the lake sediment is nitrate-rich and micro-aerobic [165]. In such conditions, the NO dioxygenase activity of SHP could protect the bacteria.

Is SHP an NO reductase?

HMP (flavohemoglobin) is also an aerobic NO dioxygenase which protects *E. coli* from nitric oxide toxicity [160]. Anaerobically, HMP can act as an NO reductase [161]. Earlier experiments showed that the expression of HMP is up-regulated by the presence of NO under both aerobic and anaerobic conditions [167]. Phenotypic studies have also been reported [168]. These show that under aerobic conditions wild type *E. coli* grows more quickly than the *hmp* knockout strain when NO is added. However, under anaerobic conditions the wild-type strain does not reveal such obvious NO protectant ability [169]. It is possible that HMP has NO detoxification ability both aerobically and anaerobically, but the efficiency of NO reduction under anaerobic conditions is not as great as that of NO dioxygenation under aerobic conditions. Consequently it is not straightforward to assess the NO protection phenotype under anaerobic conditions.

In chapter 5, the *in vitro* NO reductase ability of the SHP/DHC complex was proposed. However, the results of the anaerobic phenotypic studies in this chapter do not prove that SHP also protects *Shewanella* from nitric oxide under anaerobic conditions. Thus, anaerobically, SHP seems to lack NO detoxification activity. The reason for these different results *in vitro* and *in vivo* is possibly the same as with HMP described above. The NO elimination efficiency due to NO reduction by the SHP/DHC complex is not as great as the NO dioxygenation efficiency of SHP. As a result, when the same amount of NO (from sodium nitroprusside) was used in both aerobic and anaerobic experiments, different phenotypes are only observed under aerobic conditions. Therefore, although the anaerobic phenotypic studies do not prove that SHP is an NO reductase, they do not totally rule out this possibility.

6.4 Conclusion

Aerobically, the *Shewanella* SHP knockout strain reveals a lower NO tolerance ability than *Shewanella* WT. Therefore, the function of SHP could be as an NO dioxygenase *in vivo*. However, anaerobically, no remarkable phenotype difference was found between knockout and wild type strains. Thus, SHP can not be proved to have the ability to detoxify NO anaerobically.

Chapter VII

The Role of Asparagine 88

7 The Role of Asparagine 88

7.1 Introduction and Aims

Cytochromes *c* are normally defined as electron transfer proteins having one or more *c*-type heme groups. In these proteins the heme is covalently bound *via* two thioether bonds involving sulfhydryl groups of cysteine residues. Based upon their structures, they are divided into 4 classes (as described in section 1.3.1). Class I cytochromes *c* are monoheme proteins comprised of approximately 80-120 amino acids. Within this class, one of the axial heme iron ligands is always a histidine residue, while the other is either histidine or methionine [170, 171].

SHP (*sphaeroides* heme protein) is a monoheme cytochrome *c* of approximately 13 kDa molecular weight. This was initially isolated from *Rhodobacter sphaeroides* and its structure was reported in 2000 [3]. Based upon this structure, SHP is clearly a class I cytochrome *c* with one axial histidine ligand to the heme iron (CXXCH). Unusually, however, it has an asparagine residue as the other axial heme ligand, and as such is unique among cytochromes *c*. For this reason it may be assumed that the asparagine plays a special role.

Although asparagine is only found as a heme ligand in SHPs, this asparagine is not conserved throughout all SHP sequences [2]. Using the NCBI database [172], 43 highly-conserved SHP sequences can be found with significant homology. Ignoring two duplicates from *R. sphaeroides* and three cytochrome *b* sequences from *Magnetospirillum magnetotacticum*, this leaves SHP homologues in 38 different species from the α-, β-, and γ-proteobacteria that include *Thauera*, *Azoarcus*, *Burkholderia* and *Shewanella*. All these homologues have a similar size (~120 amino acids) and a conserved cytochrome *c* heme binding motif (CXXCH), but only 36 of the 38 have the motif containing the conserved asparagine ligand (W-F/L-X-R-N). Of the remaining two homologues' sequences (and in addition to the histidine ligand)

one is predicted to have an aspartic acid as a heme ligand (from *Magnetospirillum gryphiswaldense*), while the other (cytochrome *c″* from *Methylophilus methylotrophus*) uses a second histidine residue, as confirmed by its crystal structure [85, 173, 174].

Methylophilus methylotrophus cytochrome *c″* is very similar, both in terms of amino acid sequence and structure, to *Rhodobacter sphaeroides* SHP [3, 5, 85, 173]. Thus, it is considered a member of the SHP family. However, the different heme iron ligation raises the question of whether cytochrome *c″* also has nitric oxide dioxygenase activity.

In previous studies SHP has been shown to accept electrons from its genomic partner DHC (diheme cytochrome *c*), and a recent report reveals that SHP has nitric oxide (NO) dioxygenase activity [5]. The mechanism of NO dioxygenation is proposed to involve O_2 binding to the reduced (ferrous) SHP to form the oxy-ferrous protein. Following this, its conjugate superoxy-ferric form reacts with NO to generate nitrate and ferric SHP. Such a mechanism is similar to that proposed for another NO dioxygenase, flavohemoglobin (HMP). The difference between the two proteins is that the HMP heme iron receives electrons from the flavin in an intramolecular electron transfer step. The presence of the unique asparagine heme ligand raises the possibility that it plays some important role in NO dioxygenation. In order to elucidate this role, five site-directed mutant forms of SHP (N88A/D/H/M and K) have been constructed and characterised with respect to their NO dioxygenation activity. Substitution by aspartic acid and histidine is designed to mimic the sequences of the homologues mentioned above. The choice of methionine and lysine seeks to introduce other recognised heme ligands, while the N88A substitution may be seen as an analogue of the reduced state of SHP, in which the asparagine no longer binds to the iron.

This chapter reports the reduction potentials, electron transfer characteristics, EPR spectra, and O_2 binding characteristics of wild-type SHP and its mutant forms, and

discusses the potential role of the asparagine ligand.

7.2 Results

7.2.1 The purification of SHP mutants

Wild-type *Rhodobacter sphaeroides* SHP and N88X mutant forms were over-expressed in *E. coli* (BL21(DE3)) and purified using the method described in Chapter 2. The validity of the proteins was confirmed by SDS PAGE and heme staining, and the purity confirmed by Coomassie blue staining and UV-visible spectrophotometry. Using UV/Vis spectrophotometry, the ratio of the absorbances of the Soret band (A_{401}) and the peak at 280 nm was calculated. Ratios of $A_{401}/A_{280} >$ 4.3 are indicative of pure protein. The final yield of purified SHP (wild-type) is about 1 mgl^{-1} of cell culture. The yields of the purified N88A and N88H enzymes are about 0.5 mgl^{-1}, while those of the N88M and N88K are only 0.1 mgl^{-1}. However, the N88D enzyme can be obtained in relatively high yields of over 5 mg of pure protein per litre of culture. Once purified the proteins remain stable over the long term at -20 ^{o}C.

7.2.2 Spectral characteristics of SHP mutants

Generally speaking the UV/vis spectrum of ferric cytochromes has a major absorption peak around 410 nm (Soret peak) and other minor absorbances around 550 nm (α peak). In the ferrous form the Soret peaks tend to shift to longer wavelengths (~420-430 nm), and two other minor absorptions around 500-550 nm (α and β peaks) appear. Each cytochrome has a unique UV/vis spectrum and the positions of the Soret, α and β peaks may be used to distinguish different heme prosthetic groups [10].

	Fe^{III}			Fe^{II}		
	Soret	**α**	**β**	**Soret**	**α**	**β**
WT	401.0	627.0	497.0	426.0	548.0	
N88A	400.5	626.0	494.0	420.0	550.0	
N88H	403.0	625.0	495.0	420.5	550.0	
N88D	400.5	616.0	490.0	414.0	550.0	
N88K	406.0	523.0		420.0	549.5	
N88M	400.0	631.5	507.5	420.0	553.5	525.5

Table 7.1: Wavelength maxima of SHP and five N88X variants *(10 mM Tris, pH 7.0, 25 ^{o}C)*

As table 7.1 shows, ferric SHP and its mutants reveal similar Soret peaks around 401 nm at pH 7.0, which is at a shorter wavelength than the ferric Soret peaks of most cytochromes (410 nm). Most of the SHPs also have similar α and β peaks (around 625 nm and 500 nm), but the N88K mutant only has a α peak at 523 nm. The Soret peaks of ferrous SHP and all mutant forms are around 420 nm - 426 nm with an obvious shoulder, with the exception of the N88D mutant (Figure 7.1).

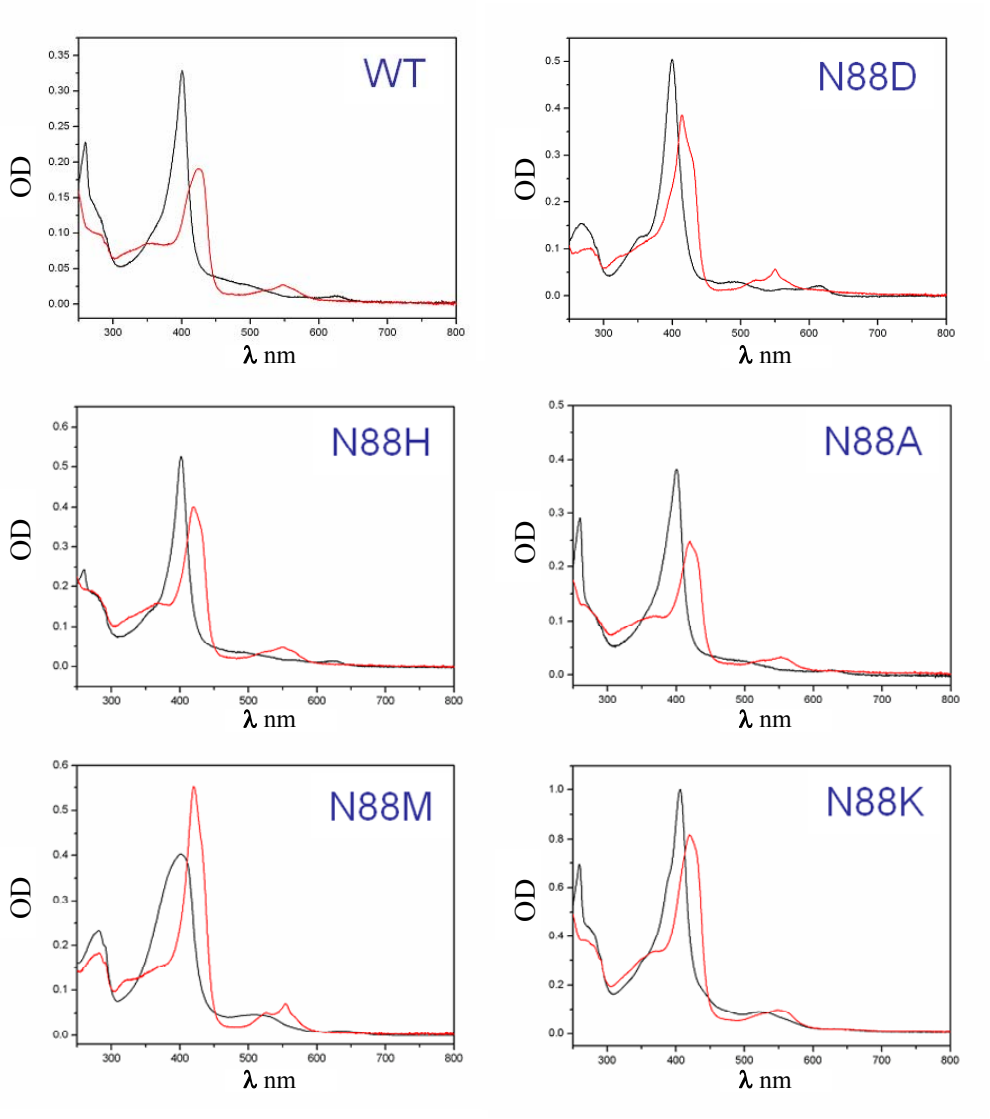

Figure 7.1: The UV-Vis spectra of SHP and five N88X variants. *The UV-Vis spectra of SHP^{3+} (black lines) and SHP^{2+} (red lines).*

The extinction coefficients for the ferric and ferrous Soret peaks were calculated by the pyridine hemochrome method [134]. In general these extinction coefficients are greater for the ferric protein (~80 $mM^{-1}cm^{-1}$) than for the ferrous state, with the exception of the N88M mutant (table 7.2). In the ferric form wild type SHP has the greatest extinction coefficient (129 $mM^{-1}cm^{-1}$), with those of the N88A/D/H/K mutants being around 100 $mM^{-1}cm^{-1}$.

SHP	oxidised		reduced	
	ε ($mM^{-1}cm^{-1}$)	relative intensity (%)	ε ($mM^{-1}cm^{-1}$)	relative intensity (%)
Wild type	129.2	100.0	81.0	100.0
N88A	137.5	106.4	91.5	109.3
N88D	93.9	72.6	74.0	87.4
N88H	104.0	80.5	71.8	88.6
N88M	53.8	41.6	83.5	91.3
N88K	98.0	75.8	70.8	103.1

Table 7.2: Extinction coefficient of the Soret peak in SHP and five N88X variants. *(10 mM Tris, pH 7.0, 25 ^{o}C)*

7.2.3 Ligand effects on redox potential

Previous studies have shown that SHP will accept electrons from DHC [5]. The ability of heme iron to accept electrons is highly dependent upon the reduction potential of the heme group, and this is greatly influenced by the nature of the axial heme iron ligand(s). Thus if the asparagine axial ligand to the heme iron is substituted, the redox potential is likely to be affected. The reduction potential of SHP and its Asn88-substituted forms were measured by the OTTLE method in 50 mM TrisHCl pH 7.0, 500 mM NaCl, 25 ^{o}C, and under anaerobic conditions. Wild type SHP has a reduction potential of -100 mV *vs* the standard hydrogen electrode (SHE), and this value is pH-independent between pH 6.0 and pH 8.0. The reduction potentials of the N88X mutant forms are raised by approximately 45, 120, 180 and 200 mV (N88H, H88A, N88K and N88M respectively). Conversely, the reduction potential of the N88D form is -405 mV, some 300 mV lower than that of the wild type protein. These reduction potentials vary in accordance with the electronegativity of sixth heme iron ligand. For example, aspartic acid is a very strong electron donor to the ferric heme iron, thus stabilising the ferric state and leading to the particularly low reduction potential of the N88D mutant (table 7.3). With the exception of the N88D mutant,

wild type SHP has the lowest redox potential, due to asparagine being less electron-withdrawing than histidine, alanine, lysine and methionine.

SHP	Redox potential (mV) vs SHE
N88M	103 ± 3
N88K	79 ± 2
N88A	19 ± 3
N88H	-55 ± 2
Wild type	-100 ± 2
N88D	-405 ± 2

Table 7.3: Redox potentials of SHP and five N88X variants. *Redox potentials were determined by OTTLE experiment, and all experiments were under the anaerobic condition with the buffer containing 100 mM Tris, pH 7.5, 500 mM NaCl, and at 25 ^{o}C. ± here is standard deviation of three observation.*

7.2.4 Ligand effects on oxygen and nitric oxide binding

7.2.4.1 k_{on} and k_{off} values for oxygen binding to ferrous SHPs

Like lots of heme proteins [175-177], SHP and its mutants can bind oxygen at the ferrous iron to form an oxy-ferrous complex [1]. The nitric oxide dioxygenase activity of SHP is proposed to involve reaction of the oxy-ferrous SHP with nitric oxide to generate nitrate and ferric SHP. Thus oxygen affinity should be important for SHP's enzymatic activity. Therefore, it is interesting to know what the effect of altering the axial heme ligand will have on the oxygen binding affinity. Stopped-flow analysis was used to obtain k_{on} and k_{off} values for O_2 binding (in 100 mM sodium phosphate pH 7.5, 10 ^{o}C). The results of this (table 7.4) indicate that the wild type, N88D, N88H and N88A SHPs have similar rate constants for oxygen binding rate constant (k_{on} = 0.17, 0.07, 0.29 and 0.22 $\mu M^{-1}s^{-1}$ respectively), while those for the N88K and N88M proteins are slightly greater (0.48 and 0.45 $\mu M^{-1}s^{-1}$ respectively). Compared to the obtained k_{on} values, the dissociation rate constants (k_{off}) are varied. The

oxy-ferrous complex of wild type, N88D and N88M have lower dissociation rate constants (3.2, 5.3, and 7.7 s^{-1} respectively) than observed for the N88H, N88A, and N88K mutant forms (62.3, 46.3 and 25.1 s^{-1} respectively).

	k_{on} ($\mu M^{-1}s^{-1}$)	k_{off} (s^{-1})	K_d (μM)
SHP-WT	0.17	3.2	18.8
N88D	0.07	5.3	75.7
N88H	0.29	62.3	214.8
N88A	0.22	46.3	210.5
N88K	0.48	25.1	52.3
N88M	0.45	7.7	16.9

Table 7.4: Kinetic constants for O_2 of wild-type SHP and five N88 variants. *The conditions were 100 mM sodium phosphate buffer pH 7.5, 10 ^oC.*

7.2.4.2 Nitric oxide binding to ferric SHP

From the crystal structure of ferric SHP from *Rhodobacter sphaeroides* it can be seen that the sixth axial heme ligand is bound to the heme iron, thus preventing nitric oxide binding. To ascertain whether there is a sixth ligand bound to ferric heme iron in the N88X mutant forms, their NO binding capabilities were tested. This was carried out as described in section 2.9.4. It was found that addition of 20 μM nitric oxide caused no spectral change in the case of wild type SHP and the N88D and N88H mutant forms, indicating no NO binding. However, in the presence of the same concentration of nitric oxide the spectra of the N88M and N88K proteins are clearly changed, indicating the formation of ferric nitrosyl complexes. The N88A mutant form also shows NO binding, but only at higher NO concentrations (≤ 100 μM) and with the spectrum indicating incomplete conversion to the ferric nitrosyl complex (Figure 7.2).

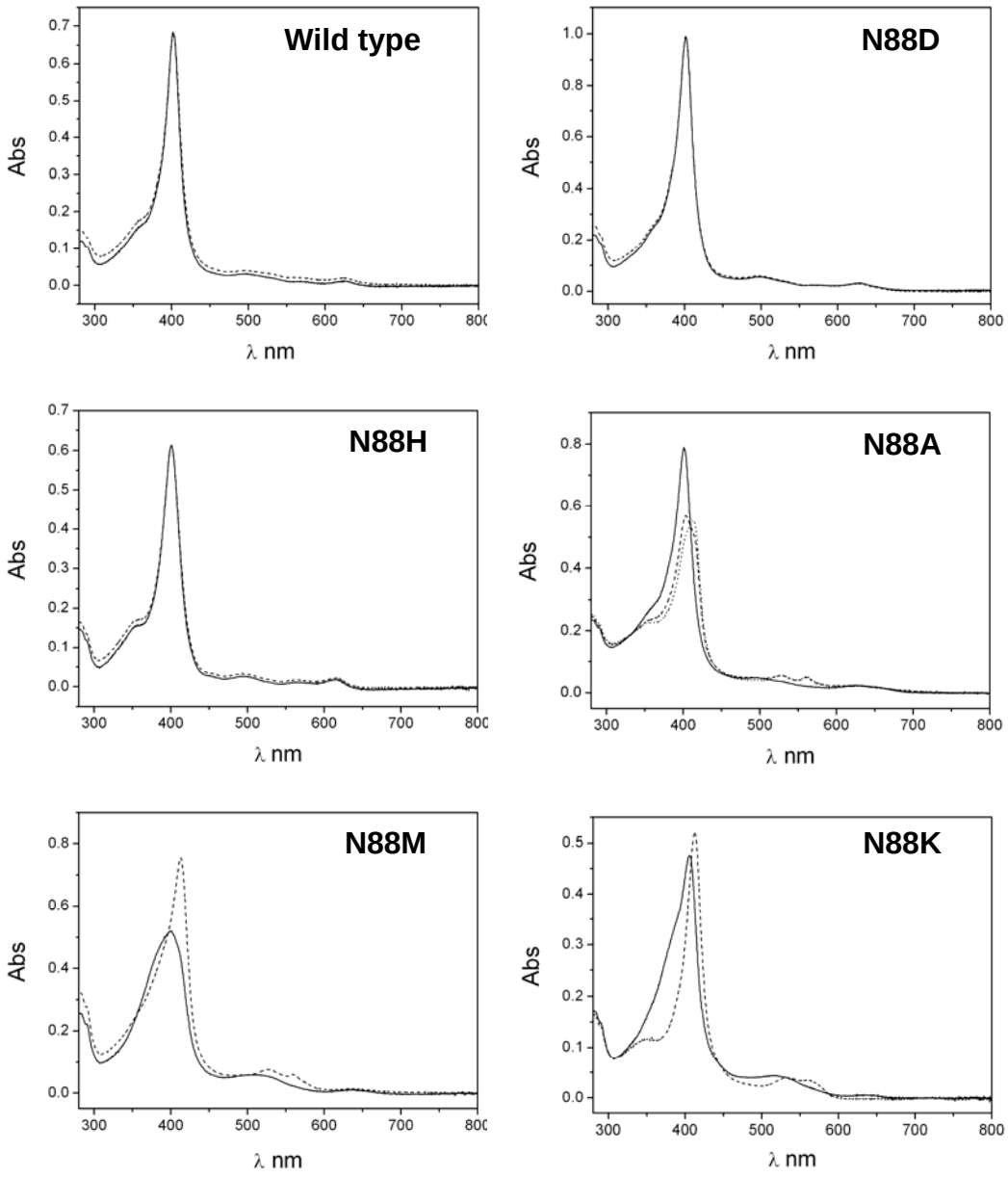

Figure 7.2: UV-Vis spectra of ferric SHP and five N88X variants with NO. *UV-Vis spectras of SHP^{3+} (solid lines) and SHP^{3+}-NO (dotted lines).*

7.2.4.3 The stability of oxy-ferrous form

Nitric oxide dioxygenation proceeds through the reaction of oxy-ferrous SHP with nitric oxide. Thus, a stable oxy-ferrous complex should be necessary for nitric oxide

dioxygenation. Like other oxygen binding cytochromes, the SHP oxy-ferrous complex slowly auto-oxidizes to produce the ferric form and superoxide at room temperature. Therefore it is interesting to know what effect the nature of the axial ligand has upon the stability of the oxy-ferrous complexes. As the data in the table 7.5 shows, the oxy-ferrous complex of wild type has the longest half life, up to 60 minutes in 100 mM phosphate buffer, pH 7.5, and 25°C. In the same conditions, the oxy-ferrous complexes of N88A, N88H, N88K, and N88M SHPs have shorter half lives (26, 31, 32 and 44 minutes respectively). However, in the case of N88D SHP the half-life is significantly shorter (0.1 minutes) in the same conditions.

SHP	Life time (min)	Rate of oxdization (s^{-1})
Wild type	60 ± 2	2.8×10^{-4}
N88D	0.10 ± 0.01	0.2
N88A	26 ± 3	6.5×10^{-4}
N88H	31± 1	5.4×10^{-4}
N88K	32 ± 2	5.2×10^{-4}
N88M	44 ± 2	3.8×10^{-4}

Table 7.5: Half-life and rate constants for the auto-oxidation of oxy-ferrous SHP and five N88X variants. *Ferrous SHP and N88X mutants were mixed with buffer containing 1 mM O_2 (100 mM sodium phosphate buffer, pH 7.5, 25 °C). The decay of oxy-ferrous complex was determined by following the absorbance change at the Soret peak.*

7.2.5 Ligand effects on electron transfer

Reduction of SHP by DHC must precede oxy-ferrous complex formation. Since the reduction potentials of the various SHP forms mentioned here range from 100 mV to -400 mV, it is of interest to see what effect the axial heme ligand has on the rate of electron transfer. Stopped-flow analysis was used to measure this, with ferric SHP (wild type or its mutants) being mixed with ferrous DHC in 100 mM Tris pH 7.5, 500 mM NaCl at 10 °C. The high salt concentration is used to avoid SHP and DHC forming a relatively long-lived complex, and to slow the process so that it occurs

within a measurable timescale. Figure 7.3 shows that oxidized SHP wild type, N88H, N88A, N88K, and N88M can rapidly receive an electron from reduced DHC [in the short time (0.2 sec)](Would it not be better to quote this as a rate?), but N88D SHP does not become reduced as quickly (Figure 7.3). This result is in line with the reduction potential of the proteins (N88D = -400mV, DHC = -240 mV and -310 mV) which make electron transfer thermodynamically unfavourable.

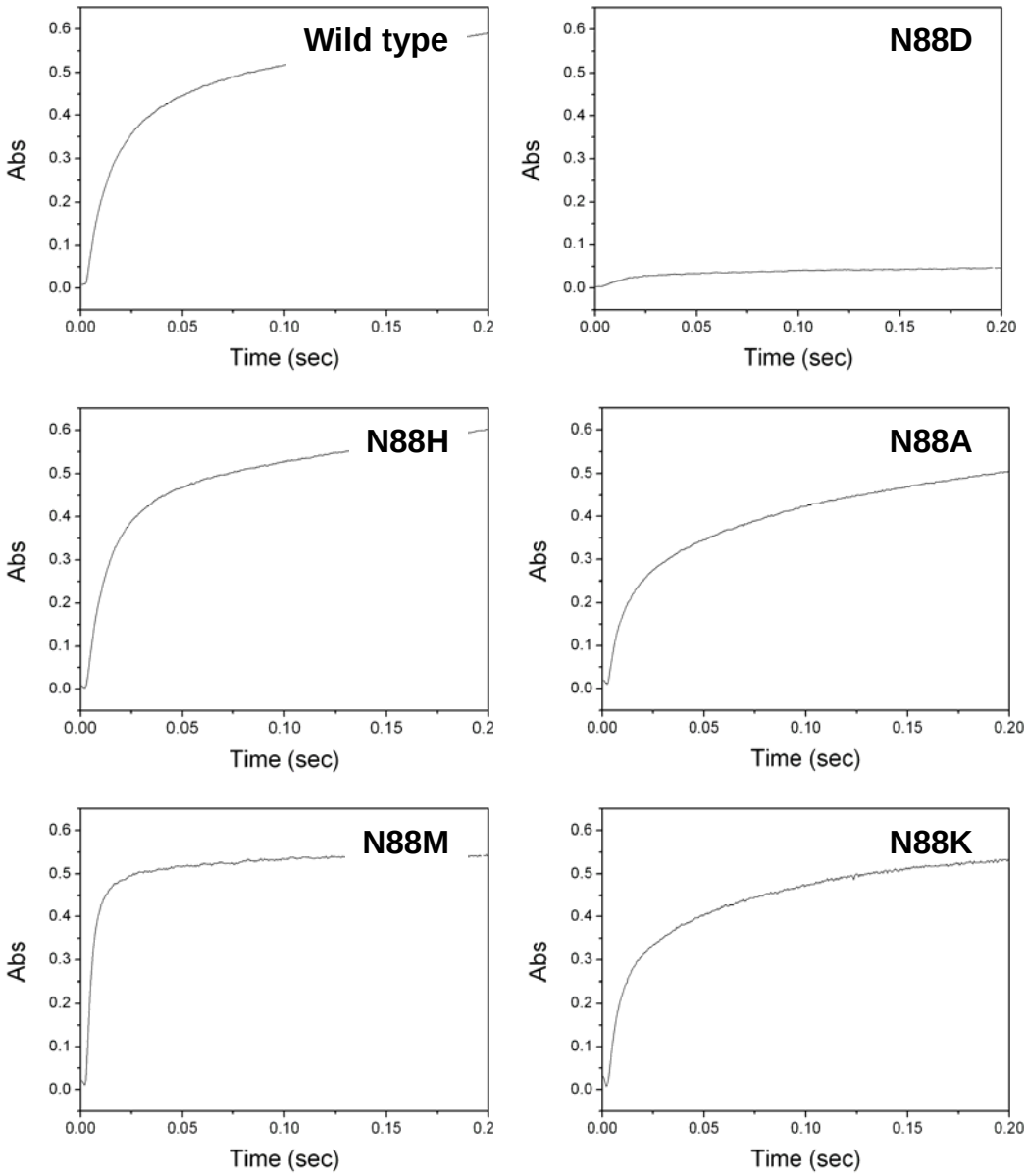

Figure 7.3: Kinetics of SHP and five N88X variants reduction by DHC.

7.2.6 Characterisation of *Methylophilus* cytochrome *c″* (obtained from Dr. Helena Santos)

The amino acid sequences of cytochrome *c″* from *Methylophilus methylotrophus* and *Rhodobacter sphaeroides* SHP show significant homology (32 % identity, 48 % similarity) [172]. Their structures are superposable (Figure 7.4), and in both the sixth heme ligand binds to the iron in the ferric form but is labile in the reduced from. These similarities suggest a similar function for the two proteins.

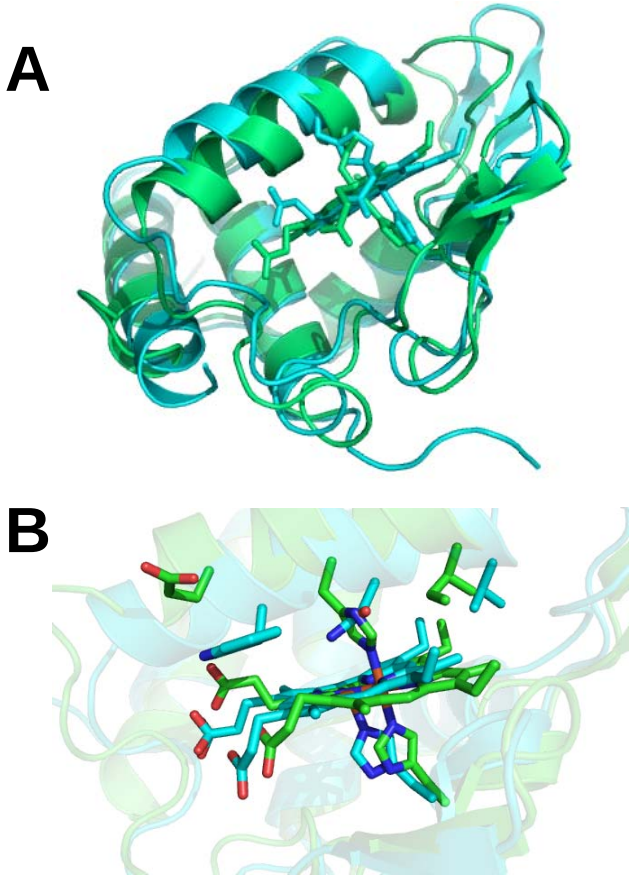

Figure 7.4: Overlay of the structure of cytochrome c″ from Methylophilus methylotrophus and Rhodobacter sphaerodies SHP. *(A) The full length SHP (green, 1DW0) is overlaid with full length cytochrome c″ (blue, 1OAE). (B) Overlay of the heme of cytochrome c″ from M. methylotrophus (light blue, 1OAE) and heme of SHP from R. sphaeroides (light green, 1DW0). Oxygen atoms are seen in red, nitrogen atoms in deep blue, and iron in orange. This Figure was generated using PyMOL (DeLano Scientific; http://pymol. sourceforge.net/).*

SHP	Life time (min)	Redox potential (mV)
N88D	0.1	-405
Wild type	60	-100
N88H	31	-55
N88A	26	19
N88K	32	79
N88M	44	103
MM cyt *c*	0.1	-43

Table 7.6: Comparison of redox potentials and half-lives of the oxy-ferrous complex. *(25 °C.)*

The reduction potential of *Methylophilus* cytochrome *c''* was determined by the OTTLE method (in 50 mM TrisHCl pH 7.0, 500 mM NaCl, 25 ^{o}C) under anaerobic conditions, and was found to be -43 mV (*vs* SHE; Figure 7.5, -60 mV at pH 7.0 in previous report [85]), while the reduction potential of SHP is -100 mV (*vs* SHE) under the same conditions. Interestingly, the potential of *Methylophilus* cytochrome *c''* shows strong pH dependence in the physiological pH range [85], but the redox potential of SHP is pH-independent between pH 6.0 and 8.5.

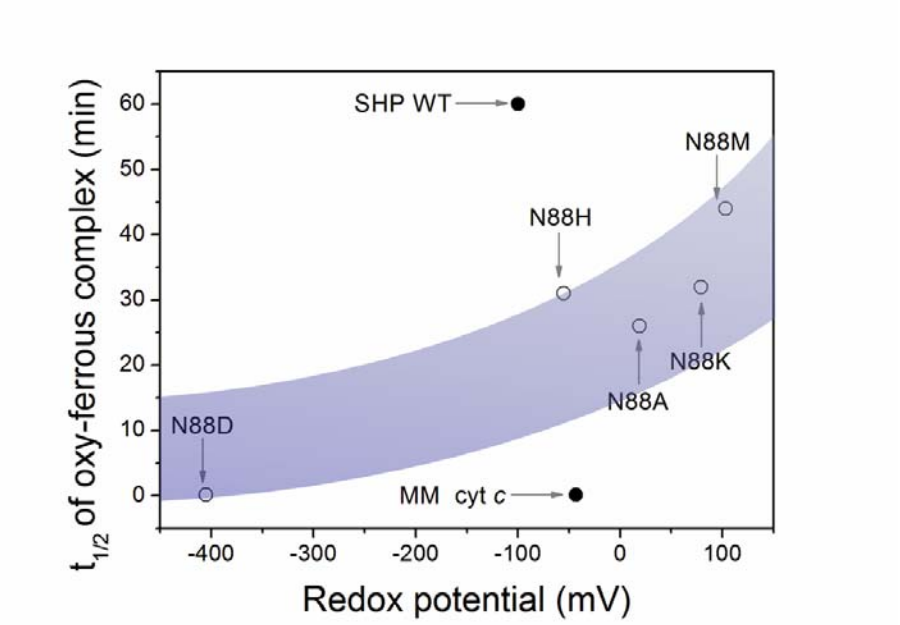

Figure 7.5: Plot of the half life of the oxy-ferrous complex against the redox potential. *The trend is shown by the red line. Methylophilus cytochrome c″ (MM cyt c) is obviously below the trend line, while the half life of SHP wild type is well above the line.*

As table 7.6 shows, the stability of the oxy-ferrous complex is normally dependent on the redox potential. Logically, a heme with lower redox potential is more stable in the ferric form, and its oxy-ferrous complex is likely to be the superoxy-ferric canonical structure which would convert to the ferric form by losing superoxide. For example, the N88D mutant, which has a very low redox potential (-405 mV), has an oxy-ferrous complex with a much shorter half life (~ 3 sec, Figure 7.5) than the wild-type protein. The redox potential of *Methylophilus* cytochrome *c″* (-43 mV) is similar to that of the N88H mutant SHP (-55 mV) and wild-type SHP (-100 mV). Therefore, the half life of the oxy-ferrous complex of *Methylophilus* cytochrome *c″* may be expected to be similar to those of the N88H mutant and wild-type SHPs. However, the oxy-ferrous complex of *Methylophilus* cytochrome *c″* is particularly unstable, and its half life is about 3 sec at 10 ^{o}C. This is much shorter than the half life of the species in N88H and wild-type SHP (>30 and >60 minutes respectively).

7.3 Discussion

Ligand effects on the redox potential and the electron transfer

The heme midpoint potential is one of the most important physical factors of cytochromes. It is influenced by the protein surrounding the cofactor, and in particular the nature of the axial ligand(s). In this study, when the sixth heme ligand of SHP (Asn88) was substituted by other five amino acids the reduction potential was altered. Although the structures of asparagine and aspartic acid are similar, the electron donating ability of two amino acids are hugely different. Thus, in the N88D mutant, the strong electron donating ability of the oxygen of aspartic acid tends to stabilize the ferric form and drops the redox potential from -100 mV to -405 mV. Conversely, in the N88M mutant the ligating sulfur atom of methionine tends to stabilize the ferrous form and increase the redox potential to 103 mV. This pattern is similar to other previous reports [2, 85, 178, 179].

SHP is proposed to be a nitric oxide dioxygenase. Ferric SHP can receive an electron from reduced DHC and then bind oxygen to become an oxy-ferrous SHP. Next, this oxy-ferrous SHP can react with nitric oxide to generate nitrate. Thus, reduction by DHC is one of the most important steps in nitric oxide dioxygenation. In previous studies, SHP and DHC were peoposed to be electron transfer partners. The redox potential of wild-type SHP is -100mV. This is higher than the redox potentials of both hemes of DHC (-240 mV and -310 mV), thus making electron transfer thermodynamically favourable. Therefore, SHP can get an electron from DHC very quickly.

However, the N88X mutants of SHP reveal various redox potentials, ranging from 100 mV to -400 mV. Indeed, the redox potential of N88D (-400 mV) is much lower than that of DHC. Consequently, the direction of electron transfer from DHC to N88D is thermodynamically unfavourable. Therefore, as Figure 7.3 shows, oxidized SHP wild type, N88H, N88A, N88K, and N88M can rapidly receives electrons from reduced DHC (~0.2 s), but N88D does not.

Ligand effects on oxygen and nitric oxide binding

To be a NO dioxygenase, a stable oxy-ferrous complex is very important for SHP because the mechanism of nitric oxide dioxygenation *is via* the oxy-ferrous complex reacting with nitric oxide. Like other oxygen binding cytochromes, the oxy-ferrous complex of SHP slowly auto-oxidizes to produce the ferric form and superoxide at room temperature. Generally speaking, lower redox potentials make the oxy-ferrous complex unstable, because of its tendency to exist as the superoxy-ferric canonical structure, which would convert to the ferric form by losing superoxide. On the other hand, higher redox potentials make the oxy-ferrous complex more stable. As the data show in the table 7.5, the oxy-ferrous complex of wild type has a longer half life of up to 60 minutes in 100 mM phosphate buffer, pH 7.5, and 25^{o}C. In the same conditions, the oxy-ferrous complexes of N88A, N88H, N88K, and N88M SHPs have shorter half lives, with the N88D having a significantly less stable oxy-ferrous complex. As the Figure 7.4 and table 7.6 show, the stabilities of the oxy-ferrous complexes are redox potential dependent; only the complex of wild type is unusually stable. According to the crystal structure (PDB ID: 1DW2), the reason for wild type SHP's stable oxy-ferrous complex is possibly due to a hydrogen bond between the asparagine and bound oxygen. The aspartic acid in N88D can also form a hydrogen bond between the sixth ligand and oxygen, but the redox potential is too low to form a stable complex. Therefore, the ferrous-O_2 complex of N88D is extremely unstable. In conclusion, forming a stable oxy-ferrous complex is possibly one of the reasons why SHP has asparagine as the sixth axial heme ligand.

Heme iron has high affinity for NO, whether ferric or ferrous. Indeed, NO binding is often irreversible, and can inactivate heme proteins. Prevention of NO binding is therefore an important issue. According to the crystal structure of ferric SHP from *Rhodobacter sphaeroides*, the sixth heme ligand (Asn88) is bound to the heme iron, thus preventing NO binding. Therefore, NO can only bind to the ferrous, five-coordinate heme iron of SHP. However, as shown in section 7.2.5.2 and Figure 7.3, only the N88D and N88H mutant SHPs are, like wild-type SHP, able to prevent

NO binding in the ferric state. This is indicated by no change in their ferric spectra in the presence of 20 μM nitric oxide. Nevertheless, under the same NO concentration, ferric N88A, N88M and N88K mutants will form dead-end nitrosyl complexes, indicating that neither methionine nor lysine are heme ligands in the ferric form.

Is asparagine the only sixth heme ligand in the SHP family?

There are 38 sequences with significant homology to SHP revealed in the NCBI database. As shown in Figure 7.8, only 36 of the 38 have the motif containing the conserved asparagine ligand (W-F/L-X-R-N). Of the remaining two homologues' sequences one is predicted to have an aspartic acid as a heme ligand (from *Magnetospirillum gryphiswaldense*), while the other (cytochrome *c″* from *Methylophilus methylotrophus*) uses a histidine residue. The question is whether these two cytochromes also have NO dioxygenase activity and whether they really belong to SHP family.

As a heme ligand aspartic acid is likely to result in a low heme reduction potential. For example, the N88D mutant of SHP reveals a particularly low redox potential which makes its oxy-ferrous complex extremely unstable and prevents its reduction by DHC. The homologue from *Magnetospirillum gryphiswaldense* is predicted to use aspartic acid as a heme ligand, and may therefore display similar behaviour to N88D SHP.

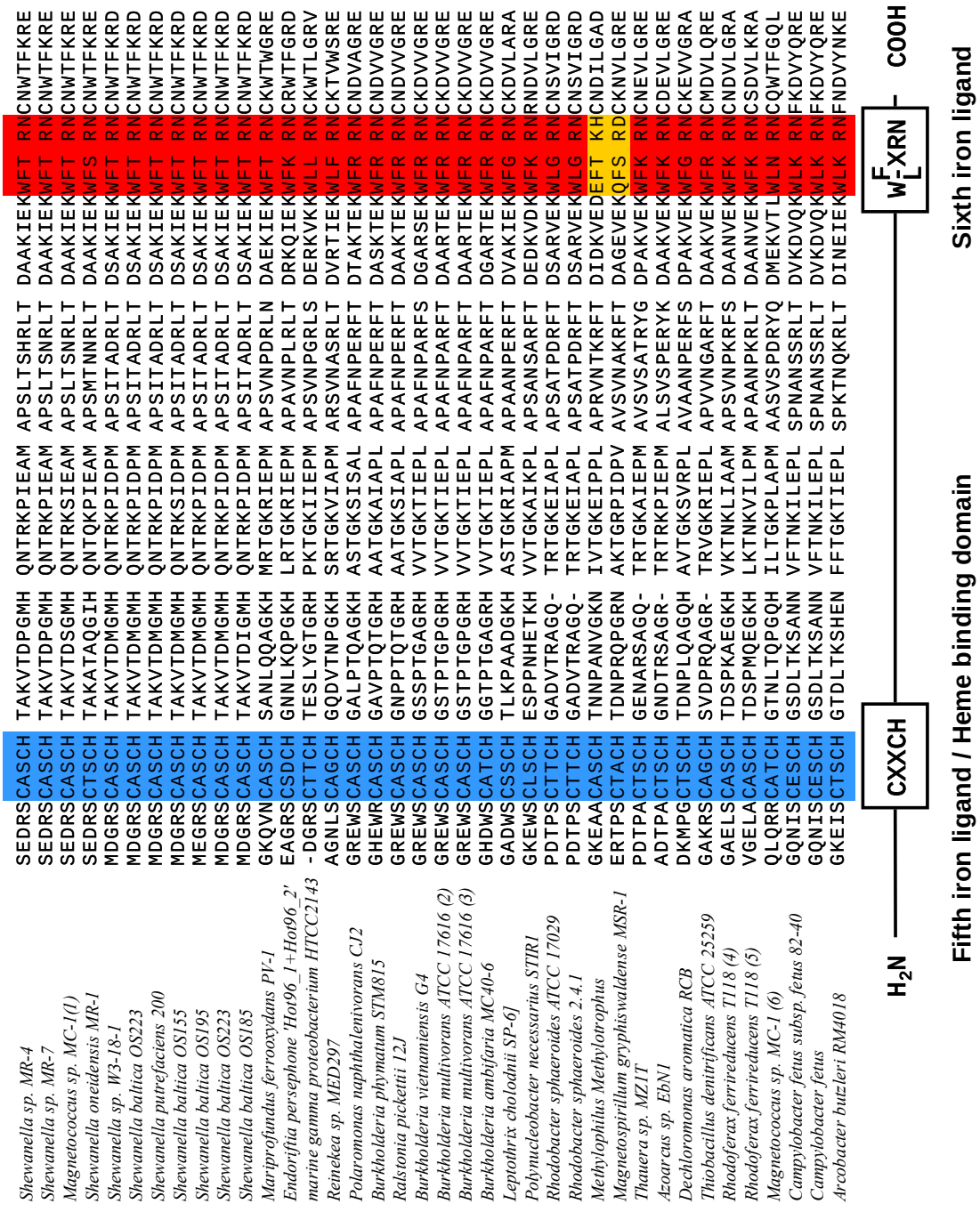

Figure 7.6: Section of sequence alignments for 38 SHP homologous sequences. *Cytochrome c conserved heme binding motif (CXXCH) highlighted in blue. The sixth heme binding residues of SHP are located in a highly conserved motive (WF/LXRN, highlighted in red), except the cytochrome c'' from Methylophilus Methylotrophus and the cytochrome c from Magnetospirillum gryphiswaldense (lighlighted in orange). (1) hypothetical protein Mmc1_0315 from Magnetococcus sp. MC-1; (2) hypothetical protein Bmul_5869 from*

Burkholderia multivorans ATCC 17616; (3) cytochrome c_{553} from Burkholderia multivorans ATCC 17616; (4) cytochrome c-like protein from Rhodoferax ferrireducens T118; (5) hypothetical protein Rfer_3817 from Rhodoferax ferrireducens T118; (6) hypothetical protein Mmc1_0315 from Magnetococcus sp. MC-1. Multiple protein alignment was using T-COFFEE servers (http://www.tcoffee.org/Projects_home_page/t_coffee_home_page.html) [180].

Another unusual case is *Methylophilus* cytochrome *c″* which uses histidine as a heme ligand. The redox potential of cytochrome *c″* (-43 mV) is similar to the redox potentials of the SHP (-100 mV) and its N88H mutant (-55 mV). Therefore, the half life of the oxy-ferrous complex of *Methylophilus* cytochrome *c″* may be expected to be similar to those of the N88H mutant and wild-type SHPs, and therefore have the same function. However, the oxy-ferrous complex of *Methylophilus* cytochrome *c″* is particularly unstable, and its half life is about 3 sec at 10 ^{o}C. This is much shorter than the half life of the species in N88H and wild-type SHP (>30 and >60 minutes respectively). Thus, it does not look to be a nitric oxide dioxygenase candidate.

The reason for the different half lives of the oxy-ferrous complexes of *Methylophilus* cytochrome *c″* and *Rhodobacter* SHP are not due to the different redox potentials, but are possibly due to structural differences at the active sites of these two cytochromes *c*. As shown in Figure 7.6, the motif (W-F/L-X-R-N) containing the sixth heme ligand also has a conserved tryptophan, except for in the homologue from *Magnetospirillum gryphiswaldense* and the cytochrome *c″* from *Methylophilus methylotrophus*. As can be seen from Figure 7.6, in SHP this tryptophan occupies the space above one side of the heme, where it prevents the asparagine from binding to the heme iron in the ferrous form. According to the crystal structure of ferrous-NO SHP, hydrogen bonds can be found between the bound NO molecule and the asparagine ligand, and also between the asparagine and the serine. These hydrogen bonds give an unusually stabilised ferrous-NO complex, and may also increase the stability of the ferrous-O_2 complex (Figure 7.7).

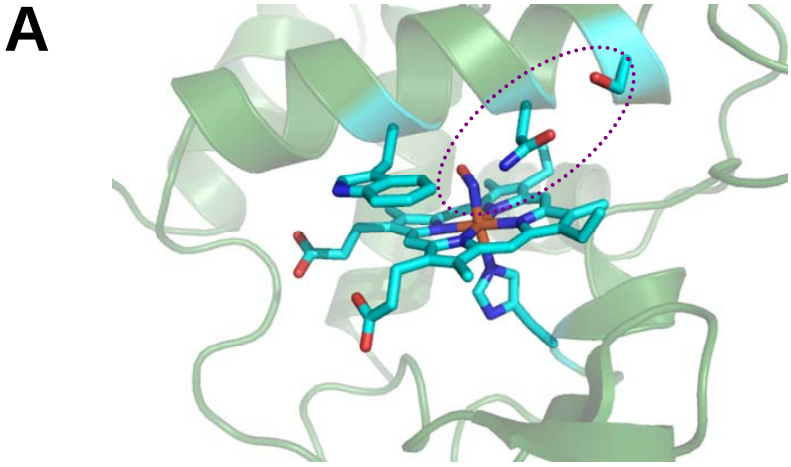

Figure 7.7: Active sites structures of Rhodobacter sphaerodies SHP and cytochrome c″ from Methylophilus methylotrophus. *The crystal structures of the active sites of Rhodobacter sphaerodies SHP (PDB: 1DW2, panel A) and cytochrome c″ from Methylophilus methylotrophus (PDB: 1GU2, lower panel B). Oxygen atoms are seen in red, nitrogen atoms in deep blue, and iron in orange. Hydrogen-bonds in the active site are found within the dotted circle line. This Figure was generated using PyMOL (DeLano Scientific; http://pymol.sourceforge.net/).*

To summarize, although the SHP homologue from *Magnetospirillum gryphiswaldense* has not been studied in detail, from its sequence it is possible that it may be similar in character to the N88D form of SHP. *Methylophilus* cytochrome *c″*

and *Rhodobacter* SHP have similar redox potentials and protein structure but have differences in the sixth axial ligand motif, different O_2 and NO binding characteristics, and a different rearrangement of the axial ligands upon reduction. Therefore, the SHP homologue from *Magnetospirillum*, *Methylophilus* cytochrome *c''*, and *Rhodobacter* SHP are unlikely to be functionally related.

7.4 Conclusions

Our studies reveal several potential reasons why SHP utilises asparagine as a heme ligand. Firstly, in the ferric form, asparagine 88 binds to heme iron to prevent small molecules binding. Secondly, in the ferrous form, it moves to allow oxygen to bind and form the oxy-ferrous complex, using hydrogen bonding for stability. Thirdly, using asparagine as heme residue creates a suitable redox potential for reduction by DHC, thus allowing NO dioxyenation.

Chapter VIII

Final conclusions and Future work

8 Final conclusions and Future work

8.1 Final conclusions

In this work the characterization of SHP, DHC and the SHP/DHC complex are reported. This includes the functions of SHP and the SHP/DHC system, and indicates the importance of the sixth heme ligand of SHP.

I. Aerobic function of SHP: Nitric oxide dioxygenase

An aerobic function for SHP, as a nitric oxide dioxygenase, is reported for the first time. The mechanism (described in section 4.2.1) of SHP is the same as in other nitric oxide dioxygenases such as flavohemoglobin and neuroglobin. However the NO-bound form of SHP rapidly reacts with superoxide, which has not yet been observed for flavohemoglobin or neuroglobin. This mechanism could be important as superoxide could be endogenously produced (via the mechanism proposed in Figure 4.7). It is possible that inactive NO-bound flavohemoglobin and neuroglobin can also be reactivated by this novel mechanism. The aerobic phenotypic experiments also show that the *Shewanella* SHP knockout strain reveals a lower NO tolerance ability than *Shewanella* WT. Therefore, the function of SHP could be as an NO dioxygenase *in vivo*.

II. An anaerobic NO reduction ability is revealed for the SHP/DHC complex

SHP can be over expressed with nitrate as the terminal electron accepter under anaerobic conditions. Thus, it is reasonable to assume that SHP has an anaerobic function. From this work, we found that SHP can reduce nitrite to generate NO *in vitro*, but its catalytic efficiency is perhaps too low to be considered a nitrite reductase *in vivo*. Although this nitrite reductase activity cannot compete with NIR or NrfA, it is still possible to reduce nitrite to generate NO, and SHP may be involved in NO signaling. Furthermore, ferrous SHP can bind but not reduce nitric oxide. Instead, the SHP/DHC complex reveals NO reduction activity. Thus, the SHP/DHC system

may function as a means of NO elimination in anaerobic conditions. However, anaerobically, no remarkable phenotype difference was found between knockout and wild type strains. Thus, SHP can not be proved to have the ability to detoxify NO anaerobically.

III. The function of sixth heme ligand of SHP

Our studies also reveal how SHP utilises asparagine, as a sixth heme ligand, in its nitric oxide dioxygenase activity. Firstly, in the ferric form, asparagine 88 binds to the heme iron to prevent small molecules binding. Secondly, in the ferrous form, it moves to allow oxygen to bind and to form the oxy-ferrous complex, using hydrogen bonding for stability. Thirdly, using asparagine as a heme ligand creates a suitable redox potential for reduction by DHC, thus allowing NO dioxyenation.

8.2 Future work

Although some functions of SHP, DHC and the SHP/DHC complex have been determined, several important questions remain to be answered with regard to these proteins.

- Firstly, the structures of SHP and DHC have been solved; however the structure of the SHP/DHC complex has not been determined. Chapter 3 revealed that SHP/DHC complex can only be formed in low salt conditions (ionic strength < 100 mM), and the optimized buffer pH is around 6.5 – 8.0. Therefore, using low salt but high glycerol concentration in the buffer is possibly an ideal condition for continuation of crystal growth trials of the SHP/DHC complex.

- Secondly, although the *in vitro* anaerobic function of the SHP/DHC system is proposed as NO reduction, such anaerobic NO detoxification has not been conclusively demonstrated *in vivo*. Further phenotypic and biochemical studies must be carried out to ascertain the anaerobic function of SHP, especially since, the *Shewanella* SHP knockout strain reveals a lower NO tolerance than

Shewanella WT. However, these results could be optimized using a system to mix O_2, N_2, and NO and to deliver gases at a constant flow rate [132].

- Thirdly, the importance of the conserved residues (W84 and R87) in the active site of SHP should be probed. As described in chapter 7, these two residues are proposed to increase stability of oxy-ferrous complex by controlling the position of the sixth heme ligand in the ferrous form. To confirm this suggestion, mutagenesis of these two key residues in SHP (W84 and R87) should be carried out to probe their importance.

- Finally, chapter 3 describes the binding of SHP and DHC. However, it was carried out using SHP^{3+} and DHC^{3+}. Therefore it would be interesting to know whether the binding behaviours are different between SHP^{2+} and DHC^{3+}, and SHP^{3+} and DHC^{2+}.

Reference:

Reference:

1. Gibson, H.R., et al., *Structural and functional studies on DHC, the diheme cytochrome c from Rhodobacter sphaeroides, and its interaction with SHP, the sphaeroides heme protein.* Biochemistry, 2006. **45**(20): p. 6363-71.
2. Klarskov, K., et al., *Ligand binding and covalent structure of an oxygen-binding heme protein from Rhodobacter sphaeroides, a representative of a new structural family of c-type cytochromes.* Biochemistry, 1998. **37**(17): p. 5995-6002.
3. Leys, D., et al., *Crystal structures of an oxygen-binding cytochrome c from Rhodobacter sphaeroides.* J Biol Chem, 2000. **275**(21): p. 16050-6.
4. Beliaev, A.S., et al., *Global transcriptome analysis of Shewanella oneidensis MR-1 exposed to different terminal electron acceptors.* J Bacteriol, 2005. **187**(20): p. 7138-45.
5. Li, B.R., et al., *Rhodobacter sphaeroides haem protein: a novel cytochrome with nitric oxide dioxygenase activity.* Biochem Soc Trans, 2008. **36**(Pt 5): p. 992-5.
6. Brunori, M., et al., *Neuroglobin, nitric oxide, and oxygen: functional pathways and conformational changes.* Proc Natl Acad Sci U S A, 2005. **102**(24): p. 8483-8.
7. Gardner, P.R., *Nitric oxide dioxygenase function and mechanism of flavohemoglobin, hemoglobin, myoglobin and their associated reductases.* J Inorg Biochem, 2005. **99**(1): p. 247-66.
8. Weber, R.E. and A. Fago, *Functional adaptation and its molecular basis in vertebrate hemoglobins, neuroglobins and cytoglobins.* Respir Physiol Neurobiol, 2004. **144**(2-3): p. 141-59.
9. Brum, G.D., L. McKane, and G. Karp, *Biology : exploring life*. 2nd ed. 1994, New York: John Wiley. 1 v. (various pagings).
10. Mathews, C.K. and K.E. Van Holde, *Biochemistry*. 2nd ed. 1996, Menlo Park, Calif.: Benjamin/Cummings Pub. Co., Inc. xxvii, 1159 p.
11. Rich, P.R., *The molecular machinery of Keilin's respiratory chain.* Biochem Soc Trans, 2003. **31**(Pt 6): p. 1095-105.
12. Haddock, B.A. and C.W. Jones, *Bacterial respiration.* Bacteriol Rev, 1977. **41**(1): p. 47-99.
13. Swanson, T.A., et al., *Biochemistry and molecular biology*. 4th ed. Board

review series. 2007, Philadelphia: Lippincott Williams & Wilkins. xii, 484 p.

14. Porter, R.K. and M.D. Brand, *Mitochondrial proton conductance and H+/O ratio are independent of electron transport rate in isolated hepatocytes.* Biochem J, 1995. **310 (Pt 2)**: p. 379-82.
15. Romano, A.H. and T. Conway, *Evolution of carbohydrate metabolic pathways.* Res Microbiol, 1996. **147**(6-7): p. 448-55.
16. Budde, R.J., et al., *Acetyl-Coenzyme A Can Regulate Activity of the Mitochondrial Pyruvate Dehydrogenase Complex in Situ.* Plant Physiol, 1991. **95**(1): p. 131-136.
17. Jackson, J.B., *Proton translocation by transhydrogenase.* FEBS Lett, 2003. **545**(1): p. 18-24.
18. Hunte, C., H. Palsdottir, and B.L. Trumpower, *Protonmotive pathways and mechanisms in the cytochrome bc1 complex.* FEBS Lett, 2003. **545**(1): p. 39-46.
19. Schultz, B.E. and S.I. Chan, *Structures and proton-pumping strategies of mitochondrial respiratory enzymes.* Annu Rev Biophys Biomol Struct, 2001. **30**: p. 23-65.
20. Arechaga, I. and P.C. Jones, *The rotor in the membrane of the ATP synthase and relatives.* FEBS Lett, 2001. **494**(1-2): p. 1-5.
21. Friedrich, T., et al., *Redox components and structure of the respiratory NADH:ubiquinone oxidoreductase (complex I).* Biochim Biophys Acta, 1998. **1365**(1-2): p. 215-9.
22. Grigorieff, N., *Three-dimensional structure of bovine NADH:ubiquinone oxidoreductase (complex I) at 22 A in ice.* J Mol Biol, 1998. **277**(5): p. 1033-46.
23. Grigorieff, N., *Structure of the respiratory NADH:ubiquinone oxidoreductase (complex I).* Curr Opin Struct Biol, 1999. **9**(4): p. 476-83.
24. Guenebaut, V., et al., *Consistent structure between bacterial and mitochondrial NADH:ubiquinone oxidoreductase (complex I).* J Mol Biol, 1998. **276**(1): p. 105-12.
25. Sickmier, E.A., et al., *X-ray structure of a Rex-family repressor/NADH complex insights into the mechanism of redox sensing.* Structure, 2005. **13**(1): p. 43-54.
26. Zickermann, V., et al., *Challenges in elucidating structure and mechanism of proton pumping NADH:ubiquinone oxidoreductase (complex I).* J Bioenerg Biomembr, 2008. **40**(5): p. 475-83.
27. Flemming, D., et al., *A possible role for iron-sulfur cluster N2 in proton translocation by the NADH: ubiquinone oxidoreductase (complex I).* J Mol Microbiol Biotechnol, 2005. **10**(2-4): p. 208-22.
28. Sazanov, L.A., P.A. Burrows, and P.J. Nixon, *The plastid ndh genes code for*

an NADH-specific dehydrogenase: isolation of a complex I analogue from pea thylakoid membranes. Proc Natl Acad Sci U S A, 1998. **95**(3): p. 1319-24.

29. Hrdy, I., et al., *Trichomonas hydrogenosomes contain the NADH dehydrogenase module of mitochondrial complex I.* Nature, 2004. **432**(7017): p. 618-22.
30. Weiss, H., et al., *The respiratory-chain NADH dehydrogenase (complex I) of mitochondria.* Eur J Biochem, 1991. **197**(3): p. 563-76.
31. Chapdelaine, Y. and L. Bonen, *The wheat mitochondrial gene for subunit I of the NADH dehydrogenase complex: a trans-splicing model for this gene-in-pieces.* Cell, 1991. **65**(3): p. 465-72.
32. Ruzicka, F.J. and F.L. Crane, *Four quinone reduction sites in the NADH dehydrogenase complex.* Biochem Biophys Res Commun, 1970. **38**(2): p. 249-54.
33. Ohnishi, T., et al., *Functional role of coenzyme Q in the energy coupling of NADH-CoQ oxidoreductase (Complex I): stabilization of the semiquinone state with the application of inside-positive membrane potential to proteoliposomes.* Biofactors, 2008. **32**(1-4): p. 13-22.
34. Ohnishi, T. and J.C. Salerno, *Conformation-driven and semiquinone-gated proton-pump mechanism in the NADH-ubiquinone oxidoreductase (complex I).* FEBS Lett, 2005. **579**(21): p. 4555-61.
35. Zhang, H., et al., *Exposing the complex III Qo semiquinone radical.* Biochim Biophys Acta, 2007. **1767**(7): p. 883-7.
36. Stock, D., et al., *The rotary mechanism of ATP synthase.* Curr Opin Struct Biol, 2000. **10**(6): p. 672-9.
37. Walker, J.E., *The regulation of catalysis in ATP synthase.* Curr Opin Struct Biol, 1994. **4**(6): p. 912-8.
38. Walker, J.E., *The NADH:ubiquinone oxidoreductase (complex I) of respiratory chains.* Q Rev Biophys, 1992. **25**(3): p. 253-324.
39. Glynn, I.M., *Involvement of a membrane potential in the synthesis of ATP by mitochondria.* Nature, 1967. **216**(5122): p. 1318-9.
40. Cockrell, R.S., E.J. Harris, and B.C. Pressman, *Synthesis of ATP driven by a potassium gradient in mitochondria.* Nature, 1967. **215**(5109): p. 1487-8.
41. Lancaster, C.R. and J. Simon, *Succinate:quinone oxidoreductases from epsilon-proteobacteria.* Biochim Biophys Acta, 2002. **1553**(1-2): p. 84-101.
42. Yankovskaya, V., et al., *Architecture of succinate dehydrogenase and reactive oxygen species generation.* Science, 2003. **299**(5607): p. 700-4.
43. Tielens, A.G. and J.J. Van Hellemond, *The electron transport chain in anaerobically functioning eukaryotes.* Biochim Biophys Acta, 1998. **1365**(1-2): p. 71-8.

44. Mulkidjanian, A.Y., *Proton translocation by the cytochrome bc1 complexes of phototrophic bacteria: introducing the activated Q-cycle.* Photochem Photobiol Sci, 2007. **6**(1): p. 19-34.

45. Darrouzet, E., et al., *Structure and function of the bacterial bc1 complex: domain movement, subunit interactions, and emerging rationale engineering attempts.* J Bioenerg Biomembr, 1999. **31**(3): p. 275-88.

46. Brandt, U. and B. Trumpower, *The protonmotive Q cycle in mitochondria and bacteria.* Crit Rev Biochem Mol Biol, 1994. **29**(3): p. 165-97.

47. Trumpower, B.L., *The protonmotive Q cycle. Energy transduction by coupling of proton translocation to electron transfer by the cytochrome bc1 complex.* J Biol Chem, 1990. **265**(20): p. 11409-12.

48. Trumpower, B.L., *Cytochrome bc1 complexes of microorganisms.* Microbiol Rev, 1990. **54**(2): p. 101-29.

49. Richter, O.M. and B. Ludwig, *Cytochrome c oxidase--structure, function, and physiology of a redox-driven molecular machine.* Rev Physiol Biochem Pharmacol, 2003. **147**: p. 47-74.

50. Michel, H., et al., *Cytochrome c oxidase: structure and spectroscopy.* Annu Rev Biophys Biomol Struct, 1998. **27**: p. 329-56.

51. Gennis, R. and S. Ferguson-Miller, *Structure of cytochrome c oxidase, energy generator of aerobic life.* Science, 1995. **269**(5227): p. 1063-4.

52. Yoshikawa, S., K. Shinzawa-Itoh, and T. Tsukihara, *X-ray structure and the reaction mechanism of bovine heart cytochrome c oxidase.* J Inorg Biochem, 2000. **82**(1-4): p. 1-7.

53. Leslie, A.G. and J.E. Walker, *Structural model of F1-ATPase and the implications for rotary catalysis.* Philos Trans R Soc Lond B Biol Sci, 2000. **355**(1396): p. 465-71.

54. Lovley, D.R., *Bug juice: harvesting electricity with microorganisms.* Nat Rev Microbiol, 2006. **4**(7): p. 497-508.

55. Prescott, L.M., J.P. Harley, and D.A. Klein, *Microbiology*. 6th ed. 2005, Dubuque, IA: McGraw-Hill Higher Education. 1 v. (various pagings).

56. Lovley, D.R., D.E. Holmes, and K.P. Nevin, *Dissimilatory Fe(III) and Mn(IV) reduction.* Adv Microb Physiol, 2004. **49**: p. 219-86.

57. Wall, J.D. and L.R. Krumholz, *Uranium reduction.* Annu Rev Microbiol, 2006. **60**: p. 149-66.

58. Ortiz-Bernad, I., et al., *Resistance of solid-phase U(VI) to microbial reduction during in situ bioremediation of uranium-contaminated groundwater.* Appl Environ Microbiol, 2004. **70**(12): p. 7558-60.

59. Holmes, D.E., et al., *Enrichment of members of the family Geobacteraceae associated with stimulation of dissimilatory metal reduction in uranium-contaminated aquifer sediments.* Appl Environ Microbiol, 2002.

68(5): p. 2300-6.

60. Lovley, D.R., *The microbe electric: conversion of organic matter to electricity.* Curr Opin Biotechnol, 2008. **19**(6): p. 564-71.
61. Lovley, D.R., *Microbial fuel cells: novel microbial physiologies and engineering approaches.* Curr Opin Biotechnol, 2006. **17**(3): p. 327-32.
62. Shriver, D.F., H.D. Kaesz, and R.D. Adams, *The Chemistry of metal cluster complexes*. 1990, New York: VCH. 439 p.
63. Mason, R.P., *Redox cycling of radical anion metabolites of toxic chemicals and drugs and the Marcus theory of electron transfer.* Environ Health Perspect, 1990. **87**: p. 237-43.
64. Gold, V. and International Union of Pure and Applied Chemistry., *Compendium of chemical terminology : IUPAC recommendations*. 1987, Oxford [Oxfordshire] ; Boston: Blackwell Scientific Publications. viii, 456 p.
65. Moser, C.C., et al., *Nature of biological electron transfer.* Nature, 1992. **355**(6363): p. 796-802.
66. Moser, C.C. and P.L. Dutton, *Engineering protein structure for electron transfer function in photosynthetic reaction centers.* Biochim Biophys Acta, 1992. **1101**(2): p. 171-6.
67. Beratan, D.N., J.N. Betts, and J.N. Onuchic, *Protein electron transfer rates set by the bridging secondary and tertiary structure.* Science, 1991. **252**(5010): p. 1285-8.
68. *Nomenclature Committee of the International Union of Biochemistry (NC-IUB). Nomenclature of electron-transfer proteins. Recommendations 1989.* Eur J Biochem, 1991. **200**(3): p. 599-611.
69. Waxman, K., K.K. Tremper, and G.R. Mason, *Blood and plasma substitutes--plasma expansion and oxygen transport properties.* West J Med, 1985. **143**(2): p. 202-6.
70. Thackray, S.J., C.G. Mowat, and S.K. Chapman, *Exploring the mechanism of tryptophan 2,3-dioxygenase.* Biochem Soc Trans, 2008. **36**(Pt 6): p. 1120-3.
71. Gilles-Gonzalez, M.A., et al., *Oxygen-sensing histidine-protein kinases: assays of ligand binding and turnover of response-regulator substrates.* Methods Enzymol, 2008. **437**: p. 173-89.
72. Wagner, P.D., *The biology of oxygen.* Eur Respir J, 2008. **31**(4): p. 887-90.
73. Imai, S., et al., *Transcriptional silencing and longevity protein Sir2 is an NAD-dependent histone deacetylase.* Nature, 2000. **403**(6771): p. 795-800.
74. Brune, B. and E.G. Lapetina, *Glyceraldehyde-3-phosphate dehydrogenase: a target for nitric oxide signaling.* Adv Pharmacol, 1995. **34**: p. 351-60.
75. Patel, M.S. and T.E. Roche, *Molecular biology and biochemistry of pyruvate dehydrogenase complexes.* FASEB J, 1990. **4**(14): p. 3224-33.

76. Skulachev, V.P., *Cytochrome c in the apoptotic and antioxidant cascades.* FEBS Lett, 1998. **423**(3): p. 275-80.

77. Liu, X., et al., *Induction of apoptotic program in cell-free extracts: requirement for dATP and cytochrome c.* Cell, 1996. **86**(1): p. 147-57.

78. Ambler, R.P., *Sequence variability in bacterial cytochromes c.* Biochim Biophys Acta, 1991. **1058**(1): p. 42-7.

79. Moore, G.R., *Bacterial 4-alpha-helical bundle cytochromes.* Biochim Biophys Acta, 1991. **1058**(1): p. 38-41.

80. Coutinho, I.B. and A.V. Xavier, *Tetraheme cytochromes.* Methods Enzymol, 1994. **243**: p. 119-40.

81. Schwalb, C., S.K. Chapman, and G.A. Reid, *The membrane-bound tetrahaem c-type cytochrome CymA interacts directly with the soluble fumarate reductase in Shewanella.* Biochem Soc Trans, 2002. **30**(4): p. 658-62.

82. Cutruzzola, F., et al., *NO production by Pseudomonas aeruginosa cd1 nitrite reductase.* IUBMB Life, 2003. **55**(10-11): p. 617-21.

83. Moura, J.J., et al., *Structural and functional approach toward a classification of the complex cytochrome c system found in sulfate-reducing bacteria.* Biochim Biophys Acta, 1991. **1058**(1): p. 61-6.

84. Distler, A.M., et al., *Mass spectrometric detection of protein, lipid and heme components of cytochrome c oxidase from R. sphaeroides and the stabilization of non-covalent complexes from the enzyme.* Eur J Mass Spectrom (Chichester, Eng), 2004. **10**(2): p. 295-308.

85. Klarskov, K., et al., *Cytochrome c" from the obligate methylotroph Methylophilus methylotrophus, an unexpected homolog of sphaeroides heme protein from the phototroph Rhodobacter sphaeroides.* Biochim Biophys Acta, 1999. **1412**(1): p. 47-55.

86. Meyer, T.E. and M.A. Cusanovich, *Soluble cytochrome composition of the purple phototrophic bacterium, Rhodopseudomonas sphaeroides ATCC 17023.* Biochim Biophys Acta, 1985. **807**(3): p. 308-19.

87. Stouthamer, A.H., *Metabolic regulation including anaerobic metabolism in Paracoccus denitrificans.* J Bioenerg Biomembr, 1991. **23**(2): p. 163-85.

88. Zumft, W.G., *Cell biology and molecular basis of denitrification.* Microbiol Mol Biol Rev, 1997. **61**(4): p. 533-616.

89. Bryan, N.S., *Nitrite in nitric oxide biology: cause or consequence? A systems-based review.* Free Radic Biol Med, 2006. **41**(5): p. 691-701.

90. Lin, J.T. and V. Stewart, *Nitrate assimilation by bacteria.* Adv Microb Physiol, 1998. **39**: p. 1-30, 379.

91. Dalsgaard, T., B. Thamdrup, and D.E. Canfield, *Anaerobic ammonium oxidation (anammox) in the marine environment.* Res Microbiol, 2005. **156**(4): p. 457-64.

92. Op den Camp, H.J., et al., *Global impact and application of the anaerobic ammonium-oxidizing (anammox) bacteria.* Biochem Soc Trans, 2006. **34**(Pt 1): p. 174-8.

93. Richardson, D.J., et al., *The diversity of redox proteins involved in bacterial heterotrophic nitrification and aerobic denitrification.* Biochem Soc Trans, 1998. **26**(3): p. 401-8.

94. Richardson, D.J., et al., *Functional, biochemical and genetic diversity of prokaryotic nitrate reductases.* Cell Mol Life Sci, 2001. **58**(2): p. 165-78.

95. Watts, C.A., et al., *Microbial reduction of selenate and nitrate: common themes and variations.* Biochem Soc Trans, 2005. **33**(Pt 1): p. 173-5.

96. Clarke, T.A., et al., *Escherichia coli cytochrome c nitrite reductase NrfA.* Methods Enzymol, 2008. **437**: p. 63-77.

97. Simon, J., *Enzymology and bioenergetics of respiratory nitrite ammonification.* FEMS Microbiol Rev, 2002. **26**(3): p. 285-309.

98. Clarke, T.A., et al., *Comparison of the structural and kinetic properties of the cytochrome c nitrite reductases from Escherichia coli, Wolinella succinogenes, Sulfurospirillum deleyianum and Desulfovibrio desulfuricans.* Biochem Soc Trans, 2006. **34**(Pt 1): p. 143-5.

99. Bamford, V.A., et al., *Structure and spectroscopy of the periplasmic cytochrome c nitrite reductase from Escherichia coli.* Biochemistry, 2002. **41**(9): p. 2921-31.

100. Clarke, T.A., et al., *The crystal structure of the pentahaem c-type cytochrome NrfB and characterization of its solution-state interaction with the pentahaem nitrite reductase NrfA.* Biochem J, 2007. **406**(1): p. 19-30.

101. Cunha, C.A., et al., *Cytochrome c nitrite reductase from Desulfovibrio desulfuricans ATCC 27774. The relevance of the two calcium sites in the structure of the catalytic subunit (NrfA).* J Biol Chem, 2003. **278**(19): p. 17455-65.

102. Atkinson, S.J., et al., *An octaheme c-type cytochrome from Shewanella oneidensis can reduce nitrite and hydroxylamine.* FEBS Lett, 2007. **581**(20): p. 3805-8.

103. Einsle, O., et al., *Mechanism of the six-electron reduction of nitrite to ammonia by cytochrome c nitrite reductase.* J Am Chem Soc, 2002. **124**(39): p. 11737-45.

104. Atlas, R.M. and R. Bartha, *Microbial ecology : fundamentals and applications*. 3rd ed. 1993, Redwood City, Calif.: Benjamin/Cummings Pub. Co. xii, 563 p.

105. Ritter, W.F. and R.P. Eastburn, *A review of denitrification in on-site wastewater treatment systems.* Environ Pollut, 1988. **51**(1): p. 49-61.

106. Einsle, O., et al., *Crystallization and preliminary X-ray analysis of the*

membrane-bound cytochrome c nitrite reductase complex (NrfHA) from Wolinella succinogenes. Acta Crystallogr D Biol Crystallogr, 2002. **58**(Pt 2): p. 341-2.

107. Dias, J.M., et al., *Crystal structure of the first dissimilatory nitrate reductase at 1.9 A solved by MAD methods.* Structure, 1999. **7**(1): p. 65-79.

108. Kern, M. and J. Simon, *Characterization of the NapGH quinol dehydrogenase complex involved in Wolinella succinogenes nitrate respiration.* Mol Microbiol, 2008. **69**(5): p. 1137-52.

109. Siddiqui, R.A., et al., *Structure and function of a periplasmic nitrate reductase in Alcaligenes eutrophus H16.* J Bacteriol, 1993. **175**(18): p. 5867-76.

110. Jepson, B.J., et al., *Spectropotentiometric and structural analysis of the periplasmic nitrate reductase from Escherichia coli.* J Biol Chem, 2007. **282**(9): p. 6425-37.

111. Jormakka, M., et al., *Architecture of NarGH reveals a structural classification of Mo-bisMGD enzymes.* Structure, 2004. **12**(1): p. 95-104.

112. Hall, N. and A.B. Tomsett, *Structure-function analysis of NADPH:nitrate reductase from Aspergillus nidulans: analysis of altered pyridine nucleotide specificity in vivo.* Microbiology, 2000. **146 (Pt 6)**: p. 1399-406.

113. Gonzalez, P.J., et al., *Bacterial nitrate reductases: Molecular and biological aspects of nitrate reduction.* J Inorg Biochem, 2006. **100**(5-6): p. 1015-23.

114. Baker, S.C., et al., *Cytochrome cd1 structure: unusual haem environments in a nitrite reductase and analysis of factors contributing to beta-propeller folds.* J Mol Biol, 1997. **269**(3): p. 440-55.

115. Oganesyan, V.S., M.R. Cheesman, and A.J. Thomson, *Magnetic circular dichroism evidence for a weakly coupled heme-radical pair at the active site of cytochrome cd1, a nitrite reductase.* Inorg Chem, 2007. **46**(26): p. 10950-2.

116. Xie, Y., et al., *Crystallization and preliminary X-ray crystallographic studies of dissimilatory nitrite reductase isolated from Hyphomicrobium denitrificans A3151.* Acta Crystallogr D Biol Crystallogr, 2004. **60**(Pt 12 Pt 2): p. 2383-6.

117. Gordon, E.H., et al., *Structure and kinetic properties of Paracoccus pantotrophus cytochrome cd1 nitrite reductase with the d1 heme active site ligand tyrosine 25 replaced by serine.* J Biol Chem, 2003. **278**(14): p. 11773-81.

118. Sjogren, T. and J. Hajdu, *Structure of the bound dioxygen species in the cytochrome oxidase reaction of cytochrome cd1 nitrite reductase.* J Biol Chem, 2001. **276**(16): p. 13072-6.

119. Causey, M.B., K.N. Beane, and J.R. Wolf, *The effects of salinity and other factors on nitrite reduction by Ochrobactrum anthropi 49187.* J Basic Microbiol, 2006. **46**(1): p. 10-21.

120. MacPherson, I.S. and M.E. Murphy, *Type-2 copper-containing enzymes.* Cell Mol Life Sci, 2007. **64**(22): p. 2887-99.

121. Kim, S.W., et al., *Eukaryotic nirK genes encoding copper-containing nitrite reductase: originating from the protomitochondrion?* Appl Environ Microbiol, 2009. **75**(9): p. 2652-8.

122. Shimizu, H., et al., *Proton delivery in NO reduction by fungal nitric-oxide reductase. Cryogenic crystallography, spectroscopy, and kinetics of ferric-NO complexes of wild-type and mutant enzymes.* J Biol Chem, 2000. **275**(7): p. 4816-26.

123. Cramm, R., *Genomic view of energy metabolism in Ralstonia eutropha H16.* J Mol Microbiol Biotechnol, 2009. **16**(1-2): p. 38-52.

124. Moenne-Loccoz, P., *Spectroscopic characterization of heme iron-nitrosyl species and their role in NO reductase mechanisms in diiron proteins.* Nat Prod Rep, 2007. **24**(3): p. 610-20.

125. Tavares, P., et al., *Metalloenzymes of the denitrification pathway.* J Inorg Biochem, 2006. **100**(12): p. 2087-100.

126. Watmough, N.J., et al., *The bacterial respiratory nitric oxide reductase.* Biochem Soc Trans, 2009. **37**(Pt 2): p. 392-9.

127. Forte, E., et al., *The cytochrome cbb3 from Pseudomonas stutzeri displays nitric oxide reductase activity.* Eur J Biochem, 2001. **268**(24): p. 6486-91.

128. Brown, K., et al., *A novel type of catalytic copper cluster in nitrous oxide reductase.* Nat Struct Biol, 2000. **7**(3): p. 191-5.

129. Wang, G. and H.D. Skipper, *Identification of denitrifying rhizobacteria from bentgrass and bermudagrass golf greens.* J Appl Microbiol, 2004. **97**(4): p. 827-37.

130. Schnappinger, D., et al., *Transcriptional Adaptation of Mycobacterium tuberculosis within Macrophages: Insights into the Phagosomal Environment.* J Exp Med, 2003. **198**(5): p. 693-704.

131. Gardner, P.R., et al., *Nitric oxide dioxygenase: an enzymic function for flavohemoglobin.* Proc Natl Acad Sci U S A, 1998. **95**(18): p. 10378-83.

132. Gardner, A.M. and P.R. Gardner, *Flavohemoglobin detoxifies nitric oxide in aerobic, but not anaerobic, Escherichia coli. Evidence for a novel inducible anaerobic nitric oxide-scavenging activity.* J Biol Chem, 2002. **277**(10): p. 8166-71.

133. Berry, E.A. and B.L. Trumpower, *Simultaneous determination of hemes a, b, and c from pyridine hemochrome spectra.* Anal Biochem, 1987. **161**(1): p. 1-15.

134. Takaichi, S. and S. Morita, *Procedures and conditions for application of the pyridine hemochrome method to photosynthetically grown cells of Rhodopseudomonas sphaeroides.* J Biochem, 1981. **89**(5): p. 1513-9.

135. *Tentative method of analysis for nitrogen dioxide content of the atmosphere (Griess-Saltzman reaction).* Health Lab Sci, 1969. **6**(2): p. 106-13.

136. Taylor, P., et al., *Structural and mechanistic mapping of a unique fumarate reductase.* Nat Struct Biol, 1999. **6**(12): p. 1108-12.

137. Summers, F.E. and J.E. Erman, *Reduction of cytochrome c peroxidase compounds I and II by ferrocytochrome c. A stopped-flow kinetic investigation.* J Biol Chem, 1988. **263**(28): p. 14267-75.

138. Orii, Y., *The cytochrome c peroxidase activity of cytochrome oxidase.* J Biol Chem, 1982. **257**(16): p. 9246-8.

139. Gardner, P.R., et al., *Nitric-oxide dioxygenase activity and function of flavohemoglobins. sensitivity to nitric oxide and carbon monoxide inhibition.* J Biol Chem, 2000. **275**(41): p. 31581-7.

140. Gardner, P.R., et al., *Hemoglobins dioxygenate nitric oxide with high fidelity.* J Inorg Biochem, 2006. **100**(4): p. 542-50.

141. Bonamore, A. and A. Boffi, *Flavohemoglobin: structure and reactivity.* IUBMB Life, 2008. **60**(1): p. 19-28.

142. Farres, J., et al., *Ligand binding properties of bacterial hemoglobins and flavohemoglobins.* Biochemistry, 2005. **44**(10): p. 4125-34.

143. Poole, R.K., *Nitric oxide and nitrosative stress tolerance in bacteria.* Biochem Soc Trans, 2005. **33**(Pt 1): p. 176-80.

144. Wakasugi, K., C. Kitatsuji, and I. Morishima, *Possible neuroprotective mechanism of human neuroglobin.* Ann N Y Acad Sci, 2005. **1053**: p. 220-30.

145. Brunori, M. and B. Vallone, *A globin for the brain.* FASEB J, 2006. **20**(13): p. 2192-7.

146. Gladwin, M.T., R. Grubina, and M.P. Doyle, *The new chemical biology of nitrite reactions with hemoglobin: R-state catalysis, oxidative denitrosylation, and nitrite reductase/anhydrase.* Acc Chem Res, 2009. **42**(1): p. 157-67.

147. Zumft, W.G., *Nitric oxide reductases of prokaryotes with emphasis on the respiratory, heme-copper oxidase type.* J Inorg Biochem, 2005. **99**(1): p. 194-215.

148. Gardner, P.R., G. Costantino, and A.L. Salzman, *Constitutive and adaptive detoxification of nitric oxide in Escherichia coli. Role of nitric-oxide dioxygenase in the protection of aconitase.* J Biol Chem, 1998. **273**(41): p. 26528-33.

149. Herold, S., et al., *Reactivity studies of the Fe(III) and Fe(II)NO forms of human neuroglobin reveal a potential role against oxidative stress.* J Biol Chem, 2004. **279**(22): p. 22841-7.

150. Brunori, M. and B. Vallone, *Neuroglobin, seven years after.* Cell Mol Life Sci, 2007. **64**(10): p. 1259-68.

151. Wakasugi, K., T. Nakano, and I. Morishima, *Association of human neuroglobin with cystatin C, a cysteine proteinase inhibitor.* Biochemistry, 2004. **43**(18): p. 5119-25.

152. Jin, K., et al., *Neuroglobin protects against nitric oxide toxicity.* Neurosci Lett, 2008. **430**(2): p. 135-7.

153. Gilberthorpe, N.J. and R.K. Poole, *Nitric oxide homeostasis in Salmonella typhimurium: roles of respiratory nitrate reductase and flavohemoglobin.* J Biol Chem, 2008. **283**(17): p. 11146-54.

154. Shikama, K. and A. Matsuoka, *Structure-function relationships in unusual nonvertebrate globins.* Crit Rev Biochem Mol Biol, 2004. **39**(4): p. 217-59.

155. Sawai, H., et al., *Structural characterization of the proximal and distal histidine environment of cytoglobin and neuroglobin.* Biochemistry, 2005. **44**(40): p. 13257-65.

156. Dewilde, S., et al., *Biochemical characterization and ligand binding properties of neuroglobin, a novel member of the globin family.* J Biol Chem, 2001. **276**(42): p. 38949-55.

157. Petersen, M.G., S. Dewilde, and A. Fago, *Reactions of ferrous neuroglobin and cytoglobin with nitrite under anaerobic conditions.* J Inorg Biochem, 2008. **102**(9): p. 1777-82.

158. Kukimoto, M., et al., *Site-directed mutagenesis of azurin from Pseudomonas aeruginosa enhances the formation of an electron-transfer complex with a copper-containing nitrite reductase from Alcaligenes faecalis S-6.* FEBS Lett, 1996. **394**(1): p. 87-90.

159. Clarke, T.A., et al., *Purification and spectropotentiometric characterization of Escherichia coli NrfB, a decaheme homodimer that transfers electrons to the decaheme periplasmic nitrite reductase complex.* J Biol Chem, 2004. **279**(40): p. 41333-9.

160. Hausladen, A., A. Gow, and J.S. Stamler, *Flavohemoglobin denitrosylase catalyzes the reaction of a nitroxyl equivalent with molecular oxygen.* Proc Natl Acad Sci U S A, 2001. **98**(18): p. 10108-12.

161. Liu, L., et al., *Protection from nitrosative stress by yeast flavohemoglobin.* Proc Natl Acad Sci U S A, 2000. **97**(9): p. 4672-6.

162. Hausladen, A., A.J. Gow, and J.S. Stamler, *Nitrosative stress: metabolic pathway involving the flavohemoglobin.* Proc Natl Acad Sci U S A, 1998. **95**(24): p. 14100-5.

163. Nicolis, S., et al., *Reactivity and endogenous modification by nitrite and hydrogen peroxide: does human neuroglobin act only as a scavenger?* Biochem J, 2007. **407**(1): p. 89-99.

164. Price, M.S., L.Y. Chao, and M.A. Marletta, *Shewanella oneidensis MR-1 H-NOX regulation of a histidine kinase by nitric oxide.* Biochemistry, 2007. **46**(48): p. 13677-83.

165. Woyke, T., et al., *Symbiosis insights through metagenomic analysis of a microbial consortium.* Nature, 2006. **443**(7114): p. 950-5.

166. Nalwaya, N. and W.M. Deen, *Nitric oxide, oxygen, and superoxide formation and consumption in macrophage cultures.* Chem Res Toxicol, 2005. **18**(3): p. 486-93.

167. Flatley, J., et al., *Transcriptional responses of Escherichia coli to S-nitrosoglutathione under defined chemostat conditions reveal major changes in methionine biosynthesis.* J Biol Chem, 2005. **280**(11): p. 10065-72.

168. Lewis, M.E., et al., *A survey of methods for the purification of microbial flavohemoglobins.* Methods Enzymol, 2008. **436**: p. 169-86.

169. Gardner, A.M., R.A. Helmick, and P.R. Gardner, *Flavorubredoxin, an inducible catalyst for nitric oxide reduction and detoxification in Escherichia coli.* J Biol Chem, 2002. **277**(10): p. 8172-7.

170. Moore, G.R. and G.W. Pettigrew, *Cytochromes c : evolutionary, structural, and physicochemical aspects*. Springer series in molecular biology. 1990, Berlin ; New York: Springer-Verlag. xvi, 478 p.

171. Pettigrew, G.W. and G.R. Moore, *Cytochromes c : biological aspects*. Springer series in molecular biology. 1987, Berlin ; New York: Springer-Verlag. xiv, 282 p.

172. Altschul, S.F., et al., *Gapped BLAST and PSI-BLAST: a new generation of protein database search programs.* Nucleic Acids Res, 1997. **25**(17): p. 3389-402.

173. Enguita, F.J., et al., *Structural evidence for a proton transfer pathway coupled with haem reduction of cytochrome c" from Methylophilus methylotrophus.* J Biol Inorg Chem, 2006. **11**(2): p. 189-96.

174. Brennan, L., et al., *Solution structure of Methylophilus methylotrophus cytochrome c": insights into the structural basis of haem-ligand detachment.* J Mol Biol, 2001. **308**(2): p. 353-65.

175. Fasano, M., G. Antonini, and P. Ascenzi, *O2-mediated oxidation of hemopexin-heme(II)-NO.* Biochem Biophys Res Commun, 2006. **345**(2): p. 704-12.

176. Abu-Soud, H.M., et al., *The ferrous-dioxy complex of neuronal nitric oxide synthase. Divergent effects of L-arginine and tetrahydrobiopterin on its stability.* J Biol Chem, 1997. **272**(28): p. 17349-53.

177. Tsuchida, E., et al., *Properties of and oxygen binding by albumin-tetraphenylporphyrinatoiron(II) derivative complexes.* Bioconjug Chem, 1997. **8**(4): p. 534-8.

178. Watanabe, M., et al., *Critical roles of Asp40 at the haem proximal side of haem-regulated phosphodiesterase from Escherichia coli in redox potential, auto-oxidation and catalytic control.* Eur J Biochem, 2004. **271**(19): p.

3937-42.

179. Yokota, N., et al., *Critical roles of Leu99 and Leu115 at the heme distal side in auto-oxidation and the redox potential of a heme-regulated phosphodiesterase from Escherichia coli.* FEBS J, 2006. **273**(6): p. 1210-23.

180. Notredame, C., D.G. Higgins, and J. Heringa, *T-Coffee: A novel method for fast and accurate multiple sequence alignment.* J Mol Biol, 2000. **302**(1): p. 205-17.

APPENDIX I

Derivation of Equation 3.1

$$ES \rightleftharpoons E + S$$

$$Kd = \frac{[E][S]}{[ES]}$$

$$\because [ES]_t = [E]_0 - [E]_t = [S]_0 - [S]_t$$
$$\Rightarrow [E]_t = [E]_0 - [ES]_t$$
$$\Rightarrow [S]_t = [S]_0 - [ES]_t$$

$$\therefore Kd = \frac{[E]_t[S]_t}{[ES]_t}$$
$$= \frac{([E]_0 - [ES]_t)\cdot([S]_0 - [ES]_t)}{[ES]_t}$$
$$= \frac{([ES]_t)^2 - ([E]_0 + [S]_0)\cdot[ES]_t + [E]_0 \cdot [S]_0}{[ES]_t}$$
$$\Rightarrow ([ES]_t)^2 - ([E]_0 + [S]_0)\cdot[ES]_t + [E]_0 \cdot [S]_0 = Kd \cdot [ES]_t$$
$$\Rightarrow ([ES]_t)^2 - ([E]_0 + [S]_0 + Kd)\cdot[ES]_t + [E]_0 \cdot [S]_0 = 0$$

$$ax^2 + bx + c = 0$$
$$x = \frac{-b \pm \sqrt{b^2 - 4ac}}{2a}$$

$\because$
$x = [ES]_t$
$a = 1,$
$b = -([E]_0 + [S]_0 + Kd)$
$c = [E]_0 \cdot [S]_0$
$$\therefore [ES]_t = \frac{([E]_0 + [S]_0 + Kd) - \sqrt{([E]_0 + [S]_0 + Kd)^2 - 4\cdot[E]_0 \cdot [S]_0}}{2}$$
and
$$A = \varepsilon \cdot l \cdot c$$
$$c = \frac{A}{\varepsilon \cdot l} = \frac{([E]_0 + [S]_0 + Kd) - \sqrt{([E]_0 + [S]_0 + Kd)^2 - 4\cdot[E]_0 \cdot [S]_0}}{2}$$

$$\therefore A = \varepsilon \cdot l \cdot \frac{([E]_0 + [S]_0 + Kd) - \sqrt{([E]_0 + [S]_0 + Kd)^2 - 4\cdot[E]_0 \cdot [S]_0}}{2}$$